STRESSES AROUND DISCONTINUITIES IN FIBRE-REINFORCED MATERIALS

by

M. J. IREMONGER, B.Sc.(Eng), A.C.G.I.

Thesis submitted for the Degree of Ph.D. in the Faculty of Engineering of the University of London and for the Diploma of Imperial College.

Mechanical Engineering Department,
City and Guilds College.

October, 1968.

SUMMARY

Stress distributions around fibre discontinuities in a composite material have been investigated by idealised two-dimensional models. These models have been analysed by the finite element method using a digital computer. Aluminium fibre/epoxy resin matrix models have been examined photoelastically to verify the elastic analyses and a steel fibre/lead alloy matrix model has been studied using the photoelastic coating and moiré methods to verify the elastic/plastic analyses.

It has been found that a fibre discontinuity is a source of severe matrix stress concentration, in excess of that associated with a single fibre end. The magnitude of this stress concentration and the corresponding length of fibre in which the axial stress is below the fully developed value depend upon the size and nature of the discontinuity (i.e. whether void or matrix filled), the inter-fibre spacing and the fibre/matrix modulus ratio. The fibres adjacent to a discontinuous one carry an elevated load the magnitude of which depends upon the same parameters. The elastic/plastic analyses show that matrix yielding reduces the stress concentration in the matrix by increases in the fibre stresses and the area of stress perturbation.

The results of these stress analyses are compared with the experimental observations of other workers and discussed in relation to published theories of failure. It is concluded that if the effects of a fibre discontinuity can be kept localised by having a ductile matrix or weak fibre/matrix interfaces the composite behaves in a quasi-homogeneous manner and its strength can be predicted by existing theories.

ACKNOWLEDGEMENTS

I wish to offer my sincere thanks

to Dr. W. G. Wood for his stimulating advice and practical assistance.

to the Science Research Council for their financial support for the project and a Research Studentship.

to the academic and technical staff of the Mechanical Engineering Department, City and Guilds College who were always ready to offer advice and assistance.

and to my parents for their continual encouragement, in particular to my mother who very ably typed the thesis.

M.J.I.

CONTENTS

	NOTATION	Page	6
1.	INTRODUCTION		
	1.1 Evolution of composites		8
	1.2 Fibre-reinforced composites		9
	1.3 The analysis of composites and its relation to composite design		10
	1.4 Micromechanics		11
	1.5 Principles of fibre reinforcement		12
	1.6 Literature survey		14
	1.7 Analysis of stresses around discontinuities		19
2.	THE FINITE ELEMENT METHOD		
	2.1 Introduction		21
	2.2 Basic theory		23
	2.3 Computer program development		25
	2.4 Accuracy		27
3.	SINGLE FIBRE COMPOSITE		
	3.1 Introduction		31
	3.2 Computed results		32
	3.3 Experiment results		34
	3.4 Discussion of results		35
4.	MULTI-FIBRE COMPOSITE NON-INTERACTING DISCONTINUITIES		
	4.1 Introduction		42
	4.2 Computer analyses		43
	4.3 Experimental analysis		44
	4.4 Elastic results		45

5. MULTI-FIBRE COMPOSITE WITH INTERACTING DISCONTINUITIES

5.1 Introduction 54

5.2 Computer analysis 55

5.3 Experimental results 56

5.4 Discussion of results 64

6. GENERAL DISCUSSION

6.1 Load transfer mechanisms 71

6.2 Composite failure 79

6.3 Improvements in composite design 87

6.4 Suggestions for future work 88

7. CONCLUSIONS 91

REFERENCES 94

FIGURES 99

APPENDICES -

1. Partial stiffness method 158

2. Finite element computer analysis 160

3. The computer program 165

NOTATION

σ direct stress

τ shear stress

e direct strain

γ shear strain

E modulus of elasticity

ν Poisson's ratio

V volume fraction

$\bar{\sigma}$ average (fully developed) stress

Subscripts:

c composite

f fibre

m matrix

Other symbols are defined in the text.

1. INTRODUCTION

1.1 EVOLUTION OF COMPOSITES

Materials systems containing two or more separate constituents have been known for a long time. Bamboo is a naturally occurring material with a structure similar to many man-made fibre composites (Slayter, 1962). The ancient Egyptians reinforced their clay bricks with straw and the Mongols made bows by glueing together bulls' tendons, wood and silk. Swords and gun barrels are other examples in which superior properties were obtained by combining together materials with dissimilar properties. In this century, concrete reinforced with steel and resin reinforced with paper or cloth have come into widespread use.

Glass reinforced plastics were first developed in the 1940's but because of their commercial success and their inherent inferiority to available structural materials they did not stimulate an interest in the general development of composite materials (Grimes, 1965). This did not occur until the potential of whiskers (Brenner, 1956) promoted tremendous interest. This coincided with the requirement in the aerospace industry for structural materials with higher specific strengths and elevated temperature properties than existing monophase materials. These are nearly at the limit of possible development. The use of whiskers with near theoretical strengths in a ductile metal matrix seemed to be the long sought breakthrough and intensive research was started, which has continued unabated.

The initial enthusiasm for whisker composites was tempered by difficulties in obtaining whiskers on a commercial scale and then incorporating them satisfactorily into the matrix. However, the enormous volume of research is now beginning to yeild fruitful results

(West, 1965). This research has also led to the development of other composite materials besides those containing whiskers and to a better, though still incomplete, knowledge of the general behaviour of composite systems. The ultimate aim is to be able to develop a composite to fit any particular design requirement.

1.2 FIBRE REINFORCED COMPOSITES

Several different types of materials system can be termed composite. Laminates and particulate systems in which the particles restrict the movementof cracks or dislocations in the matrix rather than carry a major part of the load are included as well as fibre composites. In a fibre reinforced material the load is carried primarily by the fibres, the matrix serving only to locate and protect the fibres and to transfer the stress from one fibre to another.

Fibres can be classified under three headings: metal wires, amorphous and polycrystalline fibres, and whiskers. Metal wires have been used mainly in model systems to test the concepts of fibre reinforcement (McDanels et al, 1963 and Kelly and Tyson, 1965a). Tungsten and steel are the most commonly used wire materials in these composites. Because of their availability and cheapness there is some potential for practical composite systems containing metal wires (Kobrin, 1965). The strength and stiffness of fibres lie between that of metal wires and whiskers. Carbon fibres (Watt et al, 1966) and baron fibres (Tooling and Production, 1967) are being produced on a commercial scale. These fibres which do not degrade when handled have a strength of about 300×10^3 p.s.i. and an elastic modulus equal to 60×10^6 p.s.i. which is twice that of steel. Glass fibres are also widely used, their main drawback being their low stiffness and their

susceptibility to atmospheric degradation (McGarry, 1966). Single crystal whiskers have the highest potential strengths, several million pounds per square inch (Coleman, 1964 and West, 1965) but their production, growth by vapour deposition, is difficult and costly. The main problem areas are in the incorporation of the whiskers into the matrix, that is aligning the whiskers and then bonding them to the matrix (Sutton, 1966).

The matrix is either polymeric or metallic. Examples of the former are epoxy and polyester resins. Many different metals have been used such as copper, aluminium, nickel and silver.

The composites are generally made by one of two methods:

(a) Liquid infiltration in which molten matrix material is mixed with the fibres , sometimes using pressure or vacuum.

(b) Powder metallurgy in which the fibres and powdered matrix are placed together in a mould and then compacted together by heating under pressure. Sometimes the matrix material is coated on the fibres prior to the moulding.

1.3 THE ANALYSIS OF COMPOSITES AND ITS RELATION TO COMPOSITE DESIGN

Composite systems investigated up to now have been analysed largely from an empirical point of view and have been the result of experiments with workable fibre/matrix combinations rather than a systematic study to determine the optimum properties. Parameters such as the length and diameter, volume fraction, distribution and 'in situ' strength of the fibres, the properties of the fibre/matrix interface and the relative elastic properties of fibre and matrix are important. Experimental difficulties and the interaction of these parameters make it almost impossible to analyse them separately.

It is therefore necessary to resort to a 'black box' approach to structural design. Design data is obtained from an empirical knowledge of the behaviour of the composite when subject to a given set of conditions. This macromechanical analysis ignores the individual behaviour and interaction of the constituents.

An exact analysis of composite behaviour is desirable for two reasons the first being in order to improve the properties of existing composites. Optimum properties will only be obtained when the effects of variations in the parameters such as those listed above are known quantitatively. A second reason is to enable the concept of 'tailor made' design to be realised. If it is possible to control the properties of a composite by varying the nature and distribution of the constituents it will then be possible to choose a material to give the exact range of properties sought by the designer.

1.4 MICROMECHANICS

An exact analysis of composite behaviou includes the study of micromechanics, that is the internal reactions of the constituent materials to imposed loads and the resulting stress distributions.

The need for micromechanical study is well recognised. Dixmier and Gerard (1964) in a report for the NATO Advisory Group for Aeronautical Research and Development (AGARD) state that ". . . (the) following fundamental problem areas (are) associated with the characterization of the composite in terms familiar to the solid mechanics viepoint. These include,

(a) Load transfer mechanisms for continuous and discontinuous reinforcements through the matrix.

(b) Stress distribution and concentration effects at

reinforcement-matrix interfaces.

(c) Fracture initiation at reinforcement-matrix interfaces.

(d) Fracture progression through composite."

A report prepared by the Materials Advisory Board (1965a) in the United States for the National Academy of Sciences supports the view that one of the major shortcomings in composite technology is the incomplete and inadequate understanding of the micromechanics of composite materials. This report states that such study is necessary to enable the successful development of composite materials systems and optimal structural design with composites to be carried out. It also outlines several particular areas worthy of study including,

(a) Elastic and inelastic stress analyses of single and multi-fibre composites with idealised geometrics.

(b) Stresses in the vicinity of a fibre break including the effects of the presence of adjacent fibres, variable material properties and localised plastic deformation of the matrix.

(c) Stresses in a composite with elastic fibres and matrix but an elastic/plastic interface layer.

The work reported in this thesis comprises stress analyses of various idealized composite geometrics containing fibre breaks and discontinuities. Account is taken of changes in material elastic properties (modulus of elasticity (Youngs modulus), E, and Poisson's ratio, ν) and of localised plastic deformation of the matrix.

1.5 PRINCIPLES OF FIBRE REINFORCEMENT

As explained earlier the fibres carry the major part of the load while the matrix transfers the load between the fibres.

When the fibres are continuous and aligned longitudinally both the fibres and the matrix undergo equal strains. The components carry the load in proportion to their respective moduli and no load is transferred between them, the matrix serving merely to locate and protect the fibres. A rule of mixtures relation can be used to give the material properties. Thus the composite elastic modulus, E_c, is given by,

$$E_c = V_f E_f + (1 - V_f) E_m \qquad (1.1)$$

This relation has been found to be experimentally valid (McDanels et al, 1963). In fact it represents the lower bound to the modulus and is true when the Poisson's ratios of fibre and matrix are equal (Hill, 1963).

As the fibre, matrix and composite strains are equal the composite stress, $\bar{\sigma}_c$, is given by,

$$\bar{\sigma}_c = V_f \bar{\sigma}_f + (1 - V_f) \bar{\sigma}_m \qquad (1.2)$$

This expression can also be used to give the composite strength, S_c,

$$S_c = V_f S_f + (1 - V_f) \bar{\sigma}'_m \qquad V_f > V_{min} \qquad (1.3)$$

where $\bar{\sigma}'_m$ is the stress in the matrix at the ultimate strain of the fibres (the matrix does not necessarily remain elastic). S_f is the fibre strength. The validity of equation (1.3) has been established experimentally by McDanels et al (1963) and Kelly and Tyson (1965a) for tungsten wires in a copper matrix. The fibre volume fraction must exceed a minimum value, V_{min}, in order that the strength of the composite is greater than the strength of the matrix only. This expression for composite strength is not true when premature fibre failures occur due to flaws or defects in fabrication. The presence

of discontinuous fibres also result in lower strengths.

When there is no continuous loading path the matrix plays an important part in the reinforcement by transferring load from one fibre to another. If the fibres have an elastic modulus greater than that of the matrix they inhibit its free deformation. This is shown schematically for an isolated fibre in figure 1.1 and it results in a strain perturbation in the matrix. The load is transferred from the matrix by shear stresses along the edges of the fibre and by direct stress at the fibre ends.

The axial stress in the fibre rises to a maximum value equal to that for a continuous fibre, $\bar{\sigma}_f$, while the shear stresses, high at the fibre ends diminish to zero (Figure 1.1). The transfer or critical length, L_c, is the length of fibre necessary for the continuous fibre stress, $\bar{\sigma}_f$, to be attained. It is important to note that in the literature the critical fibre length is sometimes defined as the length of fibre necessary to cause the fibre to fracture rather than pull out, which is not necessarily the same as the definition above. Fibre pull out occurs when the stress in the fibre is not sufficient to cause it to fracture before the matrix or interfacial bond fails.

As the average stress in a discontinuous fibre is less than $\bar{\sigma}_f$ due to the reduction in stress at the fibre ends the composite strength must be less than that of a continuous fibre composite (Kelly and Tyson, 1965b).

A comprehensive account of the basic principles of fibre reinforcement is given by Kelly and Davies (1965).

1.6 LITERATURE SURVEY

The first work on the internal stresses in a composite material

was that of Cox (1952). Cox presented a theoretical solution for the longitudinal stress distribution in a cylindrical elastic fibre embedded in a cylindrical elastic matrix. He also determined the resulting interfacial shear stress distribution in the matrix. This theory assumes perfect bonding between fibre and matrix, no load transfer across the ends of the fibre and that the interfacial shear stress is proportional to the difference between the displacement in the direction of the fibre at a point along the interface and the displacement in the matrix at the same point when the fibre is absent.

Dow (1963) in a similar theoretical analysis assumed that straight radial lines in the fibre and matrix remain straight after deformation. Rosen (1964) modified Dow's theory assuming that the fibre carries only tensile stresses and that the matrix carries only shear stresses. Rosen used a cylindrical model in which the fibre is surrounded by a matrix which itself is surrounded by a matrix having the average properties of the composite. These analyses predicted rapid load transfer near the fibre ends and therefore high interfacial shear stresses.

Tyson and Davies (1965) made an experimental comparison with the theories of Cox and Dow by using a plane model consisting of an aluminium alloy 'fibre' in an epoxy resin matrix and then determining the matrix stress distribution photoelastically. Their results compared well with the theoretical ones away from the fibre ends but within about two fibre widths of the ends they found shear stresses up to five times greater than those predicted by Cox and Dow.

Schuster and Scala (1964) also used photoelasticity to determine the stresses in an epoxy resin matrix surrounding an isolated sapphire

whisker. They found that the stress concentration at the fibre ends could be partly alleviated by using whiskers with finely tapered ends. The effect of the fibre end shape has since been investigated by several workers. MacLaughlin (1966), Allison and Holloway (1967) and Carrara and McGarry (1968) have all found that the nature of the stress distribution in the matrix around a fibre end is very dependent upon its shape.

The high stress concentrations that are associated with a fibre break were first reported by Schuster and Scala (1964) but they did no quantitative analysis. MacLaughlin (1966) investigated the matrix stress distributions for two dimensional models containing 'broken' steel 'fibres' in an epoxy resin matrix. The matrix was bounded on either side by continuous steel 'fibres' each one being three fibres widths from the central one. In these models the fibre/matrix modulus of elasticity ratio, E_f/E_m, equalled about 3000. Both matrix filled and void discontinuities were investigated with distances between the fibre ends equal to 1.0, 2.0 and 6.67 fibre widths. The peak interfacial shear stresses were considerably higher than those for a single ended fibre and decreased with increasing distance between the fibre ends. It made little difference whether or not the gap was filled with matrix because very little load was transferred through the matrix between the fibre ends due to its low elastic modulus.

MacLaughlin (1968) has recently extended his earlier work using photoelastic models containing epoxy resin 'fibres' giving a fibre/matrix elastic modulus ratio equal to 40. It was therefore possible to observe the stress distribution in the fibres as well as in the matrix. Geometries were varied to study the effects of lateral fibre spacing

(representing 16% and 45% fibre volume fractions) and the relative position of interacting fibre ends. He found the following:

(a) Critical fibre aspect ratios ranged from 40 to 80. The critical aspect ratio is the length of fibre in which the stress is less than the fully developed value divided by the fibre diameter.

(b) The stress increased sharply at the outside tips of the fibres to a value whose magnitude approximately equalled the applied fibre stress, $\bar{\sigma}_f$, in the case when two fibre ends were close together.

(c) Maximum interfacial shear stress concentration factors, $\tau^*_m/\bar{\sigma}_c$ rose to 13 at the fibre ends but then diminished rapidly away from the ends.

(d) The maximum interfacial shear stress increased as the fibres were brought closer together while the stress between the fibre ends decreased.

Schuster and Scala (1968) in some recent work on multi-fibre arrays using boron fibres in an epoxy resin matrix (E_f/E_m equal to 125) found that nearby fibre ends influenced one another only when they were less than one half of the critical fibre length apart. The stress concentrations were greatly increased when the lateral fibre spacing was small. Some reduction in the peak matrix interfacial shear stress at a fibre end was observed when adjacent fibres were close to one another.

The experimental studies described above used the technique of photoelasticity as a means of stress measurement. Carrara and McGarry (1968) have used the finite element method to determine the optimum end shape for an isolated cylindrical fibre in a matrix. This is the numerical analysis technique which is used for the analyses reported

in this thesis. The main differences between their analysis and that described in chapter 2 is that they used a mesh of quadrilateral instead of triangular elements and did not consider matrix yielding. The finite element method has also been used by Tsai and Chen (1967) but though their model is similar to that described in chapter 4 their work has been mainly concerned with overall composite properties, namely the stiffness of a discontinuous composite compared to a continuous one.

Several theoretical studies of fibre strengthening have appeared which involve approximations to the stress field. Hedgepeth (1961) investigated the stress concentrations in two dimentional filamentary structures resulting from a sudden fibre break using shear lag analysis (which assumes that the fibres carry only tensile forces and the matrix carries only shear forces). Zender and Deaton (1963) obtained reasonable agreement with this theory. Spencer (1965) considered a rigid/plastic matrix between rigid/brittle cylindrical fibres symmetrically arranged parallel to one another. With this model he predicted the load at which the composite fails by plastic flow of the matrix, or by fibre fracture. Piggott (1966) combined Cox's elastic analysis with Kelly and Davies' theory for plastic stress transfer in order to evolve a theory involving elastic/plastic matrix behaviour. Cohen (1967) has used elasticity principles to determine the stress and strain fields in a discontinuous fibre composite. The theory is in general agreement with the photoelastic studies of Schuster and Scala (1964) and Tyson and Davies (1965).

The analyses presented in the succeeding chapters of this thesis were commenced in 1965. Much of this work was completed before the publication of several of the papers described above. The analysis of

the stresses around a single broken fibre composite described in chapter 3 has been published (Iremonger and Wood, 1967).

The most comprehensive reviews of the principles of fibre reinforcement are by the American Society of Metals (1965), Kelly and Davies (1965), Cratchley (1965), Holister and Thomas (1966) and Moss (1967). The progress in composite technology is however so rapid that general surveys are soon outdated. A paper based on some of the work described in chapter 4 has been read at an Institute of Physics conference (Cranfield, September 1968).

1.7 ANALYSIS OF STRESSES AROUND DISCONTINUITIES

The succeeding chapters describe analyses of models representing fibre composites in which one or more of the fibres has broken either during fabrication or because of prior loading conditions. Fibre breaks during fabrication may result in the gap between the fibre ends being filled with matrix material. A similar geometry can arise from discontinuous fibres being aligned longitudinally and then butted together during fabrication of the composite. Both matrix filled and void end gap conditions are considered.

Because of the difficulties of analysis the models are essentially very simplified, being two dimensional and of regular geometry. Perfect bonding between fibre and matrix is assumed unless otherwise stated. It is also assumed that a continuous mechanics approach is valid, in other words that the fibre and interfibre dimensions are not so small that dislocation and grain boundary movement have a significant effect on the stress field. Both fibres and matrix are taken as homogeneous and isotropic.

The models are analysed by the finite element method using a digital computer. This technique of numerical stress analysis is described in chapter 2. The development of the computer program and the accuracy of the method are also discussed.

Chapter 3 describes the elastic stress analysis of a composite comprising a matrix containing a single broken fibre. The effect of variations in size and nature (i.e. void or filled with matrix material) of the discontinuity are considered.

In chapter 4 a more complex model is introduced. This model represents an idealised multifibre composite which enables the effect of fibre spacing (fibre volume fraction) to be considered. In this idealisation the fibre discontinuities are too far apart to influence one another. The analysis is extended to include elastic/plastic matrix behaviour.

Nearby breaks in adjacent fibres provide a ready path for matrix yielding and crack propagation. Chapter 5 describes an interacting discontinuity model with both elastic and elastic/plastic matrices. The effects of varying the distance between the discontinuities, of a weak fibre/matrix interface layer and of matrix fracture are also considered.

Chapter 6 presents a discussion of load trasfer and failure mechanisms. Theories of failure are described and the relevance of the results from previous chapters to these and the experimental observations of other workers is explained.

2. THE FINITE ELEMENT METHOD

2.1 INTRODUCTION

The finite element method is a generalisation of standard methods of structural analysis in which a continuous structure is represented by a finite number of elements interconnected at a finite number of nodal points. The method was evolved about 10 years ago in the aircraft industry where there was a need for accurate stress analysis of complex aircraft structures (Turner et al, 1956) and where digital computers were available. There has since been an increasing number of other applications and at present its use is growing at a faster rate than any other method of numerical or experimental stress analysis.

A continuum is idealised as an assemblage of elements (in this thesis triangular elements) and then analysed by standard techniques. Figure 2.1 shows a simple mesh of elements and illustrates the nomenclature used. The representation of the physical system is not exact but there need be no approximation in the mathematical analysis. This is, incidentally, unlike the finite difference method in which exact equations of the physical system are solved by approximate means.

The analysis involves the simultaneous satisfaction of equilibrium, compatibility and a force-deflection relationship. The resultant element forces at each nodal point must be in equilibrium with the externally applied nodal point loads; the elements must continue to meet at the nodal points when they are deformed and the relation between forces and displacements within each element must obey the stress-strain relationship for the material being simulated.

This compatibility relationship alone is not sufficient to represent the behaviour of a continuum because gaps and overlaps would

occur along the sides of the elements as they were deformed and stress concentrations would develop at the nodal points. It is necessary to have compatibility between adjacent elements. For triangular elements fully compatible deformation patterns can be prescribed by specifying that the internal displacements vary linearly in two perpendicular directions i.e. lines within an element initially straight remain straight during deformation. This requires the strains ϵ_x, ϵ_y and γ (and hence the stresses σ_x, σ_y and τ_{xy}) to be constant within each element. In regions of high strain gradient it is therefore necessary to have small elements.

It has been shown that if the deformation characteristics provide both internal compatibility within the elements and compatibility of displacements along the element boundaries, the strain energy of the idealization represents a lower bound to the strain energy of the continuum (de Venbeke, 1964). In addition it can be shown that the finite element solution converges to the true solution as the mesh size is reduced.

Marcal (1965) has developed a stiffness method for the solution of elastic-plastic problems which can conveniently be used in conjunction with the finite element method (Marcal and King, 1967).

The basic theory of the finite element and partial stiffness methods follows. A more detailed version with particular reference to its conversion into a computer program is given in the appendix. A full listing of the computer program is also included in the appendix. The development of this program and its limitations are discussed in section 2.3.

2.2 BASIC THEORY

The basis of the finite element analysis is as follows:

(a) Stiffness of an individual element

The first step in the analysis is to determine the forces at the corners of an element resulting from unit corner displacements. This relation is called the stiffness of the element and is a 6 x 6 matrix because there are both x and y forces and displacements at each of the three corners of the element.

The element strains are written in terms of nodal point displacements,

$$\underline{e} = \underline{D}.\underline{r} \qquad (2.1)$$

The matrix $\underline{D}$ is obtained from the displacement functions which ensure compatibility between adjacent elements, the requirement for which was described in the previous section.

The stress-strain relation for the material is also written in matrix form,

$$\underline{\sigma} = \underline{S}.\underline{e} \qquad (2.2)$$

The forces, $\underline{F}$, at the nodal points of the element are related to the stresses by a geometrical relation, $\underline{B}$,

$$\underline{F} = \underline{B}.\underline{\sigma} \qquad (2.3)$$

from (2.1) and (2.2)

$$\underline{\sigma} = \underline{S}.\underline{D}.\underline{r} \qquad (2.4)$$

and from (2.3) and (2.4)

$$\underline{F} = \underline{B}.\underline{S}.\underline{D}.\underline{r}$$

or

$$\underline{F} = \underline{k}.\underline{r} \qquad (2.5)$$

where

$$\underline{k} = \underline{B}.\underline{S}.\underline{D}. \qquad (2.6)$$

$\underline{k}$ is the required element stiffness matrix.

(b) Stiffness of assemblage of elements

The equilibrium equation for the assemblage of elements i.e. the whole structure can be written

$$\underline{R} = \underline{K}.\underline{r} \qquad (2.7)$$

where $\underline{K}$ is the stiffness of the whole structure obtained by summing the effects at each nodal point of all the adjacent elements.

(c) Solution of equilibrium equations

The equilibrium equations are solved by a systematic relaxation technique known as the Gauss-Seidel iteration procedure.

Equation (2.7) is solved for each nodal point using initially assumed displacements (usually zero) and thereafter the latest approximation to the displacement at the other nodal points (see Appendix 2).

To increase the rate of convergence an over-relaxation factor is used. Thus the change in displacement between cycles of iteration is calculated for each nodal point and the new estimate of displacement is taken as the old displacement plus the over-relaxation factor times the change in displacement. The over-relaxation factor for optimum convergence ranges between 1.7 and 1.95.

(d) Evaluation of stresses and strains

When the nodal point displacements have been determined substitution of these values in equation (2.1) yields the element strains. The element stresses are then evaluated from equation (2.2). Using an averaging technique, modified for boundary points, the nodal point stresses can be determined.

(e) Elastic/plastic behaviour

For an elastic/plastic analysis the elastic solution is taken as

that which just causes first yielding. The material is assumed to obey the von Mises criterion of yielding, which for plane stress is given by,

$$\sigma_x^2 - \sigma_x\sigma_y + \sigma_y^2 + 3\tau_{xy}^2 = \sigma_y^2 \qquad (2.8)$$

This expression is calculated for each element, the maximum value being taken as the equivalent yield stress, σ_y.

An increment of the elastic load is then applied and an analysis is performed similar to that described in paragraphs (a) to (c) except that the stiffnesses are modified for those elements that have yielded or are in the process of yielding. These modifications (Marcal's partial stiffness method) are described in the appendix.

Stresses and strains are determined as before except that plastic elements are assumed to obey the Prandtl-Reuss stress-strain equations.

This procedure is repeated for further increments of load as required.

2.3 COMPUTER PROGRAM DEVELOPMENT

The computer program described and listed in the appendix was evolved from one presented by Wilson (1963) for elastic analysis and later modified by Marcal and King (1967) to include his partial stiffness elastic-plastic method.

During the present development of the program the following major modifications were made.

(a) Boundary conditions

For the models described in chapters 4 and 5 which represent fundamental areas of multifibre composites, boundary conditions were required which make the boundaries remain straight and parallel when deformed. This constraint was imposed during the iteration on nodal

point displacements by requiring the nodal points along the boundary in question to undergo equal displacements. This constraint has the effect of slowing down the rate of convergence of the equilibrium equations.

(b) Preliminary approximation to nodal point displacements

In view of the slow convergence resulting from the boundary conditions discussed in the previous paragraph it was found necessary to make an initial estimate of the final displacements rather than starting with all displacements zero. The most effective, and simple, way of doing this was to consider the modal in question with continuous fibres and to apply a rule of mixtures relation to determine the nodal point displacements without recourse to iteration.

(c) Matrix yielding

During elastic loading the fibre stresses exceed the matrix stresses because of the greater modulus of elasticity of the fibrous material. In order to allow matrix yielding only it was necessary to define fibre and matrix elements differently.

Modifications were also made so that partial matrix yielding was possible i.e. only specified matrix elements were allowed to yield. This enabled composites with a weak fibre/matrix interface to be simulated.

(d) Matrix failure

Matrix failure was simulated very approximately by allowing the modulus of elasticity of an element to reduce to nearly zero when the equivalent stress and equivalent strain reached certain values. ~~Thus both ductile and brittle matrices could be investigated by choosing different plastic strains to failure (zero in the case of brittle~~

~~systems~~).

(e) Other

In Marcal's program the elastic stresses were scaled to give unit equivalent yield stress. To make a comparison with experimental results easier this was modified so that realistic yield stresses could be used. The program was split into small subroutines and the storage of variables in the program was modified to allow a greater number of elements and nodal points to be used. Extensive changes were made in the control of the quantity and layout of the output.

2.4 ACCURACY

The major inaccuracies that arise in the application of the finite element method fall into three main areas:

1. The idealisation of the continuum into a mesh of elements.
2. The simulation of actual loading conditions and boundary restrictions.
3. The iterative solution of the equilibrium equations.

The first of these is connected with the representation of the physical system. A true solution is obtained only with an infinite number of elements, but by a judicious choice of element size and distribution this inherent approximation of the method is well within acceptable limits. The accuracy of simulation of loading and boundary conditions depends upon the complexity of the model. In most cases the errors involved, particularly away from the boundary are small. There is no inherent approximation in the mathematical analysis of the equilibrium equations, provided there are enough cycles of iteration.

The rate of convergence of the solutions of the equilibrium equations depends upon the nature of the boundary conditions and the choice of over-relaxation factor.

Some particular points arising out of these considerations are discussed in the following paragraphs.

Mesh approximation

Compatibility between elements is satisfied if the strains, and hence the stresses, are assumed to be constant within each element. As in a continuum the strains can vary continuously the element size is important in determining the accuracy of the method, particularly in regions of high strain gradient.

There is a practical limit to the number of elements and nodal points set by the storage capacity of the computer. The capacity of the Imperial College IBM 7094 is about 400 elements and 230 nodal points and that of the University College IBM 360/65 is about 750 elements and 450 nodal points. The running time of the computer program is directly related to the number of elements and so this is another constraint on the number of elements used. It is therefore important to vary the element size and distribute them so that the smallest elements are in the region of highest strain gradient. Meshes constructed on this principle are shown in figures 3.1 and 4.3.

It has been found by Clough (1965) and others that even very course meshes give good results except in regions of high strain gradient. In the study of the single fibre and non-interacting multi-fibre composites presented in this thesis where high strain gradients do occur, the good agreement with experimental results confirmed that the mesh size and distribution were satisfactory.

When elastic/plastic behaviour is studied it is usually found that a region of stress concentration spreads out as the elements yield. Therefore some loss of accuracy is to be expected when using a weighted mesh specifically designed for the elastic analysis. To overcome this a mesh containing elements of equal size can be used.

Boundary and loading conditions

The deformation of the mesh is caused by loads or displacements imposed on nodal points, usually situated at the boundaries of the mesh. Continuous loading of the boundary must therefore be approximated by resultant loads at the nodal points along the boundary. For the models discussed in this thesis nodal point loads were calculated to give uniform displacement of the ' x = maximum ' boundary assuming a rule of mixtures relationship between the two phases. The effect of the discontinuity was ignored in this approximation but changes in the load distribution to compensate for this made little difference except in the region of the boundary.

One method used to deform the multi-fibre composite models was to impose equal x - displacements at the nodal points along the boundary to be loaded. Then a preliminary approximation was performed with these x - displacements, assuming continuous fibres and a rule of mixtures relation between the two phases. The points along the loaded boundary were fixed at the positions attained during the approximation procedure. The equilibrium equations for the actual composite model (i.e. with the fibre discontinuities) were then solved with these boundary conditions. For elastic deformation the results obtained were nearly identical to those obtained with equivalent nodal point loads. However for substantial elastic/plastic deformation only the 'displacement'

loading gave a boundary with equal x - displacements.

Solution of equilibrium equations

The rate of convergence of the iteration of nodal point displacements, i.e. the solution of the equilibrium equations, is very dependent upon the choice of over-relaxation factor. Figure 2.2 shows this clearly. In this figure, which is for the single fibre composite, the number of cycles necessary for convergence was halved by increasing the over-relaxation factor from 1.89 to 1.94. For the later models other values of over-relaxation factor gave the most rapid convergence; in addition the optimum value varied with the mesh, loading and boundary conditions for what was essentially the same composite.

Results to within one per cent of the best possible for the particular fineness of mesh were obtained when the displacement unbalance became less than 10^{-5}. Displacement unbalance is the ratio of the incremental change in displacement during the previous cycle of iteration and the total displacement of all the nodal points. Using an over-relaxation factor this order of convergence was attained within 100 to 500 cycles of iteration depending upon the number of elements in the mesh.

The preliminary approximation which was used for the multi-fibre composite models increased considerably the rate of convergence.

3. SINGLE FIBRE COMPOSITE

3.1 INTRODUCTION

The first problem to be considered was that of a single broken fibre in an infinite elastic matrix with uniaxial loading parallel to the fibre axis (figure 3.1).

A single isolated broken fibre was chosen as the preliminary study for the following reasons:

(a) It is a simple model.

(b) It enabled the techniques of analysis to be fairly easily tested. In particular the finite element method could be checked.

(c) There was no published work at that time on the stresses around a fibre break.

(d) The results obtained would enable the effects due to a single fibre break to be separated from those due to other geometrical factors in the analyses of more complex models.

Variations in distance between the fibre ends (end gap) ranging from 0.05 to 3.0 fibre widths were considered. The smallest of these end gaps simulates a fibre that has just broken and larger values simulate 'equilibrium' positions that are attained sometime after fibre fracture.

Kelly and Tyson (1964) and Ham and Place (1966) have published photographs of broken tungsten fibres in sopper matrices which show end gaps of between 1.2 and 0.5 fibre widths. Mullin, Berry and Gatti (1968) show boron and tungsten fibres having 0.1 to 3 fibre width end gaps.

Further analyses were performed for end gaps filled with matrix

material. These simulate behaviour in a discontinuous fibre composite where two fibre ends happen to be in close proximity to one another. The effects of variations in the ratio of the elastic modulus of the fibre and the elastic modulus of the matrix were also considered.

The investigation was conducted numerically using the finite element method described in chapter 2. The method was checked by means of a photoelastic model comprising an aluminium alloy 'fibre' in an epoxy resin matrix.

3.2 COMPUTED RESULTS

Model Specifications

Because of symmetry in both x and y directions only one quarter of the composite model shown in figure 3.1 was necessary for the finite element representation. Points along AB and AD were restricted to sliding along these lines and loads were applied in the x-direction to points along BC. For convenience A was taken as the origin of co-ordinates and its position was fixed throughout the analysis.

The basic mesh and dimensions for the analytical model, of unit thickness, are shown in figure 3.2. This mesh, except for that part within region S, was generated automatically by a computer program (Marcal, King and Leech, 1967) Region S was varied for each end gap. The cases studied were void end gaps of 0.05, 0.1, 0.2, 0.5, 1.0, 2.0 and 3.0 fibre widths and matrix filled end gaps of 0.05, 0.1, 0.2, 0.5 and 1.0 fibre widths. The mesh size varied between 300 elements (175 nodal points) and 334 elements (192 nodal points). Figure 3.3 shows region S meshes for 0.5 and 3.0 fibre width end gaps. The distribution of elements around the fibre ends was essentially the same for each

end gap. The side length of the smallest element represented about 0.002 in. on the photoelastic model. The loads applied to nodal points along BC were calculated so as to give constant displacement of that boundary in the x-direction. The total load on BC was 10,000 lb.

The photoelastic model used for checking the analytical results had small fillets of cement at the corners of the gap and these were not removed for fear of debonding between fibre and matrix under load. However, in order to fine the effect of these fillets a further finite-element calculation was carried out for the ratio of end gap to fibre width of 0.5 with the fillet shown in figure inserted in the mesh.

The material constants used in the analysis were those of the photoelastic model i.e. $E_f = 10.0 \times 10^6$ p.s.i., $\nu f = 0.32$ and $E_m = 0.47 \times 10^6$ p.s.i., $\nu_m = 0.35$.

Results

The optimum over-relaxation factor was found to be 1.94 (see page 30). This gave a displacement unbalance of about 10^{-6} after 250 cycles which meant a running time of about $3\frac{1}{2}$ minutes.

Figures 3.8 to 3.12 were plotted from the results. The values of the interfacial shear stresses in figures 3.7 and 3.12 were those of the elements adjacent to the interface.

Accuracy

The validity of the computed results are confirmed later (page 35) by a comparison with the photoelastic results. As explained on page 22 the finite element method gives a lower bound solution and the magnitudes of the displacements (and hence the stresses) increase as smaller and smaller elements are used. The effect of varying the

number of elements was examined. As an example, for a ratio of end gap to fibre width of 0.5 the mesh was increased from 284 to 301 elements by increasing the number of elements near the end gap, in both matrix and fibre. Outside a radius of 5 fibre widths measured from the centre of the end gap, the maximum shear stress changed less than 0.5%. Between radii of 1 and 5 fibre widths, changes of 2-3% occurred, and within 1 fibre width changes were mostly less than 5%. A change in interface shear stress of 10% occurred for a length of only 0.2 fibre widths right at the fibre tip and this change decreased to less than 2% within 2 fibre widths of the end. Similar mesh patterns were used for all the end gaps analysed. Therefore a comparison between the different results should be more accurate than the results themselves.

A further set of analyses were made for the 0.5 fibre width void end gap model with variations in fibre/matrix elastic modulus ratio. Results were computed for E_f/E_m ratios of 2, 5, 10, 20, 50 and 100.

3.3 EXPERIMENTAL RESULTS

The model used for the experiment is shown in figure 3.4. The 'fibre' was made of Duralumin ($E = 10.0 \times 10^6$ p.s.i., $\nu = 0.32$) and the matrix was made of Araldite CT200/HT901 epoxy resin in the ratio of 100 : 30 parts by weight ($E = 0.47 \times 10^6$ p.s.i., $\nu = 0.35$). The matrix was cast as a single plate, $\frac{1}{4}$ in. thick, polished and then machined into two strips each just under 3" wide. The aluminium fibres were also machined before being cemented to the matrix with Araldite AY103/HY951 adhesive. The model was tested in a diffined sodium light photoelastic bench shown in figure 3.5 load being applied from a scale pan and lever arm to heavy steel end grips bolted to the specimen. A

typical isochromatic fringe pattern is shown in figure 3.6. Measured values of principal stress difference (fringe order) in the matrix plotted in two directions, one along the fibre-matrix interface and the other along the y axis, that is perpendicular to the fibre, are shown as points in figure 3.7.

3.4 DISCUSSION OF RESULTS

Comparison of computed and photoelastic results

The shapes of the photoelastic model (figure 3.4) and the computed model (figure 3.2 shows one quarter of this model) are not identical. In the latter the fibre is bounded by a much larger width of matrix. This difference is not significant as the width of the experimental model was sufficient to eliminate any effects due to the influence of the free edge of the matrix on the region around the fibre break. The extra width of matrix merely means that additional end load had to be provided on the computed model to produce the same stress as that in the experimental model. The difference in length of the two models also has no effect on the stress concentration at the discontinuity. The basis of comparison between the computed and experimental results must be the size and shape of the gap between the fibre ends in the centre of the models, that is the ratio of fibre gap to fibre width. The computed output for a void end gap of 0.5 fibre widths was scaled to give an effective 'material fringe value' using the equations,

$$\sigma = \text{load/area} \qquad (3.1)$$

$$\sigma = Ee \qquad (3.2)$$

and

$$n = (\sigma_1 - \sigma_2)\, t/f \qquad (3.3)$$

where n is the isochromatic fringe order, f is the material fringe value and t is the thickness of the model. The computed and photoelastic results were then compared on the basis of fringe order (Figure 3.7).

Three sets of computed results were compiled. The full line is for a completely void end gap, the dotted line for and end gap containing small fillets such as remained on the photoelastic model, and the chain-dotted line shows the effect of applying the end load to the matrix only and not distributing it between matrix and fibre. The actual load transfer to the photoelastic model, being by frictional forces between the end grips and the specimen could have resulted in a tendency towards this condition.

There are several possible sources of inaccuracy.

(a) The inherent limitations of both photoelastic and finite element techniques.

(b) The difficulty of positioning the higher order fringes in the photoelastic model due to the magnitude of the strain gradient in the immediate neighbourhood of the fibre break.

(c) Small differences between the elastic constants (Young's modulus, E and Poisson's ratio, ν) in the experimental model and those assumed for the computed model.

(d) The effects of a small initial fringe pattern in the photoelastic model which was perhaps incompletely allowed for.

Errors due to these mean that an overall accuracy of $\pm 5\%$ ($\pm 10\%$ within one fibre width of the fibre break) is all that could be expected.

The results shown in figure 3.7 are well within these limits. A similar measure of agreement was found for stresses along directions

other than those plotted.

The agreement found between experiment and theory confirms the suitability and accuracy of the finite element method for a study of stresses in two phase composite material models. In particular it also shows that the mesh shape and distribution was suitable and that the elements near the discontinuity were sufficiently small to give results of the same order of accuracy as those obtained using photoelasticity.

This measure of agreement was not unexpected as the finite element method has been used very successful by other workers.

Stress distribution in the fibre

The growth of axial stress in the fibre, with the end gap void for a number of fibre-gap ratios is shown in figure 3.8. The axial stress builds up non-linearly, and more slowly as the size of the end gap increases and the interaction between the fibre halves decreases.

A comparison with the solutions of Cox (1952) and Dow (1963) for the fibre axial stress is not possible because their solutions are not applicable for an infinite matrix. The rate of change of axial stress along the fibre axis was found to be proportional to the interfacial shear stress except near the fibre ends where the stress varied across the width of the fibre. As the load transfer from the matrix to the fibre is by shear at the fibre/matrix interface this relationship was expected.

The variations in stress within about two fibre widths of the fibre break are very interesting. The axial stresses in this region are low at the centre line of the fibre but very high near the fibre/matrix interface where the load is being rapidly transferred by shear from matrix to fibre (figure 3.9). In addition there are high compressive

stresses across the fibre at the end but these decrease to less than one per cent of the axial stress within two or three fibre widths of the end gap. The stress concentration near the outside tips of the broken fibre (figure 3.9) increases with decreasing end gap to such an extent that, when the end gap is less than 0.2 fibre widths, either some local yielding of the fibre can be expected or conditions will be altered by the cracking, debonding or gross deformation of the matrix in order to reduce this severe concentration. Recently, MacLaughlin (1968) has reported high axial stress gradients near the fibre ends of similar magnitudes to those found in this analysis.

The length of fibre in which the axial stress reaches its maximum value increases with the size of end gap and also with the fibre/matrix modulus ratio. Figure 3.10 shows the relationship between the length in which 95% of the applied fibre axial stress is attained and the fibre/matrix modulus ratio. The less rapid increase in transfer length for the higher values of modulus ratio is partly due to poor convergence of the finite element analysis.

When the end gaps are filled with matrix material, as in a discontinuous fibre composite, the build-up of axial stress becomes quite different from that when the gaps are void (figure 3.11). This is particularly true for small end gaps, when there is a high axial stress in the fibre right to the end, because of the pull of the matrix material in the end gap. If the end gap is very small the fibres tend to behave as one continuous filament provided the interfacial bond at the end does not break down or the matrix material in the gap yield. In practice one or other of these failure conditions does occur.

Stress distribution in matrix

Figure 3.12 shows the distribution of maximum shear stress along the fibre-matrix interface for different fibre-gap ratios. When (a) the gap is void, (b) the gap is filled with matrix material. Note that the vertical scales of these figures are not the same.

When the gap is void, the stress concentration in the matrix, at the fibre tip, decreases with increasing end gap. Such high stress concentrations occur when the fibre gap ratio is small (0.2 or less) that yielding of the matrix would certainly occur at the tip of the fibre. If the matrix is not ductile then matrix or interfacial failure would take place. Similar matrix stress concentrations have been observed by MacLaughlin (1966) using a photoelastic model with end gap ratios 1, 2 and 6.67. No direct comparison is possible however because his models were bounded by continuous fibres and the fibre/matrix modulus ratio was about 3000.

When the end gap is filled with matrix material the correspondence between stress concentration and end gap completely reverses and now the shear-stress concentration in the matrix at the fibre tip increases with increasing end gap. This is because the piece of matrix filling the end gap behaves more and more like a piece of fibre as its length becomes shorter, so that for very short end gaps the fibre appear continuous and the stresses in the matrix surrounding the fibre are low. The axial stresses in the matrix filling the end gap, however, are very high, being about the same as the axial stresses in the fibre (figure 3.11). Thus matrix yielding in tension is likely to occur at low overall stress levels. The behaviour then becomes similar to the void end gap case.

It is expected that the shear stress concentration at the fibre ends will first increase with increasing end gap, as explained above, until it reaches a value about twice that for a single fibre end and then decrease to that value as the two ends of the fibre cease to influence one another. The stress concentrations at the fibre tip for end gaps of 0.5 and 1.0 fibre widths (figure 3.12) are about twice those obtained by Tyson and Davies (1965) for a single fibre, which supports this hypothesis.

The area in which the stress field is disturbed by more than 10% from its nominal value by the presence of a void end gap increases with the size of end gap from a radius of about 10 fibre widths for a small end gap to about 20 fibre widths for a large end gap. When the gap is filled with matrix material this range of affected radius varies from about 2 to 10 fibre widths for small and large gaps respectively.

The variation in maximum interfacial shear stress with fibre/matrix modulus ratio is shown in figure 3.13. The relationship is nearly linear, the non linearity at high modulus ratios being due partly to poor convergence of the finite element solutions.

Implications for further work

The occurrence of high stress concentrations around the ends of discontinuous fibres has been known for some time but this study indicates that the stress concentrations in the matrix are very much greater in the region of a fibre break (figure 3.12) particularly when the end gap is small. MacLaughlin (1966) did not show this because his fibre end gaps were large.

These high stress concentrations are a source of yielding or failure depending upon the nature of the matrix and the fibre/matrix

interface. If the matrix is ductile then yielding will occur with the result that the stress concentration is reduced and a stable condition perhaps attained. If the matrix is brittle then a crack will be initiated which will propagate either along the fibre/matrix interface if it is weak or into the body of the matrix.

The results from the study of a single broken fibre in an elastic matrix though useful, are limited in scope. They highlight the importance of a fibre break and the severe stress concentration resulting from this condition. In addition the comparative effects of variations in end gap size are probably similar in much more complex models and in actual composites.

To gain more insight into the micromechanical behaviour of fibre reinforced composites the effects of adjacent fibres and matrix yielding and failure must be taken into account.

The next chapter presents an elastic and elastic/plastic analysis of a plane model which represents an idealised multi-fibre composite.

4. MULTI-FIBRE COMPOSITE NON-INTERACTING DISCONTINUITIES

4.1 INTRODUCTION

An idealised plane composite representing a regular array of uniaxial discontinuous fibres in an elastic or elastic/plastic matrix is shown in figure 4.1. The cross-hatched fundamental region in this figure, a repeated element of the composite, was used for the computer analysis.

The boundaries of this repeated element deform as straight lines due to symmetry requirements and the computer program was modified to impose these boundary conditions. The numerical model presented in this chapter is therefore more representative of a real composite than the common experimental model in which a discontinuous fibre is bounded by continuous fibres on either side.

This study extends that of the previous chapter by introducing the effects of neighbouring fibres on the stresses around a fibre discontinuity. A systematic study is presented of the effects of fibre spacing and the size and nature of the discontinuity. Variations in elastic modulus and Poisson's ratio of both fibre and matrix are also considered.

In addition to these elastic analyses elastic/plastic behaviour of the matrix was studied. Variations are made in the work hardening characteristics of the matrix and in the spacing of the fibres.

A photoelastic model was used as an experimental verification of the elastic computed results. The verification of the elastic/plastic analyses for a similar model is described in chapter 5.

4.2 COMPUTER ANALYSIS

A typical element of the uniaxial discontinuous composite is shown in figure 4.2a. The fundamental region of the composite is a triangle (figure 4.2b) but this shape was found to be too difficult to analyse because of the unknown deformation pattern of boundary BD. The probable shape of this boundary when deformed is shown as a dotted line in figure 4.2b but the loading and boundary conditions for this deformation are difficult to apply. The boundaries of the rectangular element remain straight when uniform tensile loads are applied, in addition symmetry requires the shape to remain rectangular. The method of imposing these boundary conditions is described on page 25. It was found that for high fibre aspect ratios the line B'C' also remained straight and parallel to AD. For this reason the model shown in figure 4.2c was used for many of the computer analyses.

Three basic meshes were constructed for distances between the fibres of 0.5, 1.0 and 2.33 fibre widths. These represent fibre volume fractions 0.67, 0.5 and 0.3 respectively. Each of these meshes was varied for end gaps 0.1, 0.5 and 1.0 fibre widths and for the gaps both void and filled with matrix material. A typical mesh containing 346 elements and 190 nodal points is shown in figure 4.3.

A set of eighteen elastic stress analyses was made varying the fibre spacing and the size and nature of the discontinuity as described above. The modulus of elasticity of the fibre was taken as 50×10^6 p.s.i., and that of the matrix as 10×10^6 p.s.i. The Poisson's ratios were taken as 0.2 and 0.3 respectively. These properties are representative of a typical reinforced metal composite. Using one particular mesh, 0.5 V_f and 0.5 fibre width matrix filled end gap (hence

referred to as the typical composite model), the effects of varying the fibre/matrix elastic modulus ratio from 2 to 100 were investigated. Analyses were also performed with the Poisson's ratio of both fibre and matrix being varied from 0.2 to 0.4. In this and succeeding chapters the stresses are extrapolated to give nodal point values (see Appendix 3, page 184).

To simulate the experimental model described in the next section the elastic properties of the fibres and matrix were made similar to those of aluminium and Araldite epoxy resin. For this analysis the side boundaries of the computed model were not constrained.

Inelastic behaviour of the matrix was considered in two ways. Firstly the growth of plastic enclaves and the resulting stress changes were studied for the three fibre spacings using a 0.5 fibre width matrix filled end gap model and an elastic/perfectly plastic matrix. Secondly, changes in the work hardening characteristics of the matrix, both linear and non-linear, were studied with the 0.5 fibre volume fraction model.

4.3 EXPERIMENTAL ANALYSIS

The model used for the photoelastic experiment is shown in figure 4.1. This model had a 0.3 fibre volume fraction and a 0.5 fibre width end gap. The 'fibres' were made of aluminium alloy and the matrix was made of an epoxy resin (Araldite CT200/HT901). These materials were the same as those used for the single broken fibre model described on page 34. The assembly of the two models was similar except that in the case of the multi-fibre composite the construction was in several stages. The two side sections - outer fibre bonded to matrix - were made first and then these were joined with the broken fibre between them. Araldite AY103/HY951 adhesive was used. The mild steel end grips were also bonded to the model. The model was loaded in the same test

rig as the single fibre composite (figure 3.5). A typical isochromatic fringe pattern is shown in figure 4.5.

A comparison was made with the computed results for a model with similar geometry and material constants. Scaling was necessary to take account of the differences in loading and dimensions. Figure 4.6 shows the variation in maximum shear stress along the fibre/matrix interface. Agreement between the experimental and the numerical results was as good as that obtained previously for the single fibre composite (see page35). This is an additional verification of the applicability of the finite element method to the study of composite materials.

4.4 ELASTIC RESULTS

Stress distribution in fibres

The growth of axial stress in the fibre containing the discontinuity is similar in form to that for a single isolated fibre. The variations in stress across the width of the fibre in the region of the discontinuity are also similar in the two cases (see page 38 and figure 3.9).

The rate of increase of axial stress becomes very small as the applied fibre stress, $\bar{\sigma}_f$, is nearly reached. For this reason the length of fibre in which 99 per cent of the applied axial stress is attained is taken as the half critical length. The variation of critical fibre length with fibre volume fraction and end gap size is plotted in figure 4.7. The critical length increases with increase in the distance between the fibres. This is due to a lessening interaction between the fibres and hence an increasing perturbation of the matrix around the discontinuity (see page 48 and figure 4.14). Thus the critical length

of an isolated fibre is considerably greater than that of a fibre which is surrounded by others. This is confirmed by reference to the results for the single fibre composite which show critical lengths about ten times greater than those for the multi-fibre composite. As the fibre/matrix elastic modulus increases so does the critical fibre length (figure 4.8) though at a gradually decreasing rate.

The axial stress in anadjacent fibre is raised above its applied value in the section opposite to the discontinuity. This perturbation extends up to about 10 fibre widths either side of the centre of the fibre. The relationship between the axial stress concentration and both fibre spacing and end gap size is shown in figure 4.9. As the distance between the fibres increases (i.e. the fibre volume fraction becomes less) the influence of the discontinuity reduces. The axial stress concentration therefore decreases, eventually becoming zero when the fibre spacing is infinite. A larger end gap causes an increase in the axial stress concentration which is most severe when the discontinuity is void. There is also an increase as the ratio between the elastic modulus of fibre and matrix increases. The stress concentration reaches 1.25 at a modulus ratio of 20 and 1.5 at a modulus ratio of 100. There is negligible variation in the continuous fibre axial stress with changes in the Poisson's ratio of either fibre or matrix.

Stress distribution in matrix

The maximum interfacial shear stress was found to be virtually independent of the distance between adjacent fibres for the same applied fibre stress (figure 4.10). However the fibres carry a greater proportion of the total load on the composite when the distance between

the fibres is small and so the ratio of maximum interfacial shear stress to average composite stress increases with decreasing fibre volume fraction. This is shown in figure 4.11. The tensile and shear stress distributions in the immediate vicinity of a 0.5 fibre width void discontinuity ($V_f = 0.67$) are shown in figure 4.12. This shows clearly the severe stress concentration at the fibre tip. The shape of stress distributions are similar in the case of a matrix filled end gap but the stresses at the fibre tip are smaller in magnitude (see figure 4.10).

The variation of interfacial shear stress with size of end gap and nature of discontinuity (i.e. void or filled with matrix material) is similar to that for the single fibre composite (see page 39). The stress concentration increases with increasing end gap for an end gap filled with matrix material but decreases with increasing end gap when it is void. When the fibre ends are closer together the interaction between them increases for a void end gap but decreases in the non-void case because the matrix filled end gap behaves more and more like fibrous material. Thus in the latter case the interfacial shear stress decreases with decreasing end gap size and the load transfer takes place largely across the fibre ends, the direct stress increasing as the ends become closer together (figure 4.10).

The maximum interfacial shear is approximately linearly proportional to fibre/matrix elastic modulus ratio (figure 4.8). It is virtually independent of Poisson's ratio of the fibre but decreases with increasing matrix Poisson's ratio (figure 4.13). As the matrix Poisson's ratio increases from 0.2 to 0.4 the value of the maximum interfacial shear stress falls by about 25 per cent.

The direct stress (σ_y) in the matrix normal to the interface of a fibre adjacent and opposite to a discontinuity varies with both end gap and fibre volume fraction. Figure 4.14 shows this variation, when the discontinuity is filled with matrix, for two points in the matrix; one at the interface midway between the fibre ends (A), the other directly in line with a fibre end (B). The presence of the discontinuity creates a pull on the adjacent fibre which increases the closer the fibres are together. When the gap is very small the material between the fibre ends transmits most of the load and the small stress concentrations at the fibre corners are closely coupled and do not diffuse far into the matrix towards the adjacent fibre. As the gap is increased up to about 0.5 fibre widths more and more of the matrix in the region of the discontinuity is affected and the normal interfacial stress on the parallel fibre grows. Beyond this size of end gap only the nearest discontinuity corner influences the stress at point B and it remains essentially constant. The lateral stress at point A increases at a steadly decreasing rate.

When the end gap is void the lateral stress is about twice that when the gap is filled with matrix material. This is because the lack of matrix material between the fibre ends leaves the load to be transmitted in the main body of the matrix which results in a greater stress perturbation.

The lateral interfacial direct stress shows a slight increase with a rise in the matrix Poisson's ratio due to the increasing lateral pull of the matrix. The effect of changes in the Poisson's ratio of the fibre is negligible (figure 4.13).

Figure 4.11 shows, for a void end gap, the distance within which

The matrix stress is perturbed more than 10% from its constant value $\bar{\sigma}_m$. Both fibre volume fraction and end gap size affect the extent of matrix which is perturbed by the discontinuity.

4.5 ELASTIC/PLASTIC RESULTS

Stress distribution in fibres

With the reduction in stress concentration when the matrix yields the load transfer between matrix and fibre takes place over a longer length of fibre than when the matrix is elastic. Figure 4.16 shows the axial stress distribution near the ends of a fibre with a 0.5 fibre width matrix filled end gap. The matrix has an elastic/perfectly plastic stress-strain relation. The load transfer across the fibre ends remains nearly constant as the imposed load increases because the matrix has yielded in this region (see figure 4.20). The stress grows at a slower rate as more of the matrix yields. The dotted line in figure 4.16 shows the growth in axial stress for a 0.5 fibre width void end gap. The load transfer in this case is similar to that when some local matrix yielding has occurred except for the lack of stress between the fibre ends. The shear transfer along the edges of the discontinuous fibre results in a variation in axial stress across the fibre in the end region similar to that described on page 38 for the single fibre composite (see figure 3.9). It is for this reason that the build-up of axial stress along the centre line of the fibre in the region where the matrix has yielded is not linear as predicted by Kelly and Tyson (1965b).

The critical fibre length, L_c, in which the axial stress is less than 99% of the applied fibre stress increases as more of the matrix

yields. Figure 4.17 shows this increase and also the variation with fibre spacing. The critical length also increases with increase in end gap size because of the smaller load transfer between the fibre ends, but this effect diminishes as the yielded area of matrix grows. When the matrix work hardens the critical length decreases because of the greater load carrying capacity of the matrix. The variation is similar to that for the continuous fibre axial stresses shown in figure 4.19.

The elevation of axial stress in the middle of the fibre which is opposite to the discontinuity has been described on page 46 and is shown in figure 4.9. When the matrix yields this fibre must carry an increasing proportion of the total load applied to the composite. With the particular geometry of the model used for these analyses, half of the fibres in the plane of the discontinuities are broken. Therefore, when the composite is loaded well above the yield point of the matrix the fibres carry nearly all the load and an axial stress concentration, $\sigma_f^*/\bar{\sigma}_f$, equal to 2 results at the middle of each fibre. Figure 4.18 shows the relationship between the axial stress concentration, $\sigma_f^*/\bar{\sigma}_f$, and fibre volume fraction as the load is increased beyond that necessary to cause the initial matrix yielding. For only localised yielding the increase in stress concentration becomes more rapid when the adjacent fibres are close together but when the matrix has fully yielded and the loads are carried predominantly by the fibres the stress concentration approaches 2 even at large fibre spacings. This is shown by the dotted line in figure 4.18. The effect of the matrix work hardening coefficients on the stress concentration is shown in figure 4.19. The greater the work hardening slope then the greater the proportion of composite load that can be carried by the matrix and hence the axial

stress concentration becomes less.

Figures 4.16 and 4.18 show that as the matrix deforms plastically the extra load is carried mainly in the fibres adjacent to the one containing the discontinuity. Analyses with models containing an isolated fibre do not take account of this and may therefore give misleading results.

The lateral direct stress, σ_{fy}, in the adjacent 'continuous' fibre at a point opposite to the centre of the discontinuity varies with fibre volume fraction, end gap size and matrix work hardening coefficients in a manner similar to the axial stress, σ_f^*. The lateral stress concentration factor, $\sigma_{fy}/\bar{\sigma}_f$, increases by a factor of nine as the composite load is increased from that necessary to cause initial matrix yielding by a factor of three for the typical composite model with an elastic/perfectly plastic matrix. When all the matrix between adjacent fibres in the region of the discontinuity has yielded (see figure 4.20) the distance between fibres has only a small effect on the lateral stress concentration.

Stress distribution in matrix

The matrix first yields at the extreme outside tip of the fibre where the high interfacial shear stresses combine with high tensile stresses to produce a severe stress concentration. When the end gap is filled with matrix material this area is the next to yield followed by a general growth of the enclave area away from the discontinuity. Figure 4.20 shows the growth of plastic enclaves for the 0.5 fibre volume fraction model with a matrix filled 0.5 fibre width end gap. The enclave shapes are similar for different end gap sizes. The yielded area grows at a somewhat slower rate for a work hardening matrix because

of its greater load carrying capacity.

The interfacial shear stress reaches a peak soon after the initial yielding and then increases above the elastic loading magnitude along the length of the fibre to accommodate the greater load transfer required. When the matrix is elastic/perfectly plastic the stress cannot rise above the yield value and so a greater length of fibre is required to transfer the load. Figure 4.21 shows the shear stress distribution along the fibre/matrix interface as the load increases, for a matrix which is elastic/perfectly plastic.

The yielding is assumed to follow the von Mises criterion (see page 25) which is represented by the elliptical surface show in figure 4.22. The initial yielding of the matrix region between the fibre ends occurs in nearly uniaxial tension (point A in figure 4.22). As the load on the composite increases the lateral constraint of the fibre ends causes the lateral direct stress in this region of matrix to increase. The state of stress then approaches the point B on the yield surface (figure 4.22). Thus the matrix is able to carry a larger tensile force than it did when it originally yielded.

With the growth of the plastic enclaves, the shear stresses in the matrix necessary to transfer the load between the fibres are perturbed over a wider area. At a cross section of the typical composite model one fibre width from the fibre end matrix yielding causes the shear stress at the continuous fibre interface to increase from a quarter to a half of that at the discontinuous fibre interface.

The lateral matrix direct stress at a point on the continuous fibre interface opposite to the discontinuity varies in a similar way to the lateral direct stress in the fibre near the same point (described on

page 51). Its variation with the work hardening characteristics of the matrix is shown in figure 4.23. The greatest stress concentration occurs with an elastic/perfectly plastic matrix. With only local matrix yielding the relationship between lateral direct stress and interfibre spacing remains similar to that shown in figure 4.14 for the elastic case but when the matrix has yielded more fully the smaller variation in matrix stresses around the region of the discontinuity makes the change of lateral stress with fibre volume fraction less. At twice the load necessary for initial yielding (see figure 4.19) the difference between the lateral stress concentration for a void or matrix filled discontinuity is negligible.

5. MULTI-FIBRE COMPOSITE WITH INTERACTING DISCONTINUITIES

5.1. INTRODUCTION

Chapter 4 describes the analysis of an idealised multi-fibre composite in which the discontinuities are non-interacting i.e. the stress field in the neighbourhood of one fibre discontinuity is not influenced by the presence of any other fibre discontinuity. In a real composite material containing fibres which are not so regularly arranged the situation when fibre ends are close to one another must often occur. When this happens the stress field around each discontinuity may be altered significantly from that for a single discontinuity. As each discontinuity is a potential source of failure a knowledge of the stress field is important in deciding how the failure initiates and then propagates through the composite.

The section model used for this analysis is shown in figure 5.1. Only one fibre spacing (0.67 fibre volume fraction) and end gap size (0.5 fibre widths) are considered, the variation in stress field with these two parameters being very similar to that for the non-interacting discontinuity model. Most analyses were performed with a distance between discontinuities of 2 fibre widths though the effect of varying this distance was investigated. Both elastic and elastic/plastic behaviour of the matrix were considered.

The elastic/plastic results are verified with an experimental model containing steel 'fibres' in a lead alloy matrix. The photo-elastic coating method was used to determine the extent of the plastic enclaves and the moiré method was used to determine the plastic strains.

5.2 COMPUTER ANALYSIS

The types of analysis performed are similar to those described in the two previous chapters except that for the study of interacting discontinuities a greater emphasis is placed on elastic/plastic matrix behaviour.

Two basic meshes were constructed both representing a composite with a 0.67 fibre volume fraction. One was a coarse mesh of 170 elements and 107 nodal points and the other was a much finer mesh of 598 elements and 345 nodal points. The middle region of this finer mesh is shown in figure 5.1. The section shown in this figure shows a length of approximately 100 units compared with a total model length of 700 units. Both meshes were generated by hand because of the irregular distribution of elements required. Small changes were made in the coarse mesh to vary the distance between the discontinuities from 3/2 to 3 fibre widths. The mesh was also modified to include thin interfacial elements for the study of composites with a weak fibre/matrix interface. The finer mesh which had a discontinuity serparation of 2 fibre widths was modified to incorporate the broken fibre end bond which occurred in the experimental model.

For most analyses the 'equal displacement' boundary condition described on page 25 was used. For the experimental comparison however, the boundaries of the computed model were allowed to deform freely. The uniaxial tensile loading was imposed by nodal point loads or fixed displacements of the points along the end boundary.

Three types of composite were studied.

(a) The lead alloy/steel experimental model. Material properies: E_f = 30×10^6 p.s.i., $\nu_f = 0.29$; $E_m = 2.0 \times 10^6$ p.s.i., $\nu_m = 0.4$. Using the matrix stress-strain relation shown in figure 5.4 and the fine mesh with

the broken fibre/matrix end bond, the growth of plastic enclaves was obtained for comparison with the photoelastic results. In addition an output of nodal point displacements was obtained to collate with the moiré results.

(b) A typical reinforced metal composite. Material properties: E_f = 50 x 10^6 p.s.i., ν_f = 0.2; E_m = 10 x 10^6 p.s.i., ν_m = 0.3 (same as for the non-interacting multi-fibre composite). Using the fine mesh, elastic solutions were obtained for both matrix filled and void end gaps. Elastic/plastic analyses were performed for this discontinuity separation (2 fibre widths). The coarse mesh was used to study the effects of changing the distance between discontinuities from 3/2 to 3 fibre widths (in increments of half a fibre width). Changes in the fibre/matrix elastic modulus ratio (E_f/E_m equal to 5, 10 and 20) and the matrix work-hardening characteristics were also studied. Ductile matrix fracture was simulated by allowing the matrix elastic modulus to tend to zero when a given plastic strain is exceeded.

(c) A glass resin composite. Material properties: E_f = 10 x 10^6 p.s.i., ν_f = 0.2; E_m = 0.5 x 10^6 p.s.i., ν_m = 0.3. This system was used to investigate the effect of a weak fibre/matrix interface. One and two discontinuity models were considered with an interface having elastic/perfectly plastic and elastic/brittle characteristics.

5.3 EXPERIMENTAL RESULTS

The Model

The experimental model designed to check the numerical results for the elastic-plastic behaviour of a multi-fibre composite with interacting discontinuities is shown in figure 5.2. The 'fibres' were of mild steel (E = 30 x 10^6 p.s.i., ν = 0.29) and the matrix was a specially made

solder with the composition 85% lead, 5% tin and 10% antimony. This had an approximately elastic/perfectly plastic stress-strain relationship (figure 5.4). This curve was obtained from a tensile test on an Instron testing machine at 0.002 in/min crosshead movement. The elastic constants of this material are E = 2.0×10^6 p.s.i., and $\nu = 0.4$.

The model was cast in a steel mould comprising a machined steel plate with side and end pieces to prevent leakage of solder. The machined steel strips, which had previously been carefully tinned with the solder were clamped rigidly to the mould molten solder poured around them. Both the solder and the mould were preheated to 320°C but immediately the pouring had been completed the mould was placed on a cold steel block and a cold steel plate put on top. This produced a rapid dissipation of heat which was necessary to prevent oxidation of the solder. The excess solder on the top surface was machined with a fly cutter to within about .001 in. of the fibre surface and finally both surfaces were ground with fine emery and buffed to give highly reflective polished faces.

Photoelastic coating method

The photoelastic coating method was used to determine the shape of the elastic/plastic boundary. This was then compared with that predicted by the finite element analysis.

This method differs from photoelasticity in that no model of the structure under test is made of plastic. Instead, a thin coating of birefringent plastic is bonded to the structure which, when it is deformed transmits its surface strains to the coating. Polarised light is passed through the coating twice, being reflected at the surface of the structure, and viewed through another polariser as in conventional photoelasticity. Isochromatic fringe patterns (lines of constant principal strain difference) are produced which give the magnitude of

the maximum shear stress for an elastic structure.

The principal strain difference, $e_1 - e_2$, is related directly to the fringe order,

$$e_1 - e_2 = \frac{NR}{2tk} \qquad (5.1)$$

where N is the fring order.

R is the optical retardation corresponding to one fringe.

t is the thickness of the coating.

k is a dimensionless constant representing the optical strain sensitivity of the plastic.

The relation between stress and strain for a biaxial stress system is written,

$$\sigma_1 - \sigma_2 = \frac{E}{(1+\nu)} \quad (e_1 - e_2) \qquad (5.2)$$

If the structure is assumed to yield according to the Tresca criterion the principal stress difference, $(\sigma_1 - \sigma_2)$ yield, to cause first yield can be written

$$\frac{(\sigma_1 - \sigma_2)_{yield}}{2} = \frac{Y}{2} \qquad (5.3)$$

where Y is the yield stress in uniaxial tension of the material of the structure.

The fringe order, N_{yield}, corresponding to the elastic/plastic interface is obtained by combining equations (5.1), (5.2) and (5.3).

$$N_{yield} = \frac{2tkY(1+\nu)}{ER} \qquad (5.4)$$

This method for determining the elastic/plastic interface has been used by Dixon and Visser (1963) and Calcote and Bowman (1965). They obtained reasonable agreement with other solutions.

Araldite CT200/HT901 was used as the coating material. It has a high strain sensitivity and remains elastic up to about 30 times the yield strain of the solder. A thin sheet, 0.040 in. thick, was cast and cut to the correct size. The coating was then bonded to the model with Eastman 910 adhesive. This is a quick setting contact adhesive which gives a strong bond up to the maximum strain of the Araldite.

The steel/solder model was loaded in a 440 lb.capacity Zwick tensile testing machine and the coating was viewed with a portable reflection polariscope (Budd large field polariscope). This set up is shown in figure 5.4. Photographs of the isochromatic fringe patterns produced by a circular polariscope arrangement were taken at various intervals of loading up to a maximum load of 400 lb. (figure 5.5).

Substitution into equation (5.4) of the following values,

$t = 0.040$ in.

$k = .13$ (Constant for Araldite obtained by calibration using known stress field)

$Y = 3000$ p.s.i. (from figure 5.4)

$R = 2.27 \times 10^{-5}$ in.

$E = 20 \times 10^{6}$

$\nu = 0.4$

gives

$$N_{yield} \approx 1$$

Thus the elastic/plastic interface is given by the first order fringe. The reinforcing effect of the coating is very small because of the thinness of the coating.

Moiré Method

The moiré method was used to determine the elastic/plastic displacements in the steel/solder model. These are then compared with the

finite element results.

The moiré method is a fairly recent development in the field of experimental stress analysis in which displacement patterns are produced by the mechanical interference of coarse diffraction gratings. The gratings have usually between 300 and 2000 parallel lines per inch and are sometimes produced as orthogonal grids with two sets of parallel lines at right angles to each other. One grid (the model grid) is bonded to the surface of the structure under test while the other (the reference grid) is placed adjacent to the model grid and separated from it by an oil film. When the structure is loaded the model grid deforms with the surface of the structure and the interference pattern is produced. Sometimes the reference grid is kept remote from the structure in which case the interference is produced by the reference grid and an image (either projected or photographed) of the model grid. Fidler and Nurse (1966) and Riley (1967) give good introductory descriptions of the technique.

For the purposes of checking the computed results the displacements alone were required. The displacement surfaces must be differentiated to give the strains.

The displacement at a point in a moiré fringe pattern is given by n/p where n is the order of the moiré fringe and p is the pitch of the array.

The sensitivity of the method can be increased by using a mismatch reference grid. Consider the example of a structure in tension with an average strain of 0.001 in/in. A model grid of 500 lines/in is bonded to the structure. Superimposing a 500 line/in refernce grid will result in a distance between fringes of 2.0 in. If however a mismatch

reference grid of 505 lines/in is used to form the moiré pattern eleven fringes will occur within the two inch gauge length. Any variations within this distance will be given only by using the mismatch reference grid. Figure 5.6 illustrates this point. The actual displacement distribution using the mismatch procedure is obtained by subtracting the initial mismatch from the observed displacement distributions. A positive mismatch is used where tensile strains are predominant and a negative mismatch is used for compressive strains.

Two types of model grid were considered for use on the steel/solder test piece,

(a) A Kodak Thin Film Resist grid exposed and printed directly onto the test piece.

(b) A stripping film grid.

KTFR is a photosensitive resinous material which is sensitive to ultra-violet radiation. The resist is dip coated or sprayed onto the structure, allowed to dry and then exposed through a glass master grid to ultra-violet radiation for about 30 minutes. The model is then placed in a developer which dissolves the unexposed part of the coating and finally is dipped into a dye to give a clearer grid. Though a great amount of effort was put into developing a satisfactory method for this process, consistently good results were not achieved. The main difficulty was in obtaining enough contrast between the lines and gaps from the points of view of both colour difference and line definition.

The production of stripping film grids was quite simple. A contact exposure was made through a glass master grid (obtained from the Central Electricity Research Laboratories, Leatherhead). The film was then bonded to the steel/solder model with Eastman 910 adhesive and finally the backing was peeled off.

The reference grids were made on Ortho Type 3 film in a manner similar to the stripping film grids. Mismatch grids of 507.87 and 492.29 lines/in were made by this process in addition to 500 lines/in grids.

The fringe patterns were observed and recorded photographically by direct superimposition of the reference grid on the model. This is not quite as accurate as the 'remote' method but the latter requires very high quality optical equipment which was not available.

The grids were separated by a thin film of glycerin. This kept them in close contact but allowed sliding in the plane of the grids. A 507.87 lines/in mismatch grid was used to measure displacements in the longitudinal directions where the strains were predominantly tensile and a 492.29 lines/in grid was used in the transverse direction where the strains were mainly compressive (due to the Poisson's ratio effect).

The model was loaded in a Zwick tensile testing machine (capacity 440 lb.). Photographs were taken of the moiré fringe patterns both at zero load and at 400lb. A typical fringe pattern is shown in figure 5.7. The comparative insensitivity of the method is apparent from this figure; the gradual slopes of the fringes (which were initially straight and parallel) do not show the high strain gradients which can be seen in figure 5.5 for the same model at the same load.

X-displacements along the fibre/matrix interfaces calculated from the fring patterns are compared with computed results in figure 5.8. The computed model had similar elastic constants and numerically fitted matrix stress-strain curve as the experimental model. Scaling was necessary to take account of the loading and dimensional differences between the two models.

Comparison between computed and experimental results

(a) Photoelastic Coating Method

The photoelastic fringe pattern (figure 5.5) is compared in figure 5.9 with the computed results for a matrix with a similar stress-strain curve. The importance of choosing the correct work hardening characteristics can be seen from figure 5.17. As it was impossible to know when the yielding at the fibre tip in the experimental model first starts, the datum for comparison is taken as that load necessary to cause a large area of yielding in the steel/lead alloy composite (nine times the load necessary to cause first yielding in the computed model). The two sets of plastic enclaves agree well both in shape and in position. Any differences can be attributed to the inherent limitations of the two methods, imperfect bonding between the fibres and the matrix and in particular slight differences between the stress-strain characteristics of the steel/lead alloy model and the computed simulation.

(b) Moiré Method

The moiré and the computed results are in only fair agreement along the fibre/matrix interfaces in the region between the two discontinuities. Outside this region however, the two sets of results compare well (figure 5.8). A similar measure of agreement is obtained at other points.

There are several possible sources of error in the moiré results:

(a) Displacements of the test piece normal to the plane of the grids which produce a gap between them and result therefore in a distorted moiré fringe pattern.

(b) Some delamination along the fibre/matrix interfaces.

(c) The coarseness of the grids.

It was also difficult to ensure that the two sets of results were exactly comparable due to possible differences in the values taken for

stress/strain characteristics of the matrix and the area of matrix yielding.

In view of the fact that Marcal and King (1967) using a similar elastic/plastic computer program obtained good agreement with both experimental and theoretical results of other workers in addition to the present comparison, it is considered that the elastic/plastic method of analysis has been shown to be valid.

5.4 DISCUSSION OF RESULTS

(a) Elastic

Figure 5.10 shows the axial stress distributions in the fibres both for a single fibre break and for two breaks, in adjacent fibres, separated by a distance of two fibre widths. The presence of the second discontinuity causes a much more rapid rise in axial stress such that it exceeds the fully developed value, $\bar{\sigma}_f$, within less than one fibre width distance from the fibre end. It then rises even further before finally reducing to $\bar{\sigma}_f$. The length of fibre in which the fully developed stress is finally attained is the sum of the critical length of a broken fibre when no nearby discontinuity in an adjacent fibre is present and the distance between the discontinuities (measured in the direction of the fibre axes). This stress distribution is the result of a superposition of the stresses due to the presence of the discontinuity in the adjacent fibre onto the transient stress distribution resulting from the void end gap in the fibre. Analyses of models with different discontinuity spacings show that the axial stress does not rise to the value attained in a continuous fibre opposite a fibre break (single discontinuity case) until the discontinuities are about 8 fibre widths apart.

The interfacial shear stress reverses its sign (figure 5.11) because of the rapid growth of fibre stress beyond its fully developed value. Thus when the gradient of the fibre stress against position along the fibre curve (figure 5.10) becomes negative the interfacial shear stress changes sign. The maximum shear stress is a little higher at the fibre end nearest to the other discontinuity (figure 5.11) because the stress in the adjacent fibre is not fully developed and the matrix carries more of the load.

When the discontinuities are more than about 8 fibre widths apart the interaction between them is negligible and each behaves as a single discontinuity. The stress distributions around each discontinuity are then similar to those analysed in chapter 4. This particular value (8 fibre widths) is only true for a 0.67 fibre volume fraction and E_f/E_m ratio equal to 5. However a more general statement can be made. The stresses in both fibre and matrix are perturbed from the fully developed values ($\bar{\sigma}_f$ and $\bar{\sigma}_m$) only within a half critical length of the fibre ends ($\frac{Lc}{2}$). Thus nearby discontinuities in adjacent fibres only interact when within one critical length of one another. Schuster and Scala (1968) obtained similar values for boron/epoxy resin composites.

The shapes of the fibre axial stress and matrix interfacial shear stress curves when the discontinuities are matrix filled are similar to those shown in figures 5.10 and 5.11 and described above. The differences are that the magnitudes of the matrix shear stress are much lower in the latter case and also that the fibre has a value of axial stress at its end equal to about $0.8\,\bar{\sigma}_f$. Figure 5.12 shows the distribution of both tensile and shear matrix stress in the region between two matrix filled discontinuities.

(b) Elastic/Plastic

Stress distribution in fibres

Figure 5.13 shows the effect that a nearby fibre discontinuity has on the build-up of axial stress in a fibre as the composite load is increased beyond that necessary to cause initial matrix yielding. The results shown in figure 5.13 are for a model with the fibres separated laterally by half the width of a fibre (0.67 fibre volume fraction) and the discontinuities, each with a 0.5 fibre width matrix filled end gap, separated longitudinally by 2 fibre widths. The matrix is elastic/perfectly plastic. This can be compared qualitatively with figure 4.16 which shows the build-up in stress for an isolated fibre discontinuity (0.5 fibre volume fraction). When the matrix starts to yield locally around each discontinuity the fibres have to carry a relatively greater proportion of the composite load. Increased shear stresses in the matrix transfer this load between the fibres. The axial stress in the fibre therefore grows very rapidly above the fully developed value, $\bar{\sigma}_f$. When the matrix yielding becomes more widespread the axial stress concentration, $\sigma_f^*/\bar{\sigma}_f$, stops increasing and even decreases for a matrix which only work hardens a little (see dotted line in figure 5.13).

The effect of the matrix work hardening characteristics on this axial stress concentration is shown in figure 5.14 $\sigma_f^*/\bar{\sigma}_f$ is maximum when the matrix has fully yielded in the cross-section through the discontinuity centre and normal to the axes of the fibres. The maximum value of $\sigma_f^*/\bar{\sigma}_f$ is smaller and occurs at a higher load than for a matrix that work hardens only slightly. This is because a matrix that work hardens considerably can carry higher stresses and the growth of yielding is slower. Analyses using different fibre/matrix elastic

modulus ratios show that this parameter has little effect on $\sigma_f^*/\bar{\sigma}_f$ once the matrix has fully yielded because the fibres carry a large proportion of the total composite load.

The fully developed fibre stress is attained at about the same distance from the discontinuities in both fibres. The length of fibre in which the fully developed fibre stress is finally attained is thus the sum of that obtained for the non-interacting discontinuity model (see page 45 and figure 4.7) and the distance, in the direction of the fibres, between the discontinuities.

Stress distribution in matrix

In the case of the non-interacting discontinuity model described in chapter 4 the matrix in the region of the fibre discontinuity is in both shear and tension (figure 4.12) with the tensile stresses larger even after substantial yielding. For the model described in this chapter the matrix in the region around each of the discontinuities but in a direction away from the other discontinuity behaves in a similar manner. The matrix between the discontinuities however is under different constraints which induce a predominantly shear state of stress when it yields. The changes in the tensile and shear stress distributions when localised matrix yielding occurs are shown in figure 5.15. As the matrix yields the stress concentration at the fibre ends is relieved and the increased load is carried by the fibres, the matrix shear stresses increasing across the whole cross section of the composite between the discontinuities in order to transfer the load. The tensile stress distribution does not alter very much except for a reduction near the fibre tip. As more yielding occurs the matrix between the discontinuities becomes predominantly in shear. The reason for this is that the elastic recovery forces in the fibres increase relative to the

applied matrix forces after the matrix has yielded thus producing a large shearing couple. If the matrix work hardens this tendency lessens.

Analyses of models with different separation distances between the discontinuities show that the load required to produce a continuous path of matrix yielding across the model is almost directly proportional to the separation distance (figure 5.16). This confirms the experimental observations of Cooper and Kelly (1967b) for a tungsten/copper composite of similar geometry. When the separation becomes about 6 fibre widths their results show composite failure due to fibre fracture instead of pull out. No attempt has been made to simulate this aspect of Cooper and Kelly's experiment with the computed model but it is clear that assuming that the plastic failure stress increases with discontinuity separation beyond the values actually analysed the fibre will reach its fracture stress before the matrix yields completely at some particular value of discontinuity overlap. As the fibre overlap is further increased the composite strength will remain constant provided that the discontinuities do not interact with one another and the matrix does not work harden.

The growth of the yielded region is slower for a matrix that work hardens considerably. Figure 5.17 shows the extent of the plastic enclaves at a given load for matrices with different work-hardening characteristics. The boundary constraints also affect the plastic enclave shape and the load necessary for plastic failure. When the boundaries are not constrained (as in the experimental model) the fibres can bend in towards each discontinuity. This reduces the matrix stresses. In a real composite the constraints on a region similar to the interacting discontinuity model may well be greater than those imposed in the computer analyses because of the existance of many long

or unbroken fibres. Therefore even higher matrix stresses and earlier plastic failure will occur.

The higher elastic stress concentration at the fibre ends that results from an increase in fibre/matrix elastic modulus ratio (see figure 4.8) causes the initial yielding to occur at a lower overall composite load. Analyses show that as E_f/E_m is increased the plastic enclaves grow particularly in the region between the discontinuities. As total matrix failure occurs in this region an increase in E_f/E_m means a decrease in composite strength.

Weak fibre/matrix interface

The influence of a weak fibre/matrix interface was studied only with the coarse mesh model so the results are only qualitatively meaningful. As expected, the delamination starts at the tips of the fibres. The bond at the fibre ends then breaks in tension followed by a gradual extension of the crack along the interface due to high shear and tensile forces (see figure 4.10). When two fibre discontinuities are near to one another the failure proceeds mainly towards the other discontinuity. Early end bond failure has been observed in photo-elastic models by the author and in tungsten/copper composites by Kelly and Tyson (1965b). In the particular model analysed by the author no failure of the interface opposite a discontinuity occurs until delamination extends from the discontinuity in the adjacent fibre. As no attempt was made to introduce frictional load transfer the models are not very representative of a real composite material with a weak interface (see page 75).

Matrix fracture

Matrix fracture has been simulated in the computer model by making the elastic modulus of an element nearly zero when its plastic strain

exceeds a certain value. This very simple approximation gives some idea of the progress of ductile failure. Figure 5.18 shows the growth of the fractured area for the interacting discontinuity model and an elastic/perfectly plastic matrix that fails at about 50 times the yield strain. The shapes of the voids formed during the failure progression are similar to those observed by Hertzberg et al (1965) for a C_uAl_2/Al eutectic composite and Cooper and Kelly (1965a) for a tungsten/copper composite.

The variation in axial stress concentration, $\sigma_f{}^*/\sigma_f$ for a non-linear work hardening matrix is shown in figure 5.19. The fracture strain was chosen such that the first matrix fracture occurs at 7 times the load for initial matrix yielding. This is less than would occur in a real composite but it enabled the solution to be completed with less increments of plastic loading than would otherwise have been required. As the matrix fractures the fibre opposite the discontinuity has to carry much more of the load and the stress rapidly increases. The composite model fails completely when a completely void region is formed across the model, joining the two discontinuities.

6. GENERAL DISCUSSION

6.1 LOAD TRANSFER MECHANISMS

In a composite material the interaction between the two phases - fibres and matrix - produces a complex internal stress distribution. As the fibres are in general much stronger than the matrix, the matrix must be able to transfer load from one fibre to another. When, as in all the models presented in this thesis, a fibre is discontinuous the matrix must provide the means to build up the stress in the fibre.

Two basic types of fibre discontinuity have been analysed:

(a) Matrix filled end gap: This arises when a fibre is broken during fabrication of the composite or when two fibre ends happen to be closely butted together.

(b) Void end gap: This can also be due to a fibre break during fabrication particularly if the composite is extended or rolled to align the fibres. It can also be caused during loading of the composite by surface defects in the fibre or by some other stress concentration such as a crack or void in the matrix.

The matrix transfers the load to the fibre at the fibre/matrix interface so in the case of a void end gap the load is transferred solely along the edges of the fibre by shear forces. When the end gap is filled with matrix material the load can also be transmitted through the fibre ends.

The theories of Cox (1952) and Dow (1963) neglect the stress concentrating effect of the fibre ends and also any tensile load transfer across these ends. In the case of an isolated fibre end the latter assumption may not be important (Tyson and Davies, 1965) but the analysis in chapter 3 shows that when two fibre ends butt together

considerable load transfer can take place within the end gap. The shear lag type of analysis which has been used by several workers (Hedgepeth, 1961 and Rosen, 1964) also neglects this type of load transfer by assuming that the matrix carries only shear stresses. Furthermore the complex triaxial state of stress within the end gap in an actual composite material can have a considerable hydrostatic component which increases the matrix yield strength and provides more effective load transfer between the fibre ends (Piehler, 1965).

The shear transfer along the fibre edges takes place within a very short distance from the fibre end producing widely varying stresses across the width of the fibre (see figure 3.9). The presence of a nearby continuous length of fibre reduces the transfer length. For an elastic matrix the transfer length is usually less than 10 fibre widths and is even less when the lateral fibre spacing is small (figure 4.7). These compare well with experimental values for copper/tungsten composites ($E_f/E_m = 3$) reported by Kelly and Tyson (1965), Weeton and Signorelli (1966) and Cooper and Kelly (1967b). These workers obtained values for $L_c/2d$ ranging from about 3 to 6.

Cooper & Kelly (1967a) derived a solution for the build-up of stress in a broken fibre bounded by an elastic matrix and continuous fibres. Their two-dimensional model is similar to that analysed in chapter 4. A comparison between their solution and the finite element analyses is shown in figure 6.1. The variation with fibre spacing is qualitatively similar for the two theories. The differences shown in figure 6.1 can be explained in terms of the following assumptions made by Cooper and Kelly:

(i) The stress is assumed constant across the width of the broken fibre. Figure 3.9 shows that this is far from true.

(ii) The stress concentrating effect of a fibre end is ignored by assuming that the shear stress is constant in each cross-section of the matrix. This has been shown to be untrue by Tyson and Davies (1965), and Carrara and McGarry (1968) as well as by the present author. The stress near the fibre end should therefore be greater than that predicted by Cooper and Kelly's theory.

(iii) The interaction between the two ends of the broken fibre is ignored. The finite element results show that the smaller the end gap the more rapid is the build-up in fibre axial stress.

Similar assumptions are made in the theories of Cox (1952), Dow (1963) and Rosen (1964).

The reason that the critical fibre lengths are so small for high fibre volume fractions is that the adjacent fibre carries a large part of the extra load caused by the presence of a discontinuity. The closer the fibres are together the larger is the part carried by the adjacent fibres (see figure 4.9). The importance of the axial stress concentration caused by the presence of a nearby discontinuity in another fibre is shown in figure 5.9. The axial stress in the fibre which is itself broken exceeds the fully developed stress, $\bar{\sigma}_f$, within only two fibre widths from the broken end because of the existance of a void in a fibre only 0.5 fibre widths away.

It therefore appears that the efficiency of load transfer between fibres is governed to a large extent by the fibre volume fraction of the composite and that care must be taken when using the results of an analysis for an isolated fibre model because it neglects the effects of interaction between adjacent fibres.

The extremely severe concentration of both direct and shear stresses is shown clearly in figure 4.12. When there is considerable load

transfer between the fibre ends for a matrix filled end gap the interfacial shear stress concentration is decreased (see figure 4.10). As explained on page 39 the load transfer mechanism between the fibre ends is quite different for the two types of discontinuity i.e. matrix filled or void for small end gaps and elastic matrix behaviour. The constraint on the matrix between the fibre ends makes it behave more like the fibre as the end gap decreases therefore increasing the direct stress transfer and decreasing the interfacial shear stress concentration. When the end gap is void the severity of stress concentration increases as the end gap gets smaller. This difference in behaviour is independent of the lateral distance between adjacent fibres.

A void end gap if produced by the fracture of the fibre during loading of the composite is initially a very narrow crack. The discontinuity can therefore be expected to behave in a similar way to a crack in a homogeneous material. Inglis (1913) has shown that the elastic stress concentration, k, due to an elliptical crack is given by,

$$k = \left(1 + \frac{2c}{h} \right) \qquad (6.1)$$

where c is the major axis of the ellipse normal to the load and h is the minor axis.

Figure 6.2 shows the values of the matrix stress concentration due to a break in an isolated fibre plotted on the basis. An empirical factor has been used to make the finite element and Inglis' values of k equal for a 3 fibre width end gap. Bearing in mind that the finite element analysis is less accurate at the smaller end gaps where it is difficult to have a fine enough mesh the two sets of values compare very well. They do show that, at least qualitatively, a fibre fracture is a similar source of stress concentration to a crack in a homogeneous

material.

The stress fields around discontinuities in adjacent fibres interact when the distance between the two sets of fibre ends is small. Schuster and Scala (1968) observed from their experiments that single fibre ends interact only when within about the half critical fibre length of one another. The analyses in chapter 5 confirm that this is also true for fibre discontinuities.

The presence of a fibre discontinuity and the greatly perturbed stress field associated with it causes some failure in the region of the discontinuity at low overall composite loads. This localised failure can be in the form of interfacial delamination, matrix cracking or matrix yielding. More will be said of the consequences of this failure in section 6.2 but even assuming this process is gradual and no extensive composite failure takes place the effect on the stress field in the region of the discontinuity is considerable.

(a) Fibre/matrix interfacial failure

If the fibre/matrix interfaces in the region of the fibre discontinuity are weak the high shear stresses associated with a fibre end can cause delamination along the edges of the fibre. This is particularly true for glass fibre reinforced resins (Outwater, 1956) and for ceramic whisker reinforced metals (Sutton, 1966). If the composite is initially unstressed delamination produces an ineffective length of fibre. In practice the composite fabrication process produces residual stresses due to the different coefficients of thermal expansion of fibre and matrix (Sutton and Chorné, 1965). Schuster and Scala (1968) have reported that smaller stress concentrations around the fibre ends are to be expected as a result of these residual stresses. The nature of the residual stress pattern is such that the matrix exerts compressive

stresses on the fibres and in the event of delamination a certain amount of frictional traction along the interface occurs. When two discontinuities are near to one another (chapter 5) the delamination proceeds more quickly in the region between the discontinuities.

The interfacial bond at the end of a discontinuous fibre is particularly likely to be weak when another fibre end is butted against it because of the difficulty of filling the space between the fibre ends during fabrication. As, in addition, the tensile stresses on this interface are very large (see figure 4.10) early delamination in this region is to be expected. The region then behaves in a similar manner to a void discontinuity and the stresses become considerably higher.

The critical fibre lengths are higher if either the end bond or the interface along the side of the fibres fail. Higher axial stress concentrations occur in the adjacent fibres because of the ineffectiveness of the matrix filled end gap and there is less effective load transfer along the discontinuous fibre. Interfacial failure may also occur along the adjacent continuous sections of fibre because of these increased stresses and the higher lateral direct stresses at the continuous fibre interface (Cook and Gordon, 1964) associated with them (see figure 4.14).

(b) Brittle matrix failure

If the matrix is brittle but the fibre/matrix interfaces are as strong or stronger than the matrix then the stress concentration at the fibre ends can only be relieved, as the overall composite load is increased, by crack extension into the body of the matrix. From the point of view of load transfer mechanisms the nucleation and propagation of a crack will tend to make the portion of the matrix between the fibre ends ineffective thus causing increases in the critical fibre length

and the axial stress concentration in adjacent fibres. Severe stress concentrations also occur at the crack tips thereby introducing a complex state of stress in the matrix.

(c) Ductile matrix failure

If the matrix is ductile the stress concentration at the fibre ends is relieved by matrix yielding. Figure 5.15 shows the reduction in peak stress concentration due to localised matrix yielding around the fibre ends. This smaller concentration of stress has the effect of spreading the load transfer over a wider area of both fibres and matrix. Thus there are increases in critical fibre length (figure 4.17), interfacial matrix shear stresses away from the fibre ends (figure 4.21) and axial stress concentrations in the adjacent fibres (figure 4.18). The state of stress when the matrix has yielded in the gap between the fibre ends in qualitatively similar to the elastic state of stress for a void end gap particularly if the fibres are much stiffer than the matrix (figure 4.16).

The growth of the yielded region is away from the fibre ends primarily at about 45° to the fibre axes. Cooper and Kelly (1967a) observed a similar pattern of matrix yielding in a tungsten reinforced copper composite. When discontinuities in adjacent fibres are close to one another (i.e. less than about 10 fibre widths separation) the yielded regions around each are drawn towards one another and eventually join (figure 5.16). The state of stress between the two discontinuities then becomes predominantly shear as explained on page 67.

When the matrix work hardens, as is usually the case, the state of stress is altered less from the elastic state the greater the work hardening. The effect of the work hardening characteristics on the fibre and matrix stresses is shown in figures 4.19 and 4.23. When the

lateral separation of the fibres is small it is believed that the work hardening characteristics of the matrix may be different from that predicted by tensile tests on the matrix alone (Kelly and Davies, 1965).

Even when the matrix is ductile the stress concentration at the fibre ends will initiate matrix or interface fracture when the strains are large. This has the effect of increasing the loads that are carried by the adjacent fibres.

The internal stress distribution inside a composite material is affected by the elastic properties of the constituents. The interfacial shear stress concentration at the fibre ends is almost linearly proportional to the fibre/matrix elastic modulus ratio for values of E_f/E_m less than about 30 (see figure 4.8). The critical fibre length also increases with an increase in E_f/E_m (figure 4.8). A high matrix stress concentration means that early matrix yielding will occur if it is ductile (if not matrix or interfacial fracture is likely). The elastic properties of the matrix are then less important. The Poisson's ratios of the fibre and matrix are far less important parameters. Indeed the stress distribution in the multi-fibre model with non-interacting discontinuities is almost independent of ν_f and varies only a little with ν_m (figure 4.13).

The dynamic effect of fibre failure has not been taken into account in any of the analyses presented in this thesis. Hedgepeth (1961) predicted that the dynamic response to a fibre fracture increases the stresses in adjacent fibres by up to 30% above the values obtained from a static analysis.

Recent work by Sadowsky et el (1964) states the importance of couple stresses in the stress distribution around very small whiskers.

These effects, which are negligible for fibres with a diameter exceeding 0.001 inches, have been ignored.

The analyses described in chapters 3, 4 and 5 also neglect the effects of three dimensionality and the influence of dislocations and grain boundary movement which may be significant in composites containing whiskers a few microns thick. Two dimensional studies do however have a direct application because one of the most promising methods of manufacturing composite material components is by laminating together two dimensional tapes (Kelly and Tyson, 1965 and Tooling and Production, 1967).

6.2 COMPOSITE FAILURE

In the preceeding chapters stress distribtions are described for situations in which a fibre break has occurred but no further fracture in either the fibres or the matrix is actually taking place (with the exception of the analyses described on pages 69 to 70). The matrix filled end gap composite represents a similar type of situation. The elastic analyses apply when the composite is in a state of static equilibrium.

As explained on page 71 fibre discontinuities can arise during fabrication or prior loading of the composite. The response of the region around the fibre end depends upon the nature of the constituents but in general the high stress concentrations cannot be accommodated by elastic behaviour of the matrix. If the matrix is 'notch' tough or ductile or the fibre/matrix interfaces weak a fibre fracture which starts as a hairline crack can grow to about one fibre width in size without necessarily causing any further fracture of fibre or matrix.

The dynamic effects of a fibre fracture may cause composite failure

over a wider area than predicted by static analyses. Ham and Place (1966) observed double fibre breaks in copper/tungsten composites which they attributed to the formation of a compressive shock wave as the result of the initial break. This is reflected at the end of the fibre as a tensile wave causing a second fracture at that point where the fibre is least restrained. Gatti et al (1967) showed that the dynamic effect of a single fibre break can in some instances be sufficient to cause total composite failure. Composite failure may nucleate from cracks initiated in the matrix of the interface layer instead of the fibres but the bulk of experimental evidence points to the fibres fracturing first (Bouc, 1962 and Rosen, 1964).

The localised failure around the fibre discontinuities depends upon the geometrical conditions in the region, such as fibre spacing and whether or not the end gaps are filled with matrix material. As mentioned before the initial failure that emanates from a fibre discontinuity and the consequent propagation of these effects until there is total composite failure also depends upon whether the fibre/matrix interface in weak or strong and the matrix ductile or brittle. The possible failure modes for these different systems in the light of the stress distributions determined in chapters 3 to 5, experimental evidence by other workers and the various theories of composite failure are discussed after a brief review of the existing composite failure theories. This discussion is limited to the tensile failure of composites containing uniaxially aligned fibres.

Tensile failure theories

The simplest tensile failure theory is that assuming equal strain in both fibre and matrix (Jech et al, 1959). The composite is assumed to fail when the fracture strain of the fibres is reached. The

strength of the composite is then given by equation (1.3). This theory for continuous fibres and the modification by Kelly (1964) for discontinuous fibre systems are true for certain model systems containing thin wire 'fibres' but predict higher strengths than are actually obtained for composites containing fibres and whiskers. This is because these latter materials fail prematurely due to surface flaws and imperfections.

Parrat (1960) introduced statistically distributed fibre flaws and proposed that composite failure occurs when the accumulation of fibre fractures resulting from increased load shortens the fibre lengths to the point when further increases in load cannot be transmitted to the fibres because the maximum shear stress of the matrix is exceeded. Total composite failure follows by shear failure of the matrix.

Rosen (1964) considered that composite failure is caused by an accumulation of individual tensile fibre fractures resulting from a statistical flaw distribution. Around each fibre break there is an ineffective length of fibre which carries only a small load. The composite fails when there are a sufficient number of these ineffective lengths of fibre in one cross-section to provide a weak surface.

By considering the energy released when one fibre breaks Arridge (1964) derived a criterion for composite failure based on a statistical distribution of fibre strengths, the critical fibre length and the geometrical composition of the composite. The theory assumes elastic matrix behaviour.

Plastic matrix behaviour has been considered by Spencer (1965) and Piggott (1966) who derived composite strength values assuming approximate stress distributions and neglecting the stress concentrating effects of fibre ends.

Riley and Reddaway (1968) have predicted composite tensile strengths by combining the theories of Parratt(1960) and Kelly (1964).

Elastic/brittle matrix with strong interfacial bond

Composite systems containing an elastic/brittle matrix and yet a strong bond between the fibres and matrix are unusual. Metal matrices are mostly ductile and polymeric matrices though often having elastic/brittle stress-strain characteristics seldom have good adhesion to fibres, particularly when the composite is being manufactured on a commercial scale. This type of composite only occurs therefore under laboratory conditions where great care can be taken to obtain strong interfacial bonds.

The stress concentration that arises due to a fibre discontinuity can only be relieved by matrix cracking. The nucleation and subsequent propagation of these cracks depend upon the fracture toughness of the matrix. If the matrix cannot absorb sufficient energy the crack grows away from the fibre ends. Mullin et al (1968) observed that in a boron/epoxy resin single fibre composite the crack followed the line of maximum tensile stress, that is initially at 45° to the fibre axis and then veering normal to the axis within a short distance from the fibre end. If the crack propagates across the matrix to an adjacent fibre and if there is a coherent interface in this region the crack is not prevented from fracturing the fibre (Clarke, 1967) and then continuing across the composite. Because of this and as the load must then be carried by a smaller number of fibres catastrophic failure of the composite is inevitable.

The inability of the fibres to deflect cracks at a coherent fibre/matrix interface and the high velocity at which these cracks travel across the matrix (Pugh, 1967) means that each fibre discontinuity

is a potential source of total composite failure. The composite strengths are below those predicted by theories based on the assumption that individual fibre breaks do not by themselves cause total collapse of the whole composite.

Matrix fracture can be initiated between the fibre ends for a matrix filled end gap because of the high tensile stresses in this region (figure 4.10). The stress distribution then becomes similar to that determined for a void end gap. When discontinuities in adjacent fibres are near to one another the region between them provides a ready path for crack propagation.

The higher the fibre/matrix elastic modulus ratio the higher is the elevation of matrix stresses at the fibre tips (figure 4.8) and the sooner the nucleation of a matrix crack. When this crack extends into the body of the matrix it goes into a region where the stresses are comparatively low. The higher the peak stress concentration the lower are the stresses away from the fibre ends at the time of crack initiation. The matrix fracture is therefore more easily arrested because the low stressed region can absorb the elastic energy required for crack extension. It is therefore probable that composites containing fibres and matrix where elastic moduli are very dissimilar are less liable to catastophic failure due to a single fibre discontinuity.

Elastic matrix with weak interfacial bonding

One of the major problem areas in composite technology is that concerned with the interface between fibres and matrix. The absorbtion of water into glass reinforced plastics produces weak interfacial layers (Bott and Barker, 1965). Inadequate fibre/matrix wetting in ceramic reinforced metals (Sutton, 1966) and certain chemical reactions between the constituents (Weeton et al, 1966) also result in weak

fibre/matrix interfaces. Failure in such materials is usually initiated in and propagates through these weak interfaces.

As the composite load is increased the severe stress concentration around a fibre discontinuity causes failure of both the end bond and the interface along the sides of the fibre (see page 75). If the end bond fails first there exists a narrow crack normal to the direction of loading. This can result in a crack extending into the body of the matrix as described in the previous section. When a fibre is broken the elastic recovery forces in the fibre break the interfacial bond (Bonc, 1962 and Mullin et al, 1968). With this delamination, load is transferred across the interface due to frictional effects. When the stress concentration has been relieved and the crack has extended a little way along the interface static equilibrium can again be attained. Failure can therefore be gradual with random fibre breaks occurring without catastrophic composite failure. Thus the failure theories of Rosen (1964) and Riley and Reddaway (1968) are applicable.

The computer analyses show that there are high lateral stresses acting on the interface of a fibre opposite a discontinuity (figure 4.14). These high stresses have been predicted by Cook and Gordon (1964). Delamination can therefore occur along a continuous fibre particularly when the fibre volume fraction is high (Grinius, 1966). The broken bond can act as a means of blunting a crack which is propagating across the matrix. This applies particularly in fatigue when crazing of the matrix takes place (Grinius, 1966). Such localised failure has been observed by Baker and Cratchley (1964), Baker (1966), Ham and Place (1966) and Gates and Wood (1967). Total composite failure follows by a process of delamination and fibre fracture. A crack propagates along an interface until it reaches a

fibre discontinuity which turns the crack at right angles to the fibre axes until it intercepts another fibre causing further delamination. If a crack extending along the interface meets a surface flaw in the fibre this can cause fibre fracture at that point.

When the fibre/matrix elastic modulus ratio is high the delamination occurs at a low composite load (see figure 4.8). The strength of the composite is then less (Grinius, 1966).

The fact that weak interfaces are a ready path for crack propagation can lead to increased rather than reduced composite strengths. As explained in the previous section rapidly moving cracks are not arrested by a coherent interface which results in total failure being initiated from one point in the composite. When the interfaces easily debond the effects of a fibre break can be more easily absorbed (in a similar way to matrix yielding) and cracks in the body of the matrix can be blunted. It is for these reasons that glass reinforced epoxy resins are tough despite both constituents being brittle.

Poor bonding has now been recognised as increasing composite strengths in many cases (Outwater and Carnes, 1967).

Ductile matrix

Composites with the highest potential strengths and retention of strength at elevated temperatures consist of brittle ceramic fibres in a ductile metal matrix. Although much effort has been put into obtaining good interfacial bonds in these composite systems poor adhesion between fibres and matrix is still common (Sutton, 1956). Plastic deformation of the matrix may be influenced by the interface depending upon whether or not it is an effective source for dislocations (Materials Advisory Board, 1965b).

Matrix yielding allows the stress concentration around a fibre

discontinuity to be relieved (figure 5.15) without the formation of a matrix crack (Kershaw and Shepard, 1965). The effects of the discontinuity are then localised. This is the basis on which the tensile failure theories of Rosen (1964) etc. (see page 81) are derived. Random fibre failure in tungsten/copper composites with low fibre volume fractions have been observed by Kelly and Tyson (1965).

The random fibre break mode of composite failure does not always occur particularly at high fibre volume fractions. Parikh (1964) observed that in a composite comprising short aligned steel fibres in a silver matrix the mode of failure was by ductile matrix failure when the fibre content was low and by brittle fibre fracture at high fibre volume fractions. Gatti et al (1967) reported composite failure due to a single fibre break even for a ductile matrix.

As has been shown in the preceeding chapters matrix yielding causes an increase in stress in the fibres adjacent to a fibre break (figure 4.9). These stress concentrations can cause fibre failure without any cracks being formed in the matrix (Cooper and Kelly, 1967a). At high fibre volume fractions the fibre stress concentrations are even greater (figure 4.9). Under these conditions the effect of a fibre discontinuity causes more than just localised yielding of the surrounding matrix and catastrophic composite failure occurs without random individual fibre breaks.

The stress analyses of the interacting discontinuity model show that the region between the discontinuities offers a ready path for both matrix yielding (figure 5.16) and fracture (figure 5.18). Hertzberg et al (1965) observed this type of failure in a $CuAl_2/Al$ eutectic composite. When the fibre overlap is small the fibres pull out of the matrix without reaching their fracture stress (Cooper and Kelly, 1967).

Except when made under carefully controlled laboratory conditions a uniaxial fibre composite contains fibres which are irregularly spaced and have discontinuities and flaws randomly distributed. The mode of failure is then a combination of those described above, namely fibre fracture where fibres are in close contact and matrix failure with fibre pull out when fibre ends are near to one another. Delamination can also occur in a similar way to that described in the previous section. Kelly and Tyson (1965) observed that above 250°C debonding of a fibre end occurred in a composite system (tungsten/copper) which at room temperature has strong interfacial bonds.

Fatigue failure has similar characteristics. Baker and Cratchley (1964) using silica reinforced aluminium observed matrix cracks propagating from a fibre break at 45° to the fibre axis (see page 82). These cracks were deflected by adjacent fibres at some distance from the interface. Baker (1966) testing aluminium reinforced with stainless steel wires observed delamination prior to composite failure where the interfacial bonds were poor. Ham and Place (1966) and Bomford (1967) have also reported fatigue failure accompanied by 45° matrix cracking, delamination and fibre fracture.

6.3 IMPROVEMENTS IN COMPOSITE DESIGN

A knowledge of the internal stress distribution in a composite material is only of value if it leads to a better understanding of the mechanics of fibrous reinforcement and enables more efficient use to be made of the constituents.

The analyses described in earlier chapters have shown that the stress perturbation and concentration around a fibre discontinuity is a very localised effect and interaction between discontinuities in adjacent

fibres occurs only when they are within a few fibre widths distance of one another. It is for this reason that the strengths of discontinuous fibre composites have been found to approach those of continuous fibre composites (McDanels et al, 1963).

The high stress concentration associated with a fibre discontinuity means that some matrix or interfacial failure in such a region is inevitable. In order to restrict this failure to the immediate neighbourhood of the discontinuity and prevent it linking up with other such regions any cracks formed in the matrix or along the interfaces must be arrested. The composite then behaves in a quasi-homogeneous way and the strength criteria based on randomly distributed fibre fractures are valid.

It is therefore important to choose materials for the two phases which allow either matrix yielding or some interfacial delamination. In the latter case it is necessary to have a laterally compressive residual state of stress after fabrication so that load can be transferred from matrix to fibres by frictional forces. By these means the effect of individual fibre discontinuities which occur either during fabrication or loading can be localised and catastrophic failure emanating from only a few points in the composite can be prevented.

It is important to avoid fibre/fibre contact as this also has a stress concentrating effect and is a ready fracture path. The method of composite manufacture in which the fibres are coated with matrix material before being compacted together is ideal in this respect.

6.4 SUGGESTIONS FOR FURTHER WORK

The analyses presented in chapters 3 to 5 are of simple two dimensional models. An extension to three dimensions would be very

valuable. There are in existance computer programs for studying three dimensional problems using the finite element method.

The computer program described in this thesis could easily be adapted for the study of more sophisticated composite models. A completely separate interface layer could be introduced with elastic and inelastic properties different to both fibre and matrix. A more major modification of the program would allow 'frictional' forces to act on the fibre once the interface had failed. Matrix failure could also be studied in a more accurate way than that used in chapter 5. To study the state of stress when some matrix failure has taken place (either yielding or fracture) with the same accuracy as the elastic solution requires a modified size weighting of the elements to take account of the movement of the region of stress concentration. This can only be done by having elements of a similar small regular size over most of the area of the model.

The main difficulties that would be encountered in the study of these more complicated and accurate models are those of computer storage space and job running time. For a typical elastic/plastic analysis of the interacting discontinuity model described in chapter 5 (mesh size about 600 elements) with 10 increments of plastic loading, the job took about 30 minutes to run. The program in its present form allows 750 elements and about 450 nodal points, the number being limited by the computer (University College IBM 360/65). More complex models would require between 1000 and 2000 elements. In addition the job time would be more than one hour. It would therefore be necessary to have access to a computer larger and faster than those available at present.

The job running time for a given accuracy of solution is very

dependent upon the choice of over-relaxation factor used in the iteration of nodal point displacements (see page 30 and figure 2.2). Some means of determining the optimum value of this parameter would be advantageous.

7. CONCLUSIONS

The model analyses described in this thesis show that severe stress concentrations occur around fibre discontinuities in composite materials. These stresses are much higher than those associated with an isolated fibre end particularly when a discontinuity is void.

The load transfer mechanism depends upon whether the gap between the fibre ends is filled with matrix material or void and therefore whether or not the load is transferred between fibre and matrix partly through the fibre ends. The constraint on the matrix between these ends makes it behave like the fibre for a small end gap which causes an increase in the direct stress transfer and a decrease in the interfacial shear stress concentration is more severe and it increases as the end gap becomes smaller.

The area of stress perturbation in which the fibre stress is not fully developed is localised around the fibre ends. The multi-fibre analyses showed that when the lateral spacing between adjacent fibres is small the length of under-stressed fibre seldom extends more than ten fibre widths either side of the discontinuity. The exact value of the critical fibre length depends upon the size of the discontinuity, the inter-fibre spacing and the fibre/matrix elastic modulus ratio (it grows larger as the value of each of these parameters increases).

The axial stress in the adjacent fibres is elevated in the regions opposite to a discontinuity. When discontinuities in adjacent fibres are near to one another this axial stress elevation can cause a more rapid build-up in stress along the fibre thereby reducing the transfer length to only two or three fibre widths. Thus, even in the region of a fibre break the major part of the load is carried by the fibres. The

lateral pull exerted by the discontinuity on adjacent fibres was also found to be considerable.

The stress distribution in the region of a fibre break was found to vary with the ratio of the elastic moduli of fibre and matrix. The matrix stress concentration is approximately linearly proportional to this ratio and as a result the critical fibre length also increases. The Poisson's ratio of the fibre has little effect upon the stress distribution but the matrix stress concentration decreases a little as the matrix Poisson's ratio increases.

The severe stress concentrations described above can only be relieved as the overall composite load is increased by yielding or fracture of the matrix or the fibre/matrix interface.

When the matrix is brittle either the interface delaminates or a crack extends into the body of the matrix. As the latter condition can easily lead to further fibre fracture some interfacial delamination is preferable. Thus, composites such as glass fibre reinforced epoxy resin are tough despite both constituents being brittle. If the matrix is ductile the perturbed region around the discontinuity increases in size as the stress concentration is relieved by plastic flow. The fibres, which under elastic conditions carry the predominant part of the composite load now carry an even greater proportion and the strength of the composite depends upon the strength of the fibres so long as the matrix can transfer load between them. If the matrix work-hardens considerably there is little change from the elastic state of stress.

To prevent early composite failure it is necessary to keep the effects of the fibre discontinuity localised. This can best be done by having a matrix which is either ductile or does not adhere perfectly to the fibres. The composite then behaves in a quasi-homogeneous manner

and its strength can be predicted by existing theories.

The work described in this thesis also shows the great potential of the finite element method for numerical stress analysis. Its main advantage in the analysis of idealised models is the case by which a single parameter can be varied whilst the others are kept constant.

REFERENCES

Allison, I.M. & Holloway, L.C. (1967) Brit. J. Appl. Phys. 18,7,979

American Society for Metals (1965) "Fiber Composite Materials" ASM

Arridge, R.G.C. (1964) Rolls Royce Rept. RR(OH)202

Baker, A.A. (1966) Appl. Matls. Res. 5, 3, 143

Baker, A.A. & Cratchley, D. (1964) Appl. Matls. Res. 3, 4, 215

Bott, T.R. & Barker, A.J. (1965) Trans. J. Plastics Inst. 33,107,153

Bouc, C.A. (1962) AD 290280

Brenner, S.S. (1956) J. Appl. Phys. 27, 1484

Calcote, L.R. & Bowman, G.E. (1965) Exp. Mech. 5, 8, 262

Carrara, A.S. & McGarry, F.J. (1968) J. Comp. Matls. 2, 2, 222

Clarke, F.J.P. (1967) unpublished paper presented at 'Properties and Design of Composite Matls' course held at Woolwich Polytechnic, 24-26th May, 1967

Clough, R.W. (1965) "Stress Analysis" ed. Zienkiewicz, O.C. & Holister, G.S. Chap 7

Cohen, L.J. (1967) Israel J. Tech. 5, 4, 261

Coleman, R.V. (1964) Met. Rev. 9, 35, 261

Cook, J. & Gordon, J.E. (1964) Proc. Roy. Soc. A 282, 63

Cooper, G.A. & Kelly, A. (1967a) J. Mech. Phys. Solids 15, 4, 279

Cooper, G.A. & Kelly, A. (1967b) "The Contribution to the work of Fracture of a Composite Material of 'Pull-out' of Fibres" Metallurgy Dept., Cambridge University.

Cox, H.L. (1952) Brit. J. Appl. Phys. 3, 3, 72

Cratchley, D. (1965) Met. Rev. 10, 37, 79

Dixmier, G. & Gerard, G. (1964) NATO AGARD Rept. 524

Dixon, J.R. & Visser, W. (1963) "Photoelasticity" ed. Frocht, M.M.
(Proc. Symposium on Photoelasticity at Illinois
Inst. of Tech. Oct. 1961)

Dow, N.F. (1963) Gen. Elec. Co. Rept. R635D61

Fidler, R. & Nurse, P. (1966) VDI - Berichte 102, 59

Gates, R.G. & Wood, W.A. (1967) AD 656427

Gatti, A., Berry, J.M., Gebhart, E.J. & Feingold, E. (1967) NASA CR 84872

Grimes, D.L. (1965) NATO AGARD Rept. 523

Grinius, V.G. (1966) AD 638921

Ham, R.K. & Place, T.A. (1966) J. Mech. Phys. Solids 14, 5, 271

Hedgepeth, J.M. (1961) TN D - 882

Hertzberg, R.W., Lemkey, F.D. & Ford, J.A. (1965) Trans. AIME Met.
Soc. 233, 2, 342

Hill, R. (1963) J. Mech. Phys. Solids 11, 5, 357

Holister, G.S. & Thomas, C. (1966) "Fibre Reinforced Materials" Elsevier

Inglis, C.E. (1913) Trans. Inst. Naval Arch. 55, 219

Iremonger, M.J. & Wood, W.G. (1967) J. Strain Analysis 2, 3, 239

Jech, R.W., McDanels, D.L. & Weeton, J.W. (1959) Proc. 6th. Sagamore
Ordnance Matls. Conf.

Kelly, A. (1964) Proc. Roy. Soc. A 282, 63

Kelly, A. & Davies, G.J. (1965) Met. Rev. 10, 37, 1

Kelly, A. & Tyson, W.R. (1965a) J. Mech. Phys. Solids 13, 6, 329

Kelly, A. & Tyson, W.R. (1965b) "High Strength Materials" Chap 13, Wiley

Kershaw, J.P. & Shepard, L.A. (1965) AD 638621

Kobrin, C.L. (1965) Iron Age 196, 15, 109

MacLaughlin, T.F. (1966) Exp. Mech. 6, 10, 481

MacLaughlin, T.F. (1968) J. Comp. Matls. 2, 1, 44

Marcal, P.V. (1965) Int. J. Mech. Sci. 7, 4, 229

Marcal, P.V. & King, I.P. (1967) Int. J. Mech. Sci. 9, 3, 143

Marcal, P.V., King, I.P. & Leech, A. (1967) "Finite Element User's Manual" Imperial College

Materials Advisory Board (1965a) Nat. Acad. Sci. Rept. MAB-207-M

Materials Advisory Board (1965b) Nat. Acad. Sci. Rept. MAB-214-M

McDanels, D.L., Jech, R.W. & Weeton, J.W. (1963) NASA TN D-1881

McGarry, F.J. (1966) Exp. Mech. 6, 6, 331

Moss, R.G. (1967) NASA CR94040

Mullin, J., Berry, J.M., & Gatti, A. (1968) J. Comp. Matls. 2, 1, 82

Outwater, J.O. (1956) Modern Plastics 33, 156

Outwater, J.O. & Carnes, W.O. (1967) AD 659363

Parikh, N.M. (1964) AD 604190

Parratt, N.J. (1960) Rubber and Plastics Age 41, 3, 263

Pichler, H.R. (1965) Trans. AIME Met. Soc. 233, 1, 12

Piggott, M.R. (1966) Acta Met. 14, 11, 1429

Pugh, S.F. (1967) unpublished paper presented at 'Properties and Design of Composite Materials' Course held at Woolwich Polytechnic, 24-26th May, 1967

Riley, W.F. (1967) Exp. Mech. 7, 2, 19A

Riley, V.R. & Reddaway, J.L. (1968) J. Matls. Sci. 3, 41

Rosen, B.W. (1964) AIAA Journal 2, 11, 1985

Sadowsky, M.A., Hsu, Y.C. & Hussain, M.A. (1964) Watervliet Arsenal Tech. Rept. WVT-RR-6407

Schuster, D.M. & Scala, E. (1964) Trans. AIME Met. Soc. 230, 12, 1635

Schuster, D.M. & Scala, E. (1968) AIAA Journal 6, 3, 527

Slayter, G. (1962) Scientific American 206, 1, 124

Spencer, A.J.M. (1965) Int. J. Mech. Sci. 7, 3, 197

Sutton, W.H. (1966) Gen. Elec. Co. Rept. R66SD4

Sutton, W.H. & Chorné, J. (1965) "Fiber Composite Materials" Chap. 9, American Society for Metals

Tooling and Production (1967) 33, 6, 83

Tsai, S.W. & Chen, P.E. (1967) "High Performance Composites", 2nd Annual Review Monsanto/Washington Univ. HPC 67-28 p.13

Turner, M.J., Clough, R.W., Martin, H.C. & Topp, L.J. (1965) J. Aer. Sci. 23, 9, 805

Tyson, W.R. & Davies, G.J. (1965) Brit. J. Appl. Phys. 13, 2, 199

de Venbeke, B.F. (1964) Proc. 14th. Meeting AGARD Structures and Materials Panel, AGARDograph 72

Watt, W., Phillips, L.N. & Johnson, W. (1966) The Engineer 221,5757,815

Weeton, J.W. & Signorelli, R.A. (1966) NASA TN D-3530

West, P. (1965) Matls. in Design Eng. 61, 6, 112

Wilson, E.L. (1963) Structural Eng. Lab. Rept. No. 63-2 California Univ. (Berkeley)

Zender, G.W. & Deaton, J.W. (1963) NASA TN D-1609

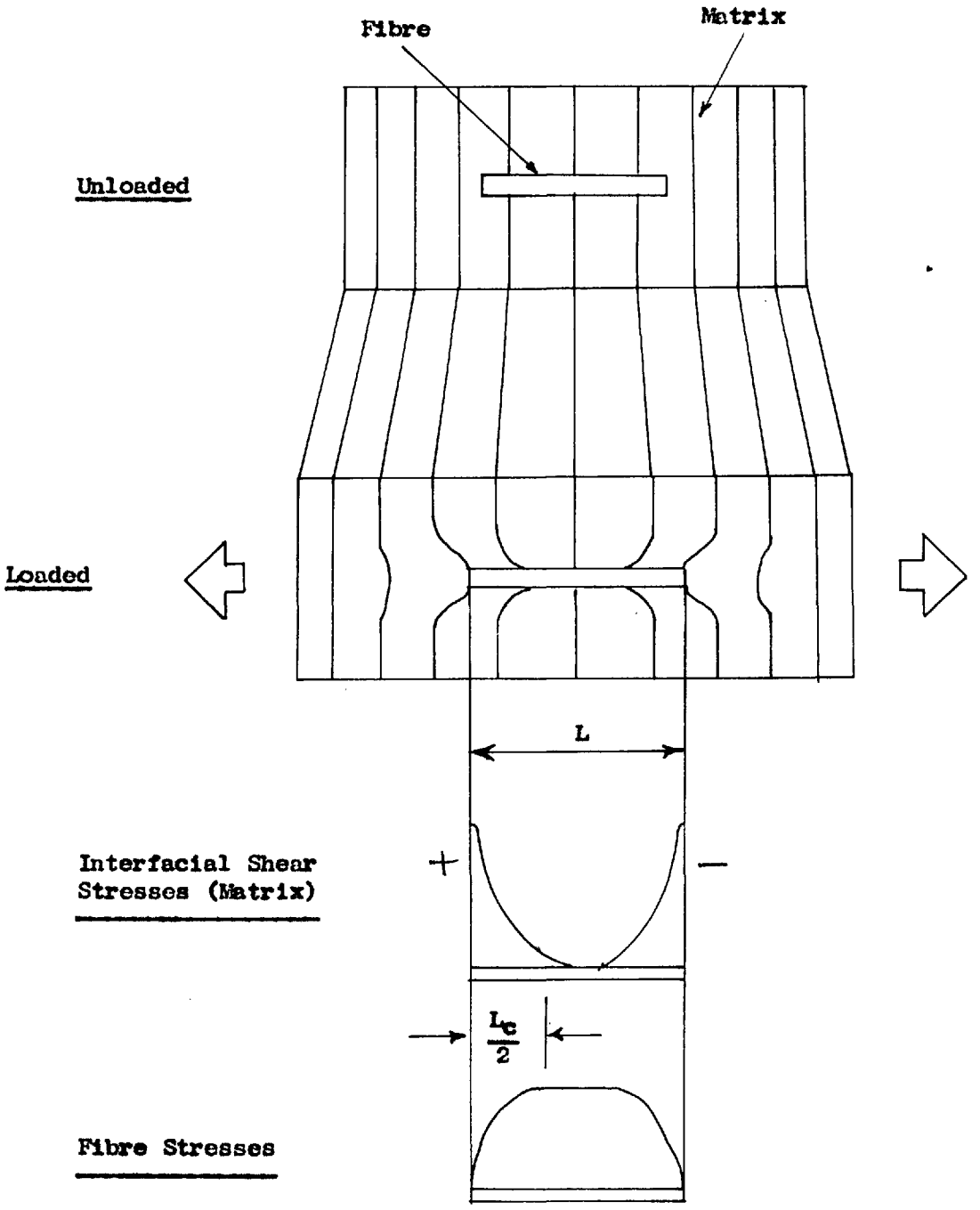

Fig. 1.1 : Schematic Representation of Stresses around a Fibre

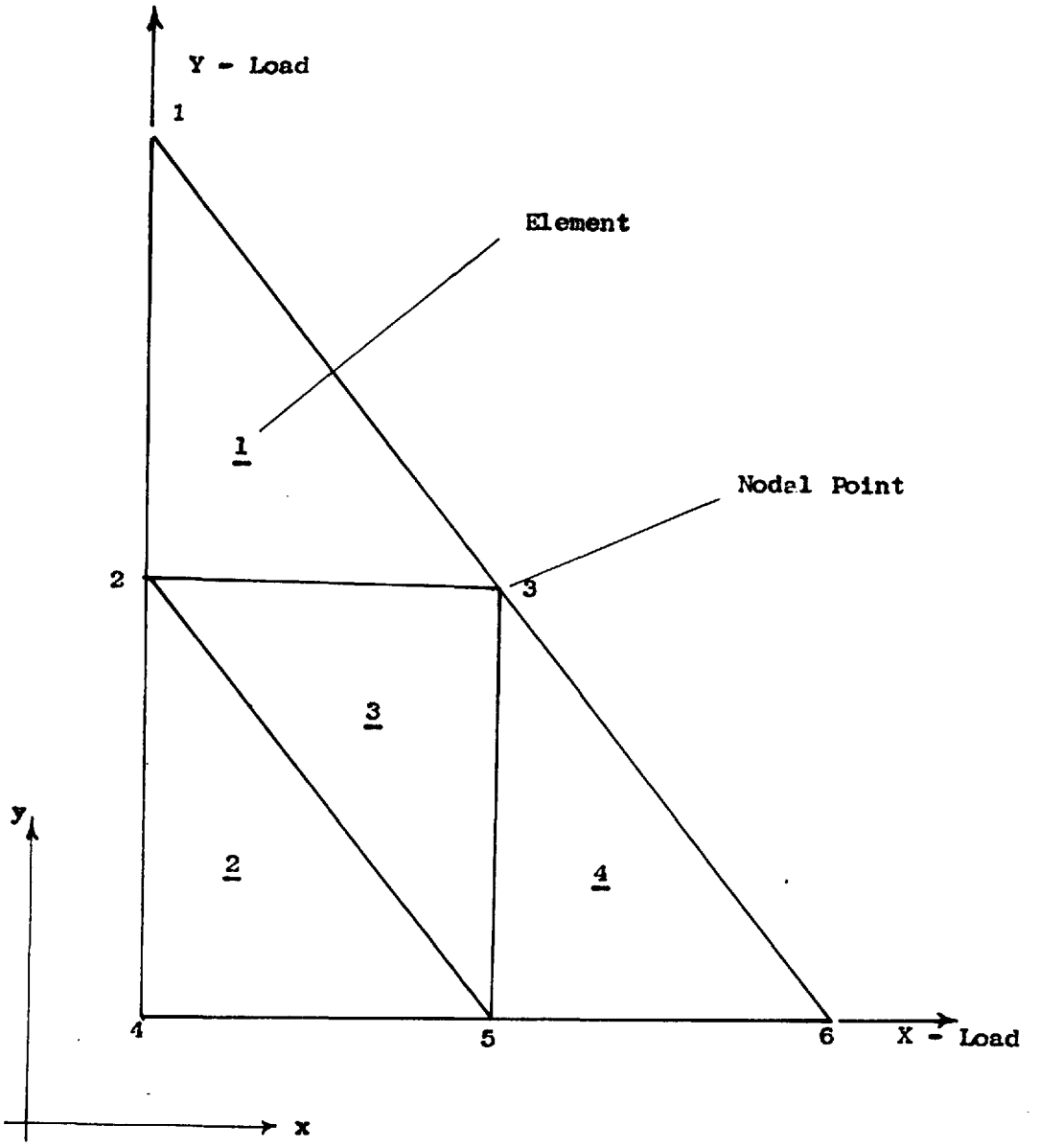

Fig. 2.1 : Finite Element Nomenclature

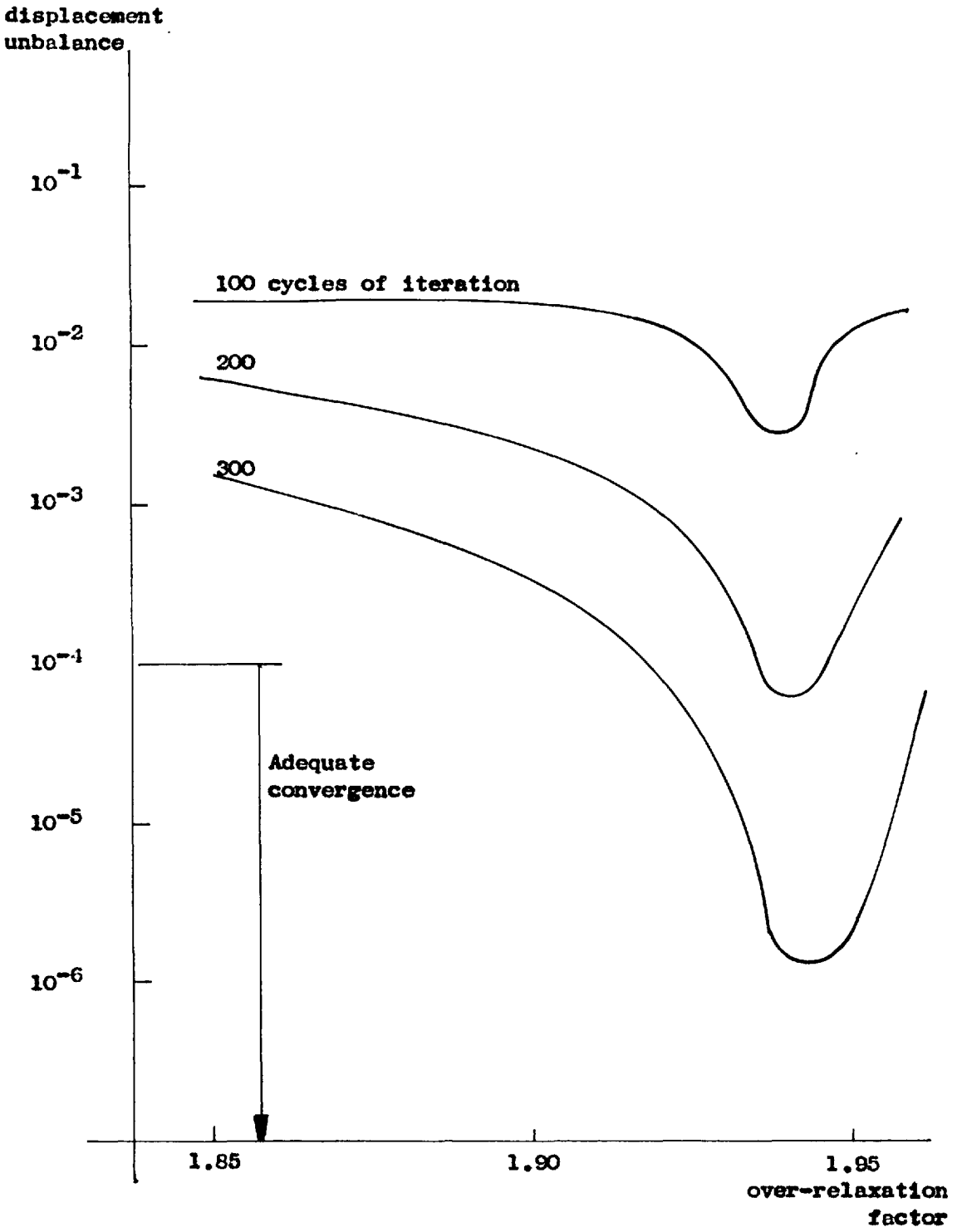

Fig. 2.2 : Convergence Curves

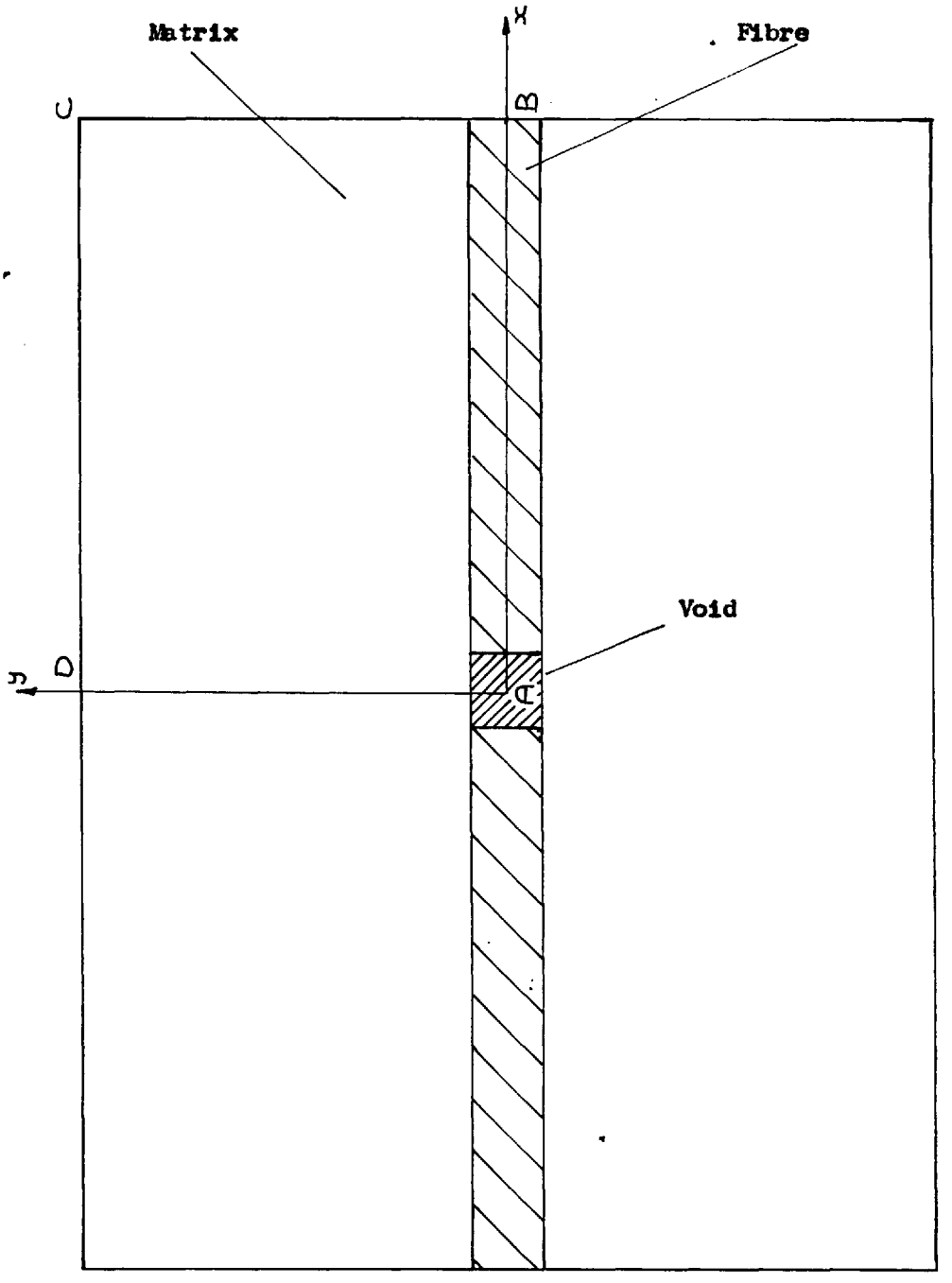

Fig. 3.1 : Single Broken Fibre Composite

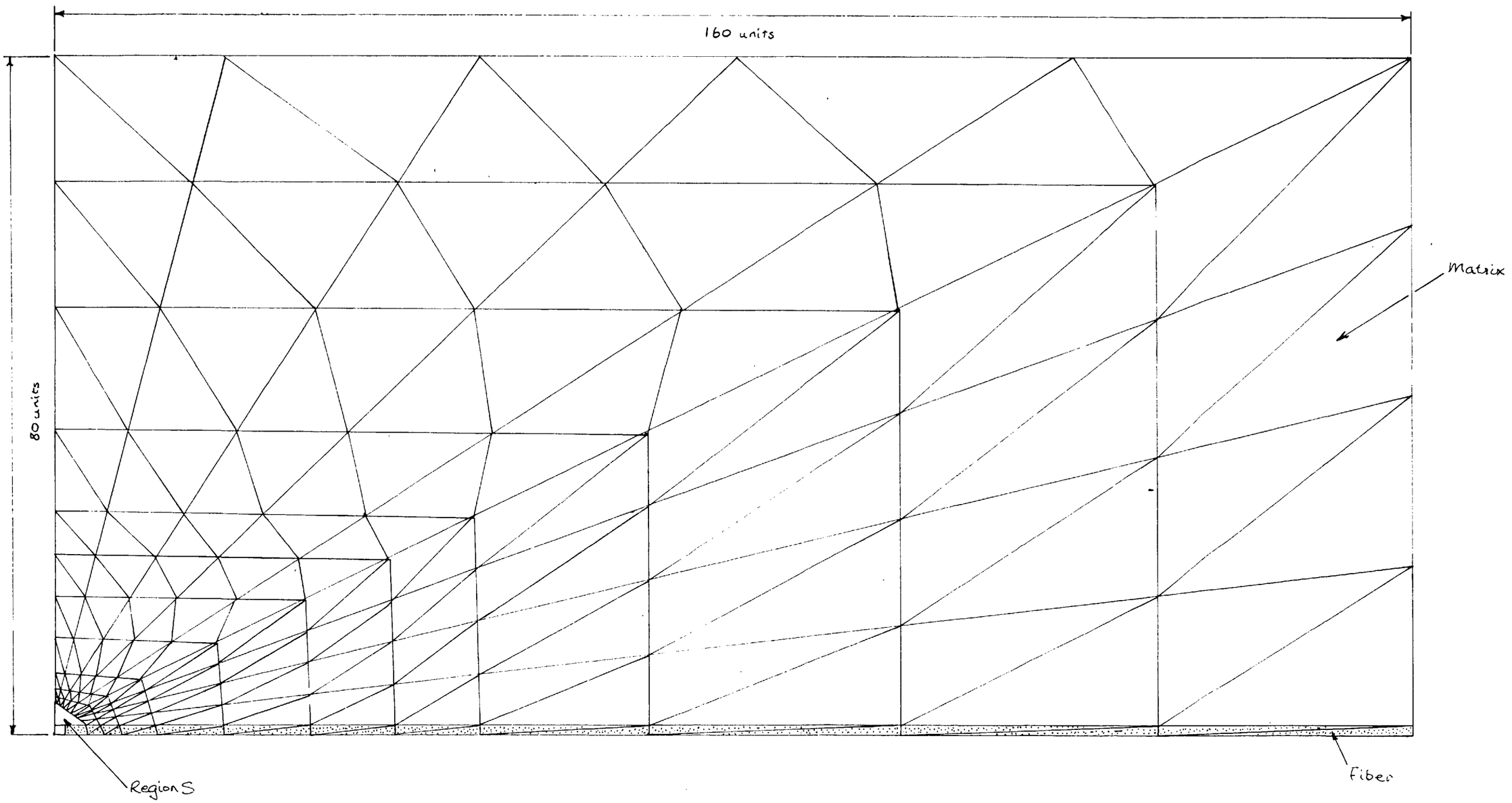

FIG. 3·2: BASIC MESH

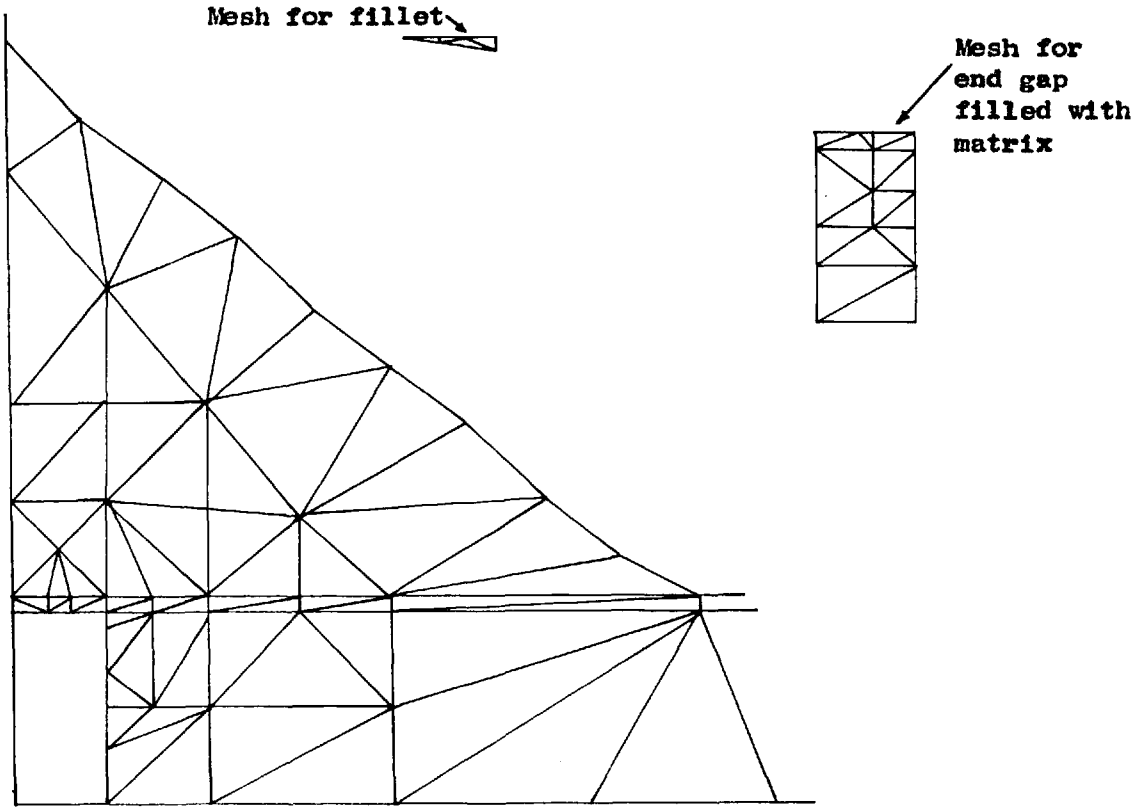

End Gap 0.5 fibre widths

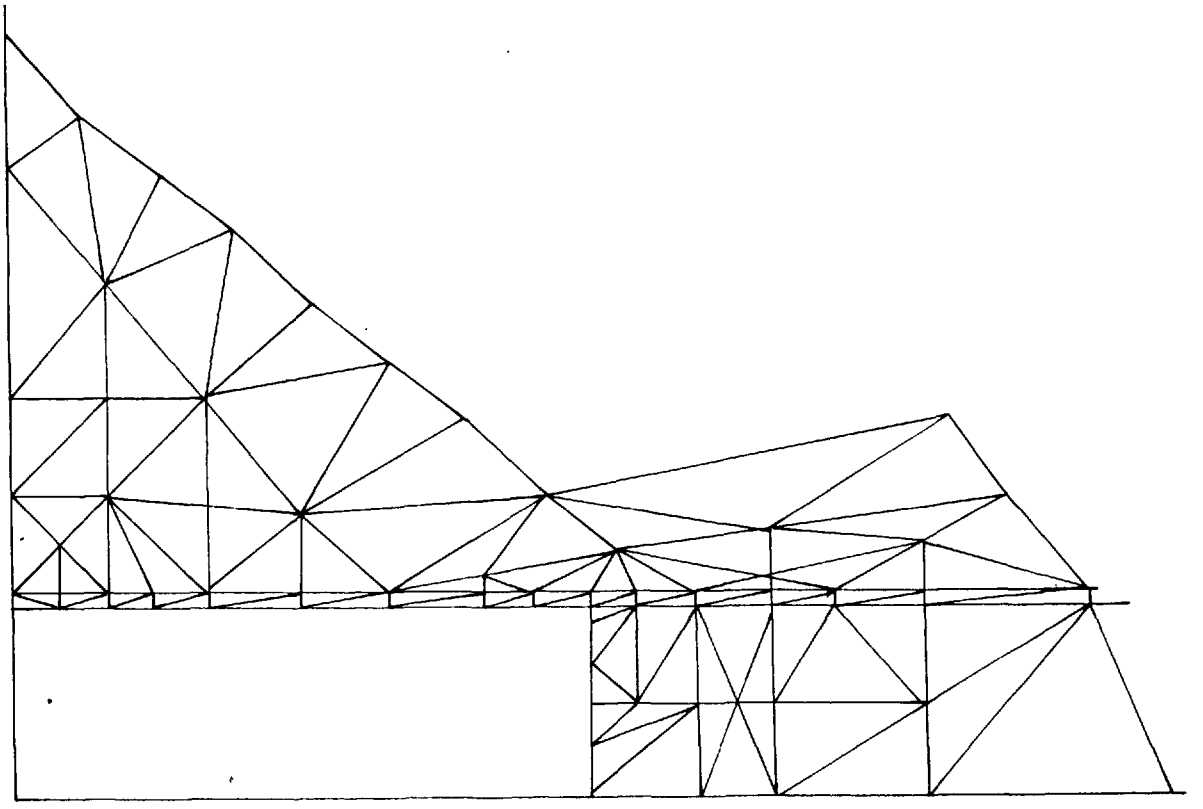

End Gap 3.0 fibre widths

Fig. 3.3 : Region S Meshes

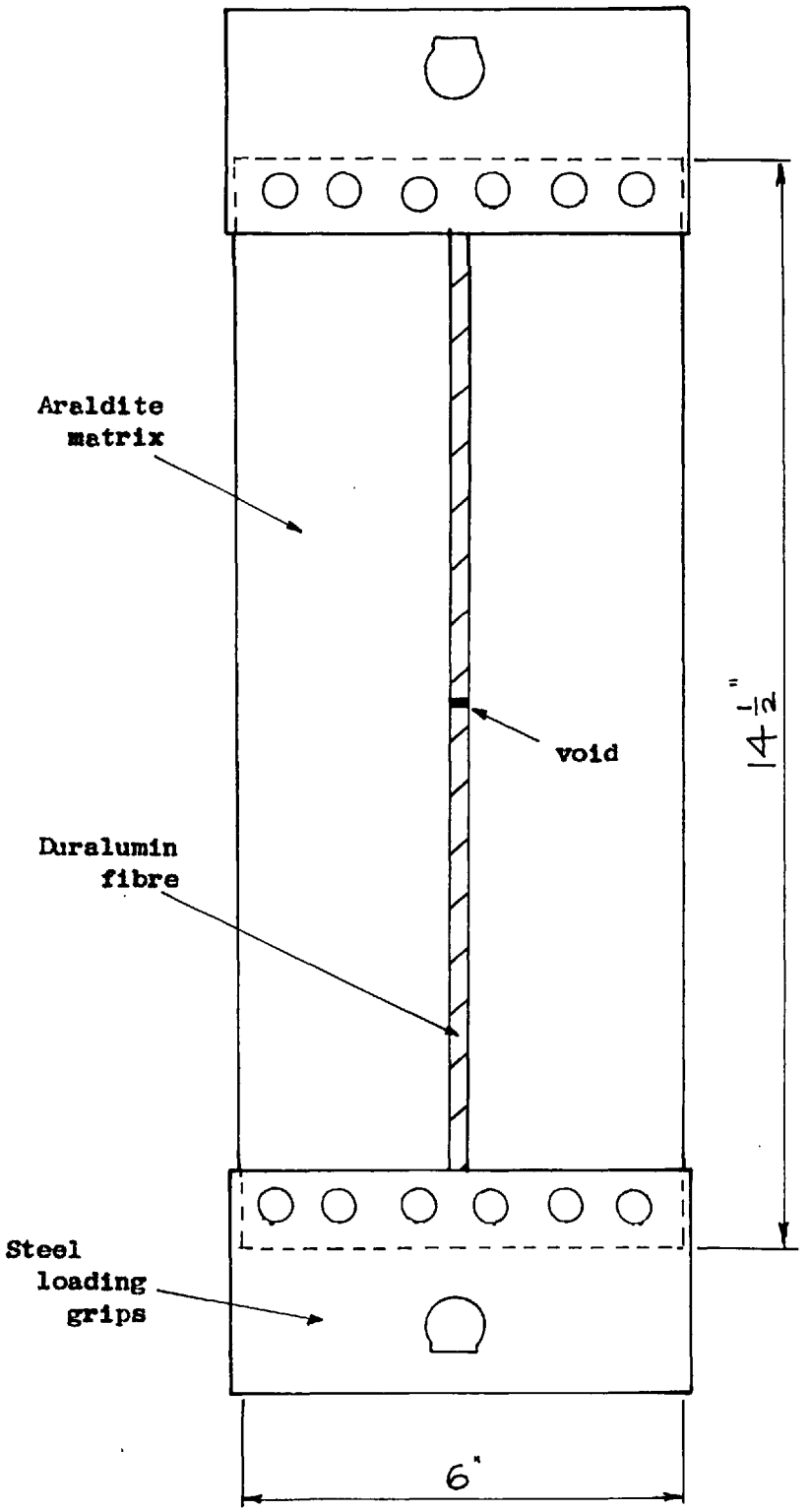

Fig. 3.4 : Photoelastic Model

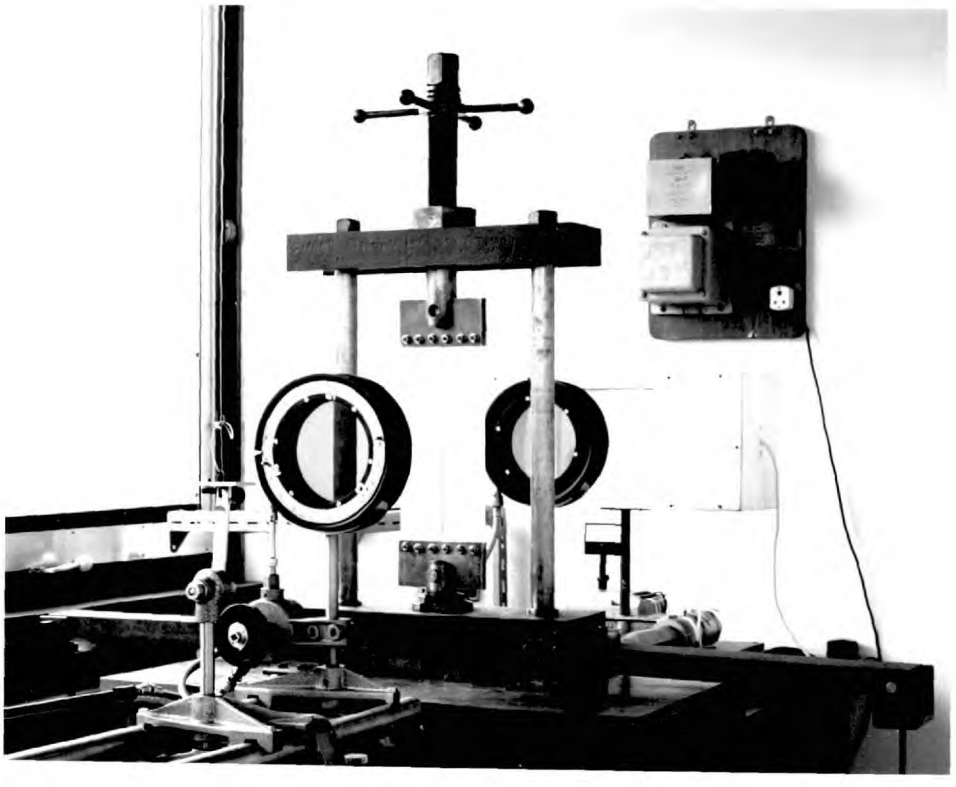

Fig. 3.5 : Photoelastic Bench

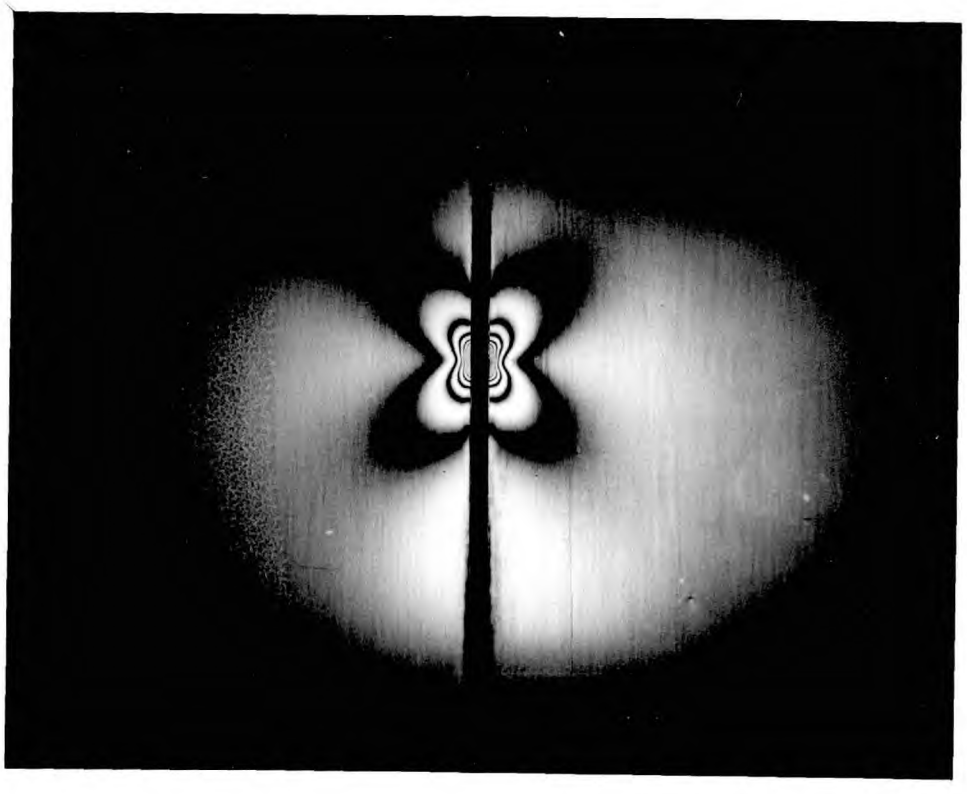

Fig. 3.6 : Typical Isochromatic Fringe Pattern - Single Fibre Composite

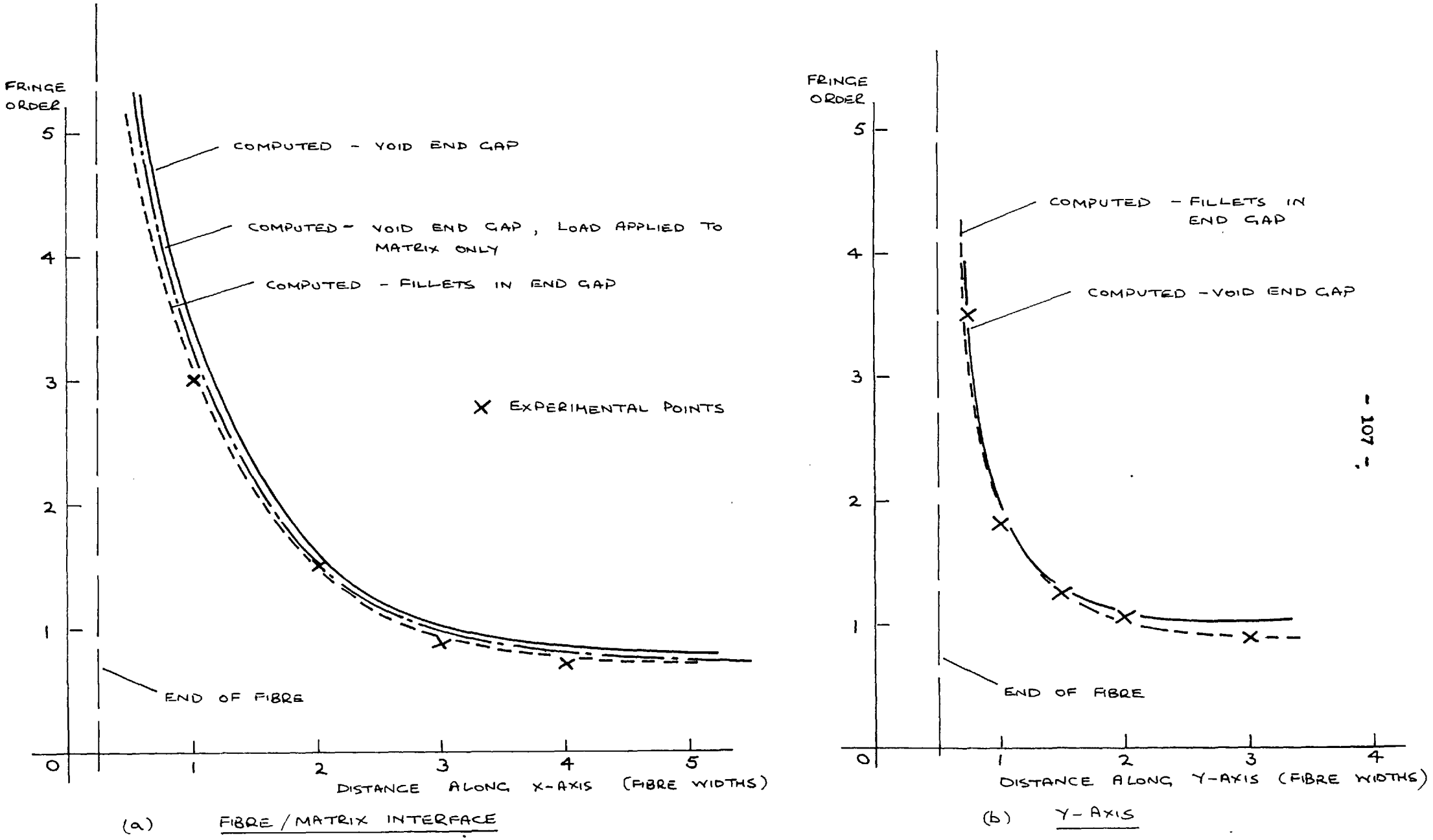

FIG. 3.7 : COMPARISON OF COMPUTED AND PHOTOELASTIC RESULTS

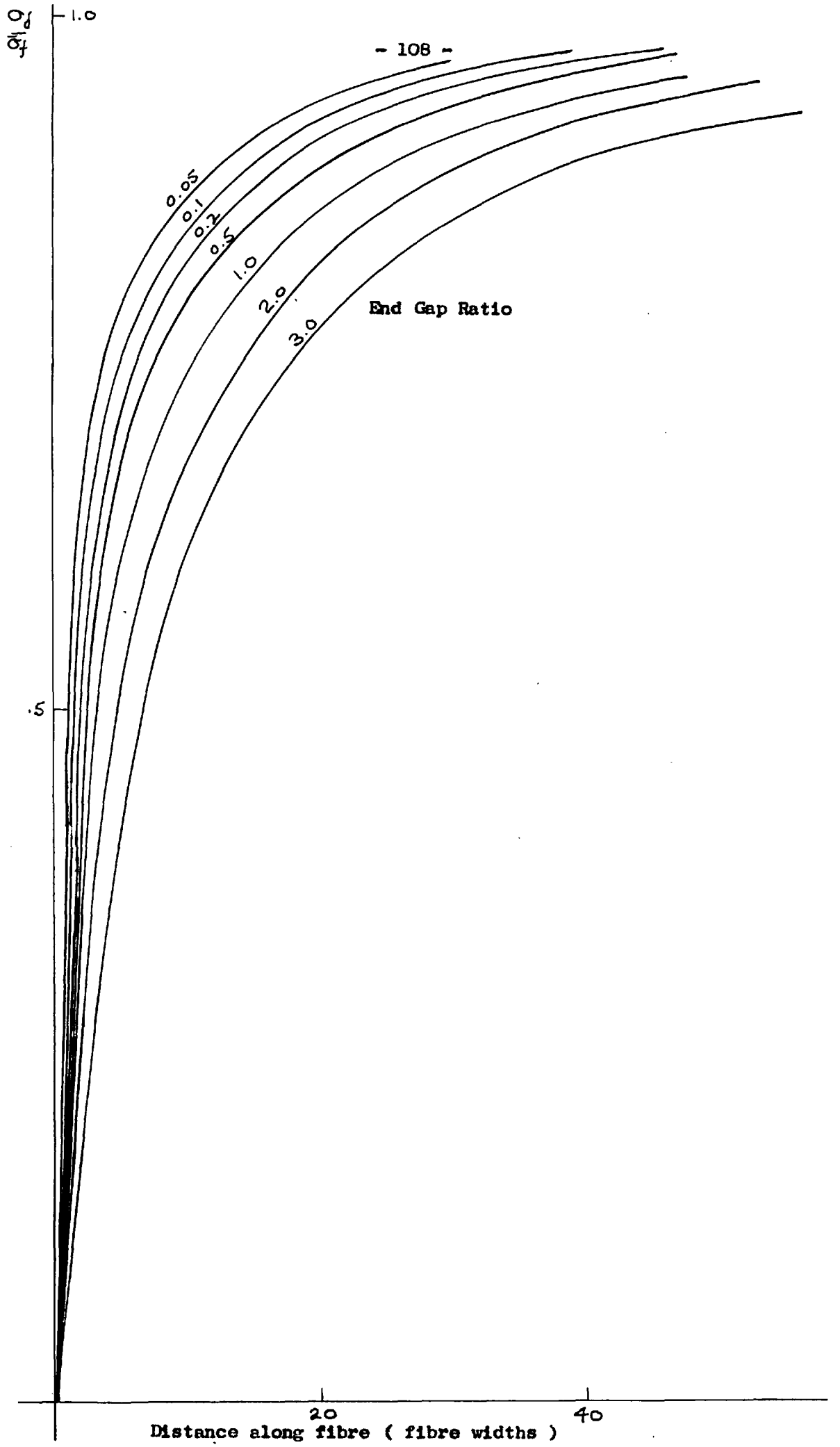

Fig. 3.8 : Distribution of Axial stress in Fibre - Void End Gap

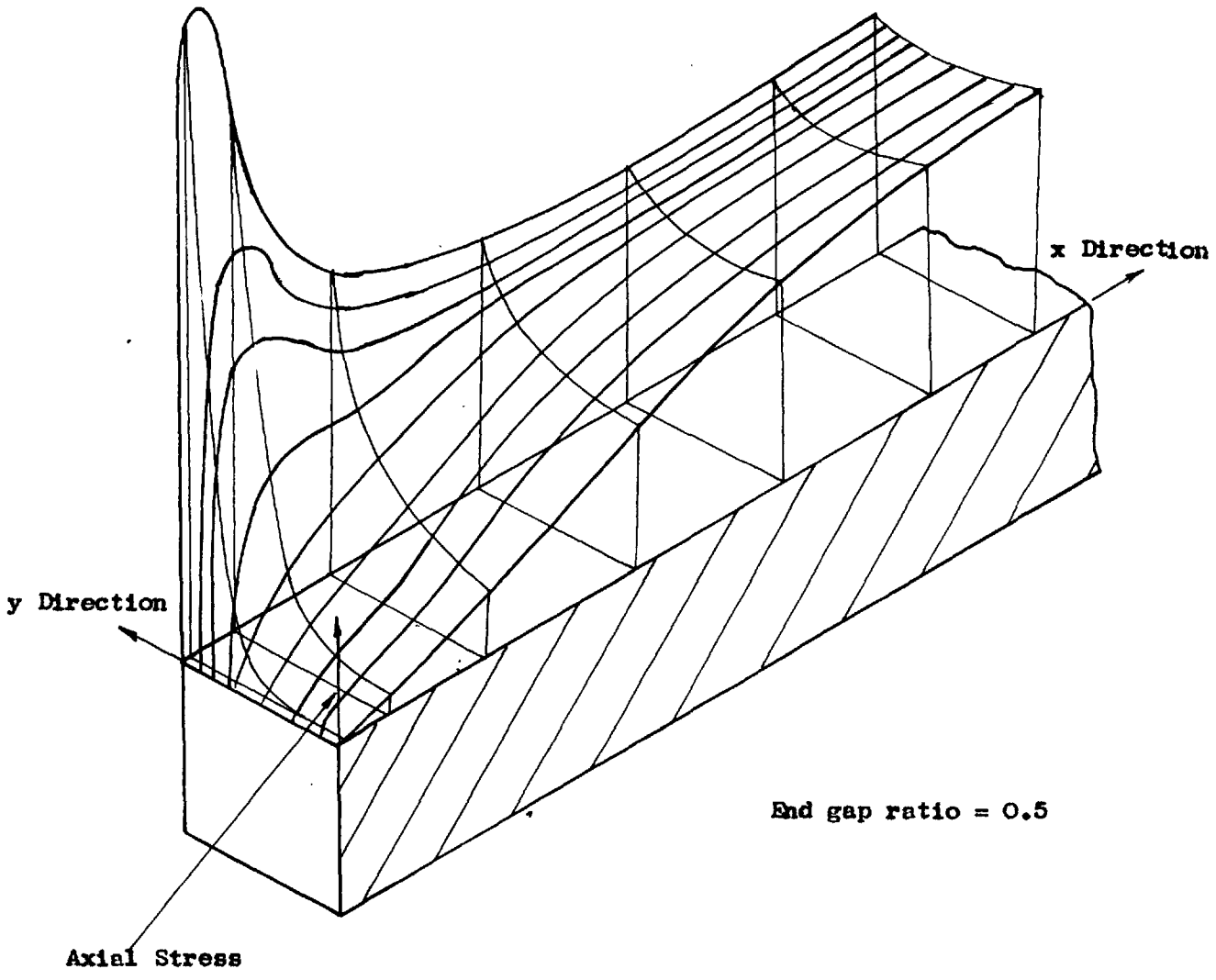

Fig. 3.9 : Distribution of Axial Stress in Half Width of Fibre for the Region of the End Gap

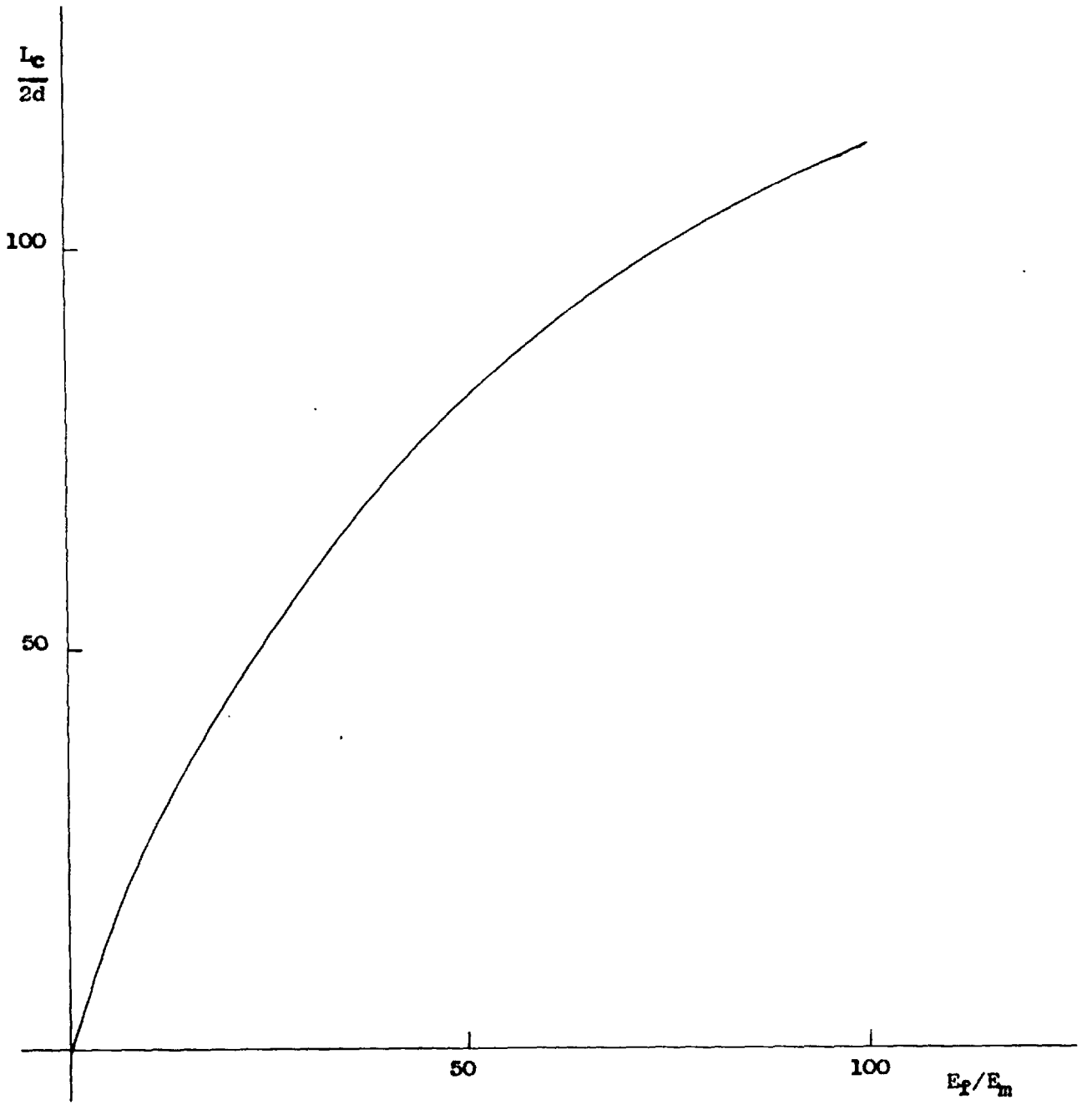

Fig. 3.10 : Critical fibre length v E_f/E_m ratio

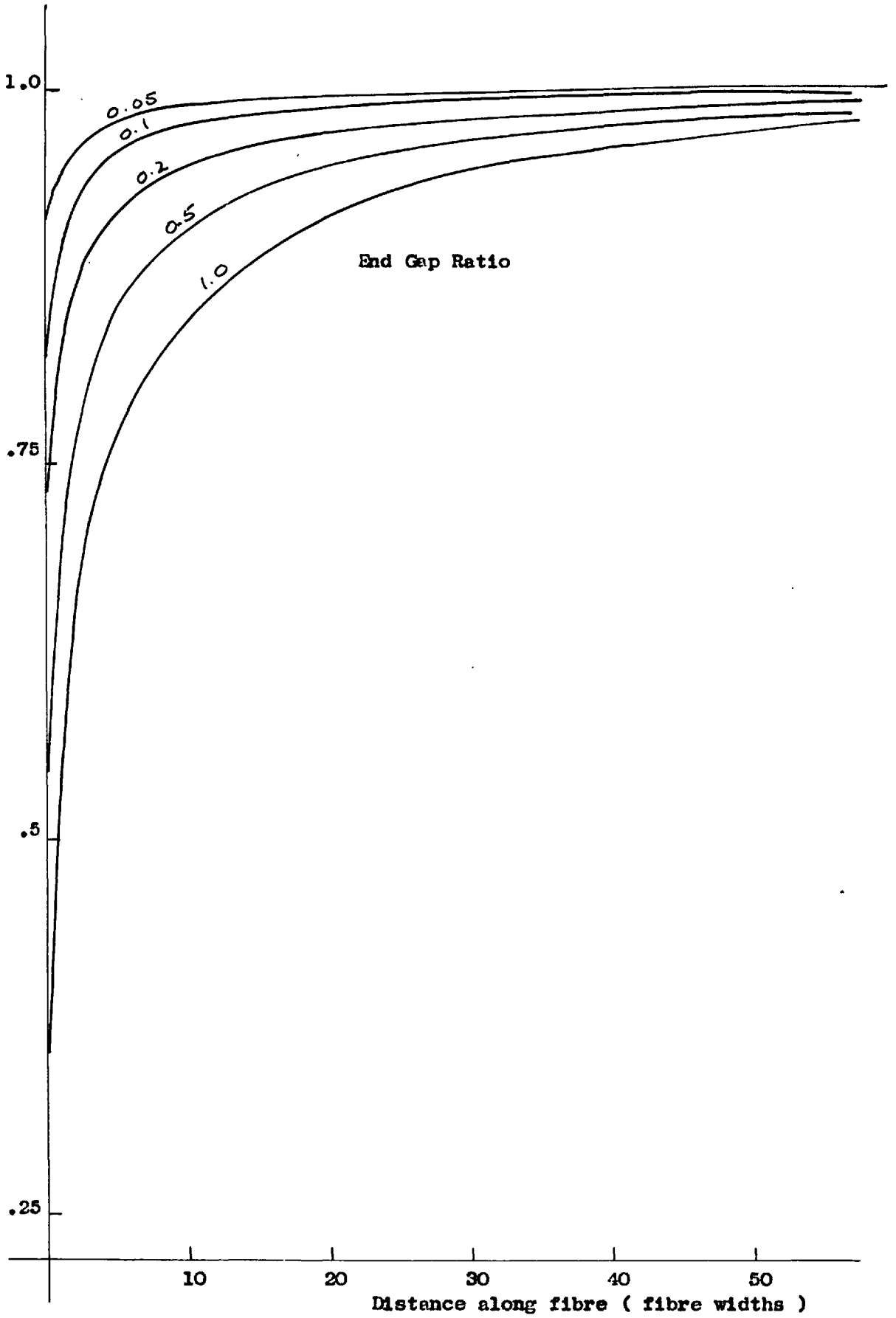

Fig. 3.11 : Distribution of Axial Stress in Fibre - Matrix Field End Gap

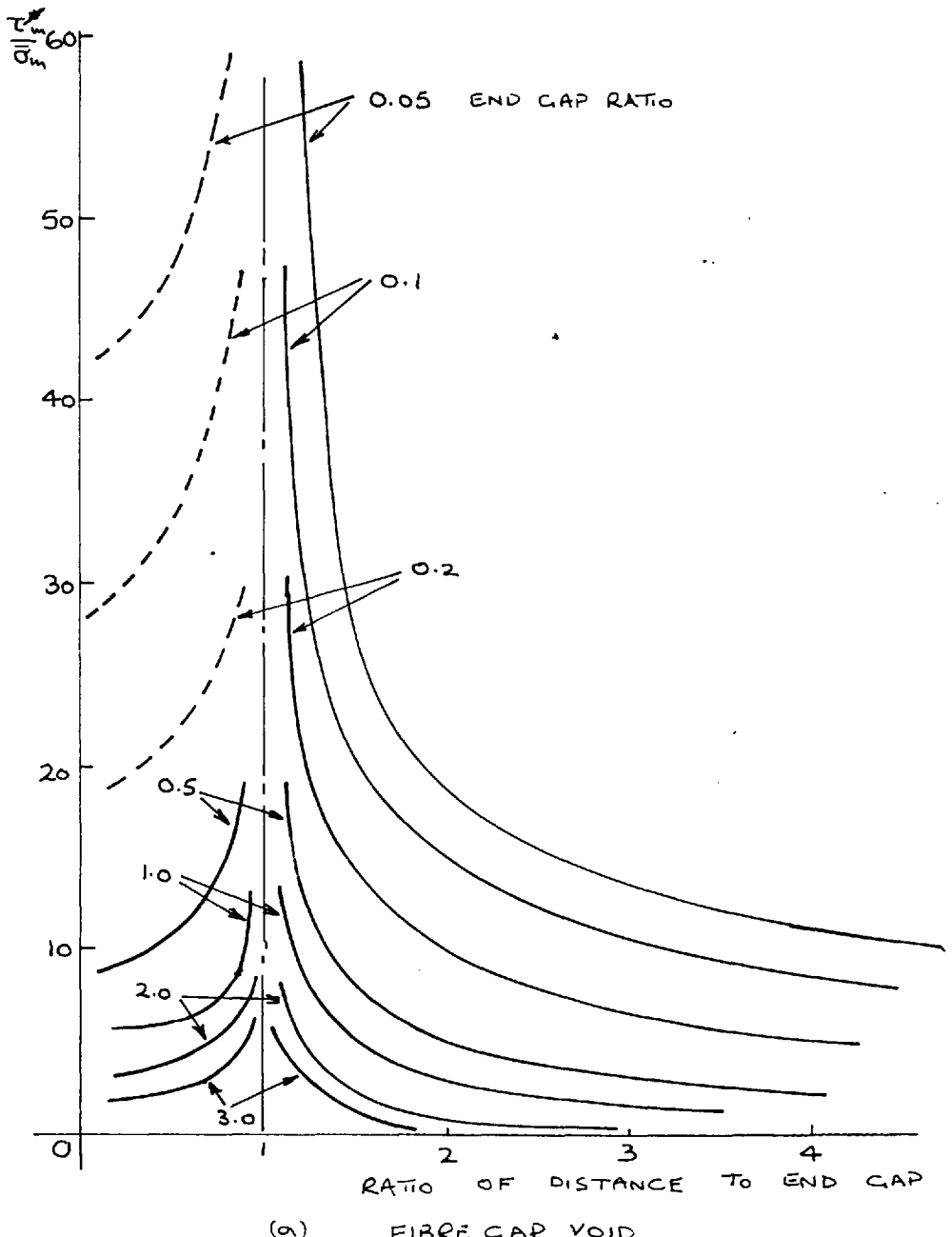

(a) FIBRE GAP VOID

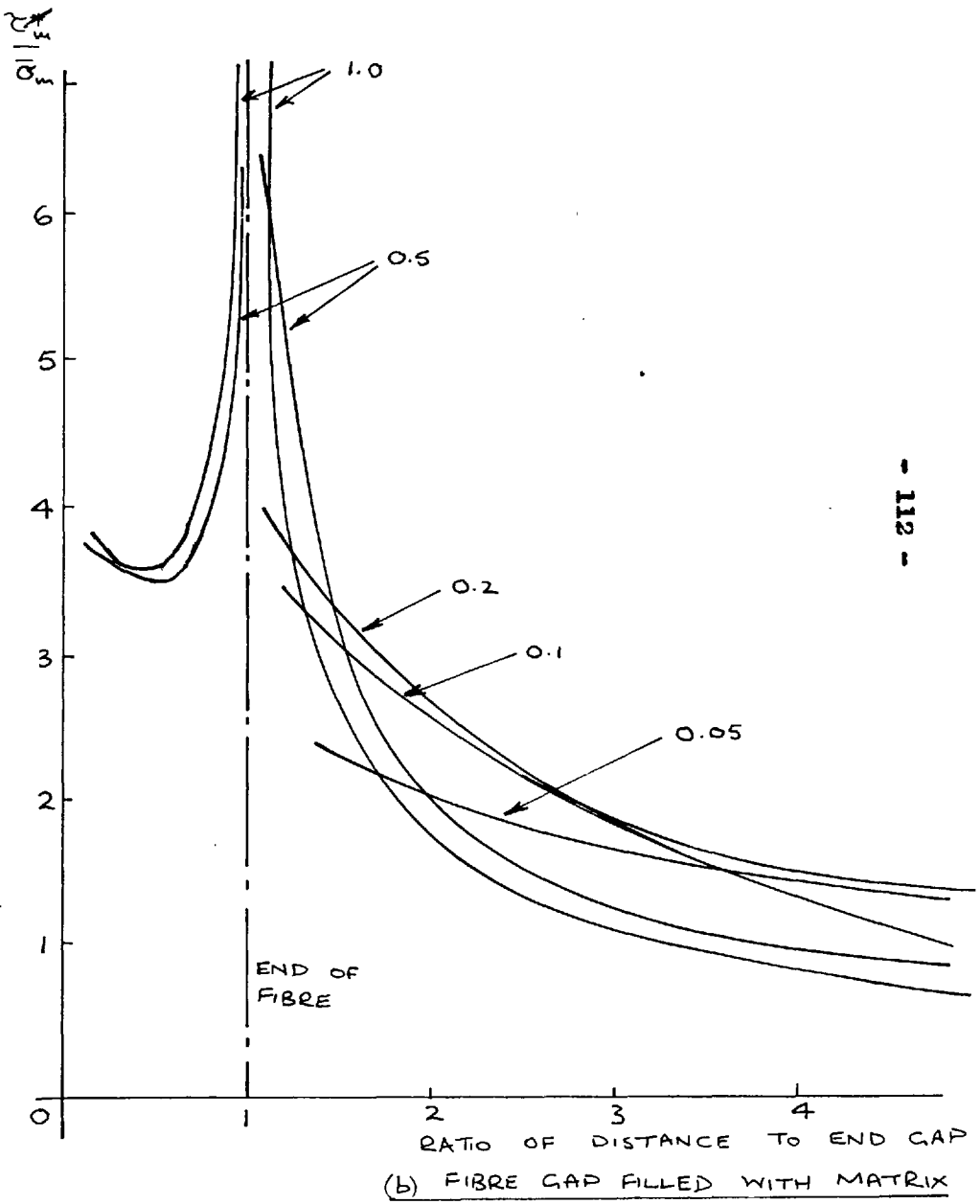

(b) FIBRE GAP FILLED WITH MATRIX

Fig. 3.12 : Distribution of Maximum Shear Stress in Matrix/Fibre Interface

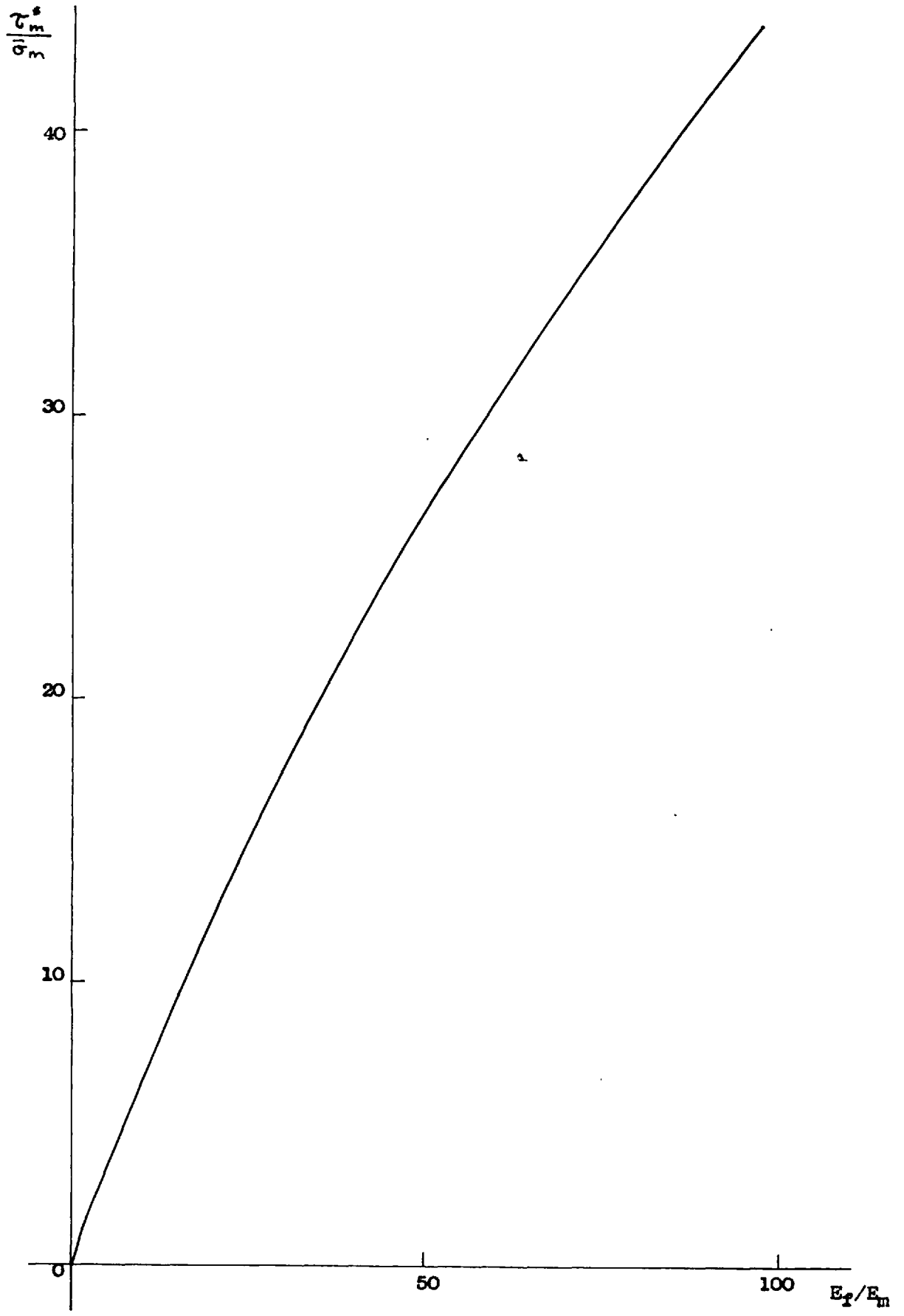

Fig. 3.13 : Maximum interfacial shear stress v E_f/E_m ratio

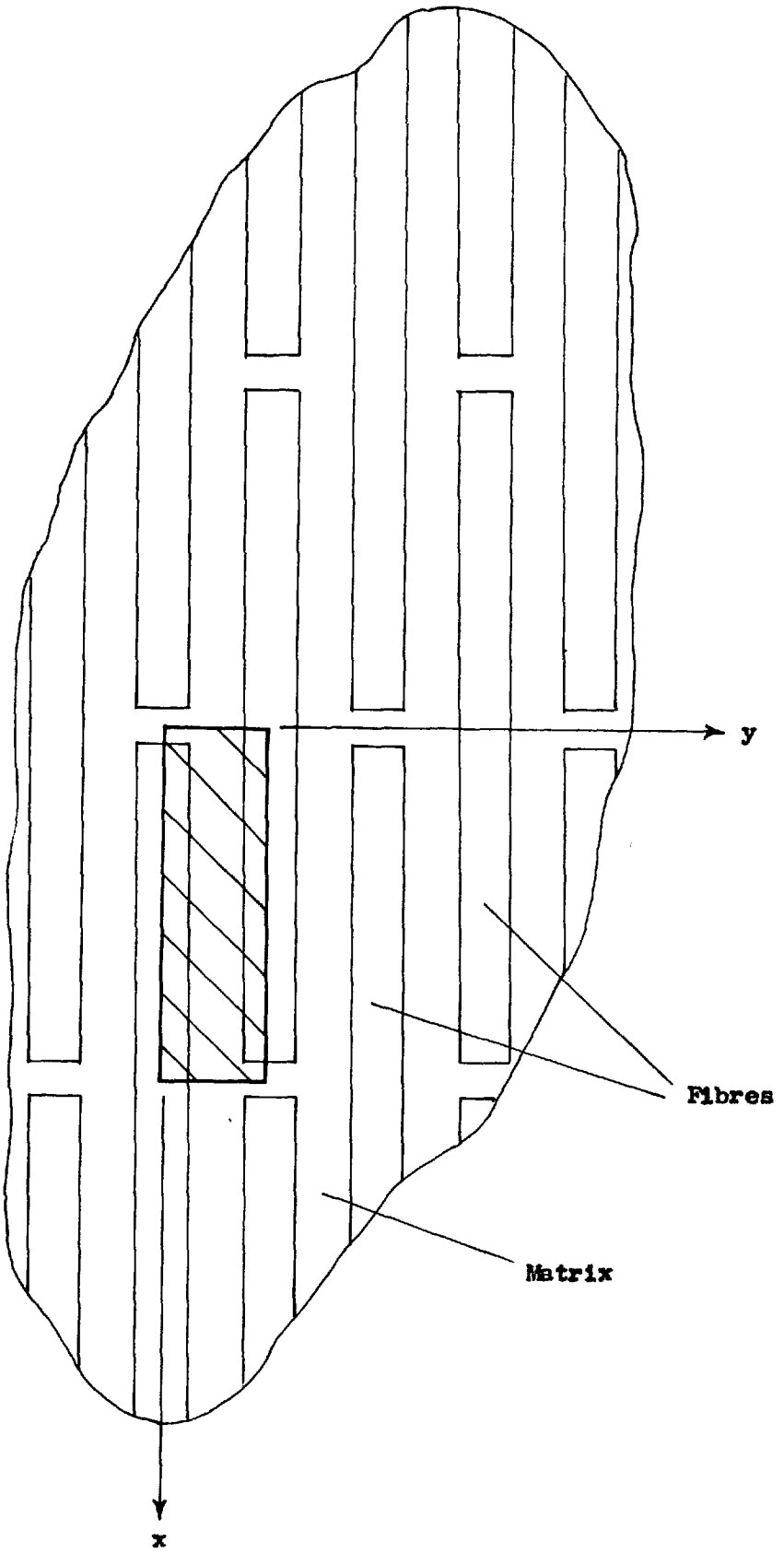

Fig. 4.1 : Idealised Discontinuous Composite

(a)

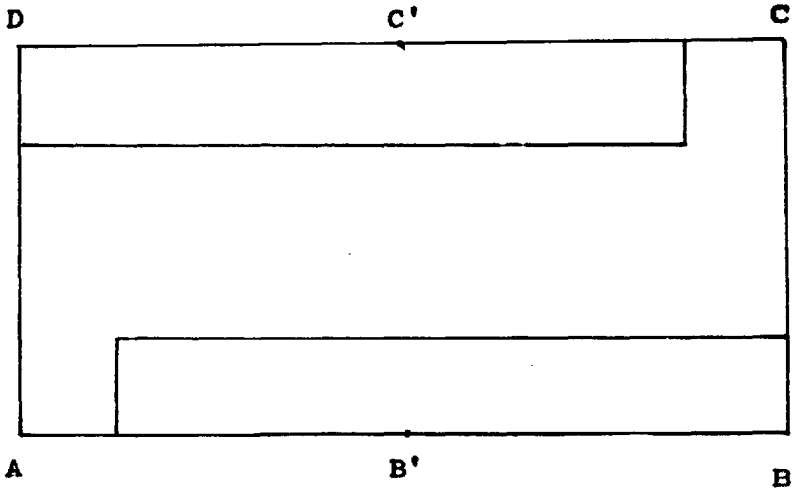

(b)

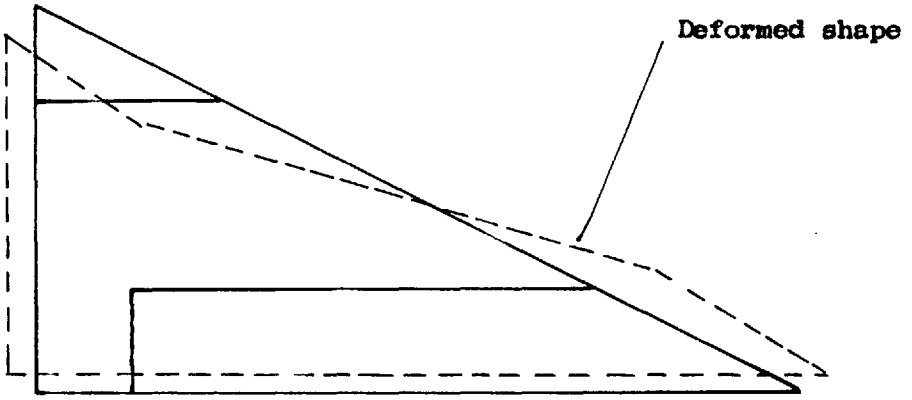

(c)

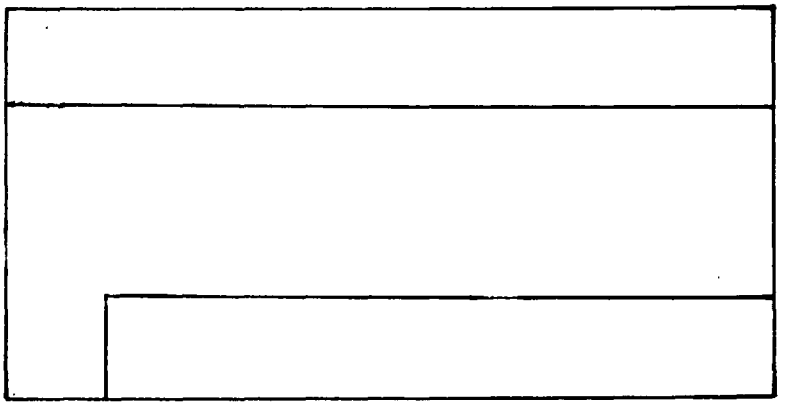

Fig. 4.2 : Finite Element Models

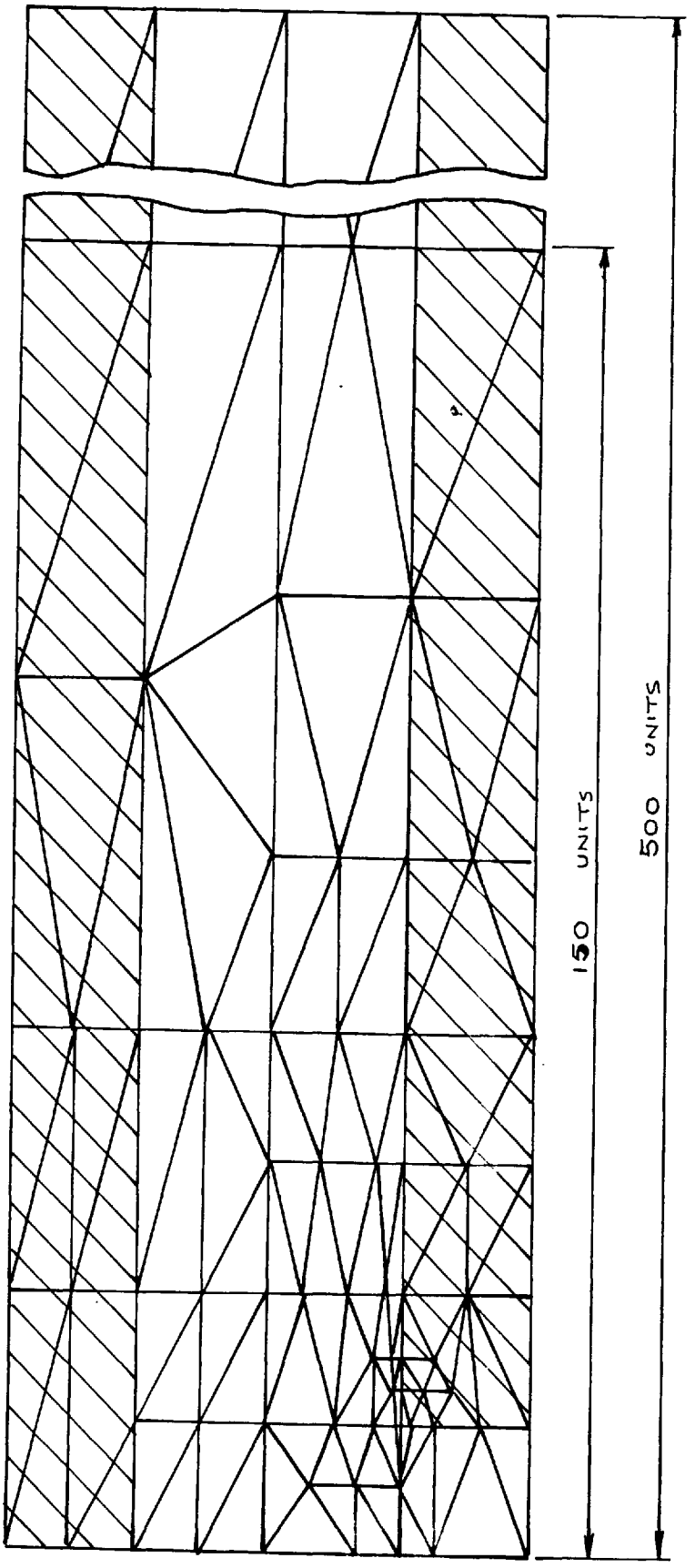

Fig. 4.3 : Typical Mesh

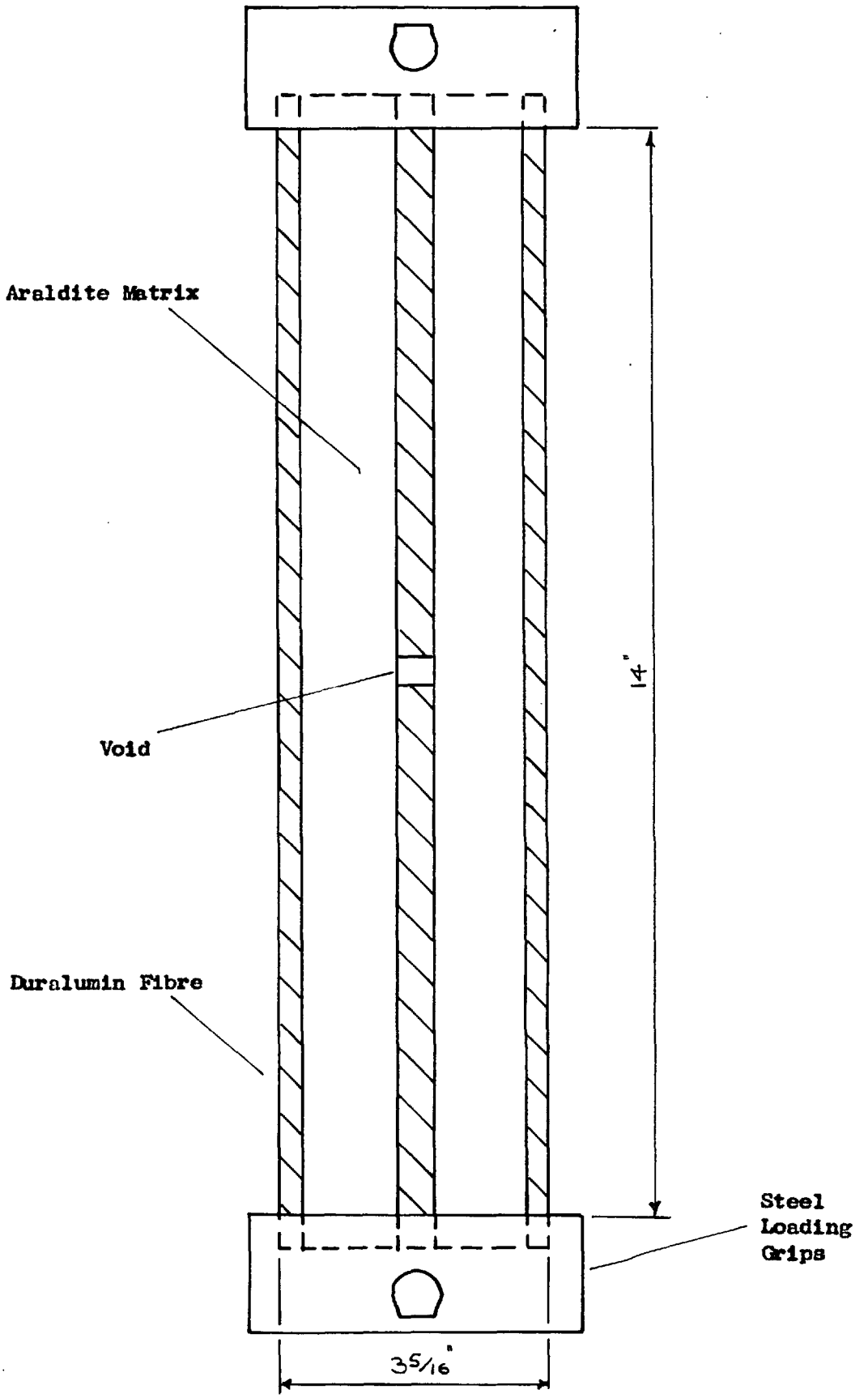

Fig. 4.4 : Experimental Model

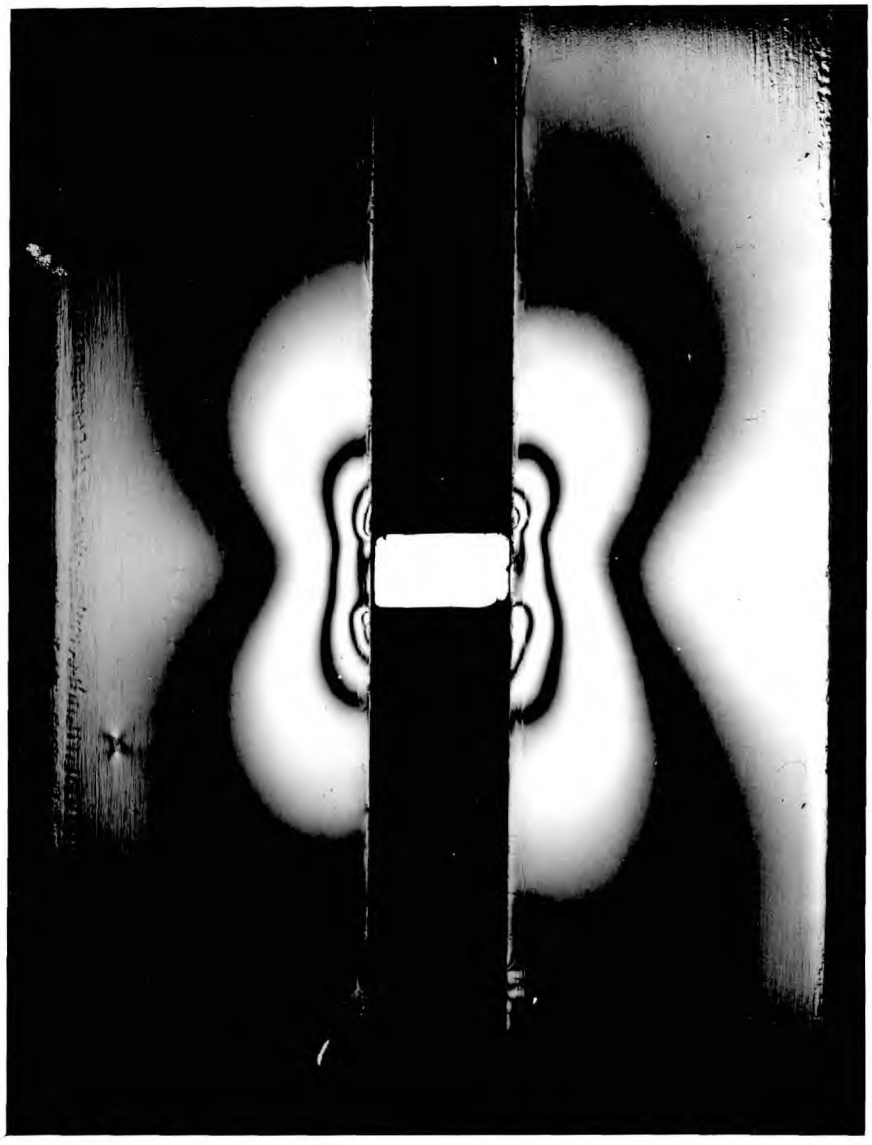

Fig. 4.5 : Typical Isochromatic Fringe Pattern - Multi Fibre Composite

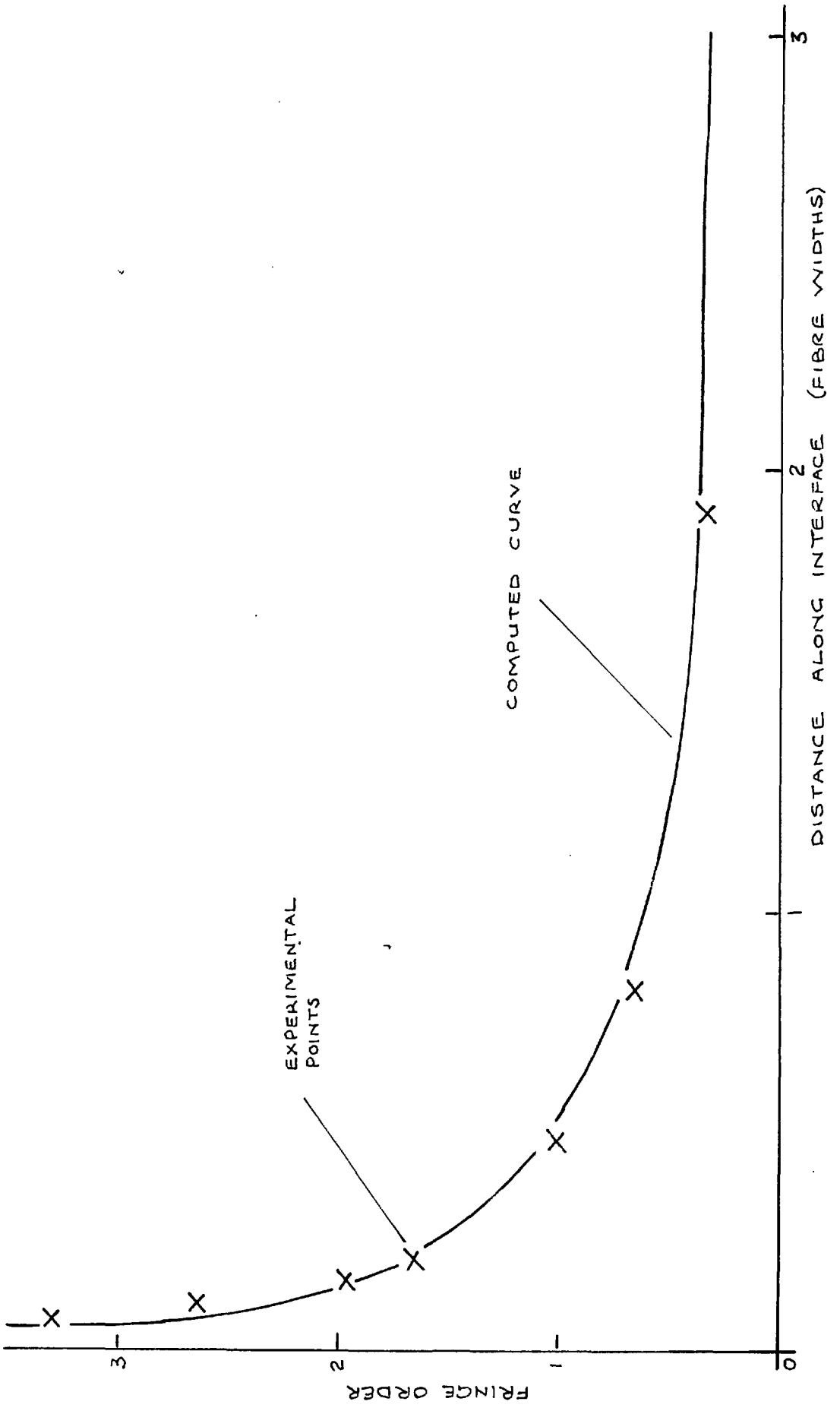

Fig. 4.6 : Comparison Between Experimental and Computed Results

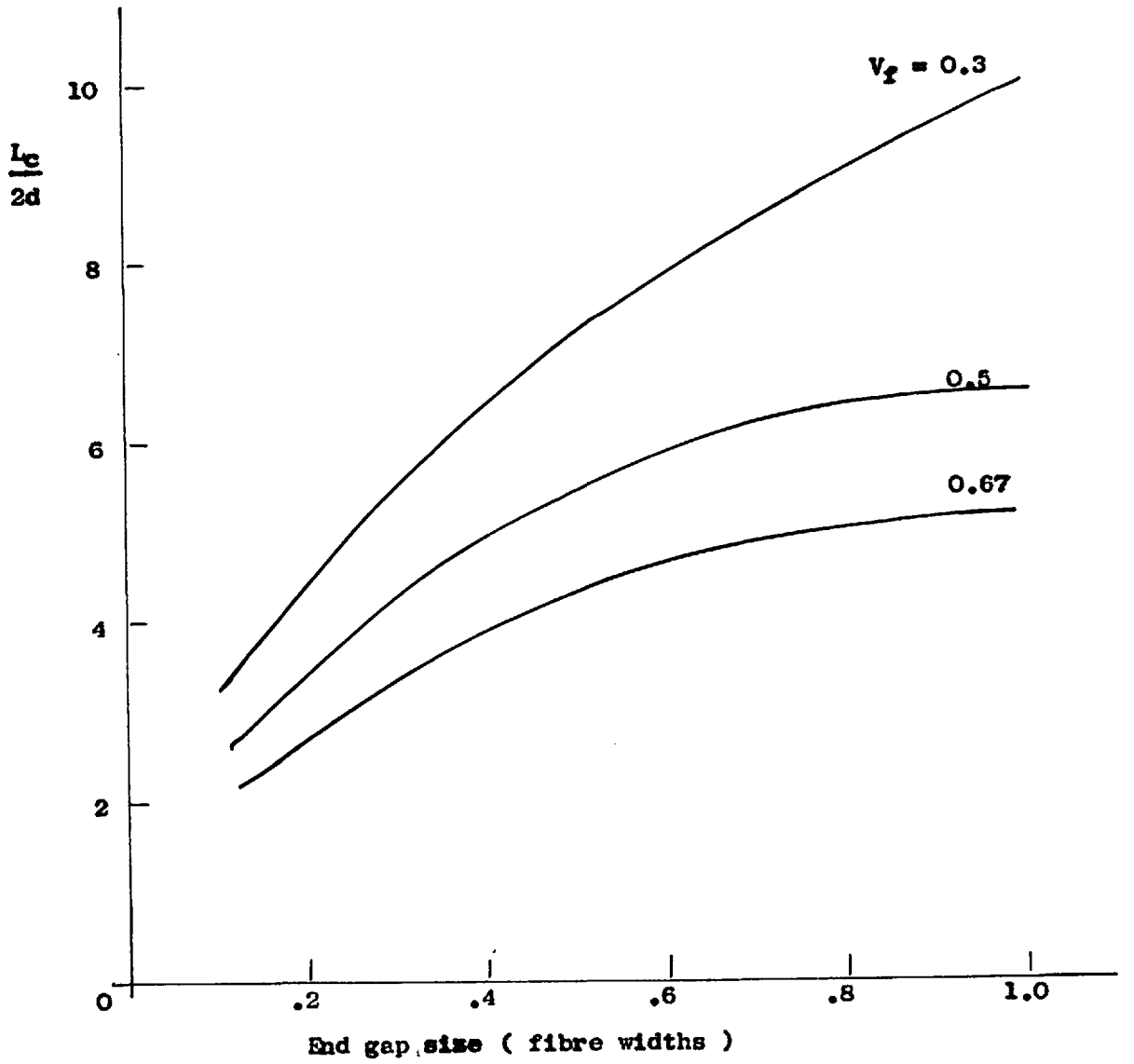

Fig. 4.7 : Critical Fibre Length v End Gap Size

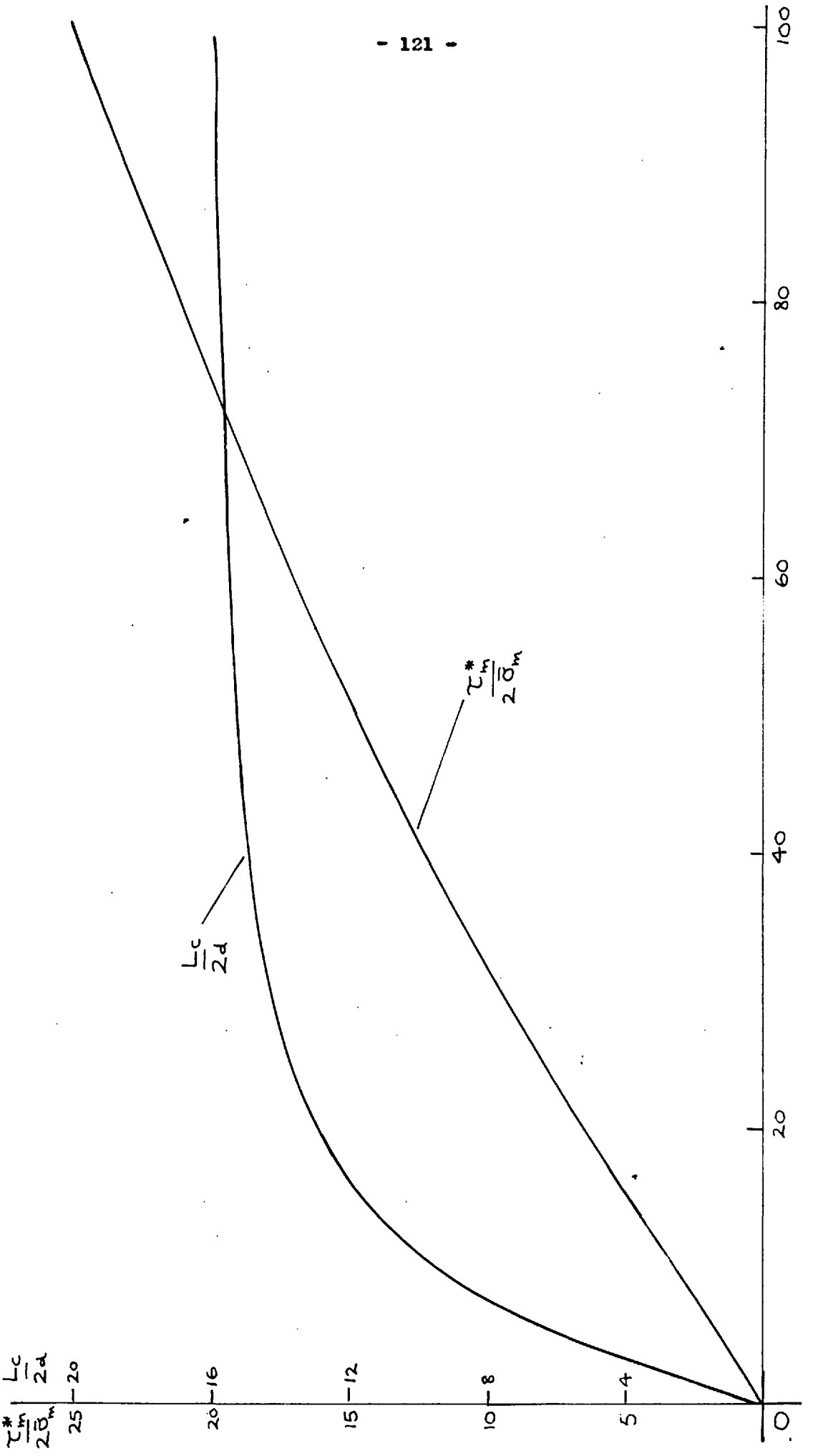

Fig. 4.8 : Effects of Varying Fibre/Matrix Elastic Ratio

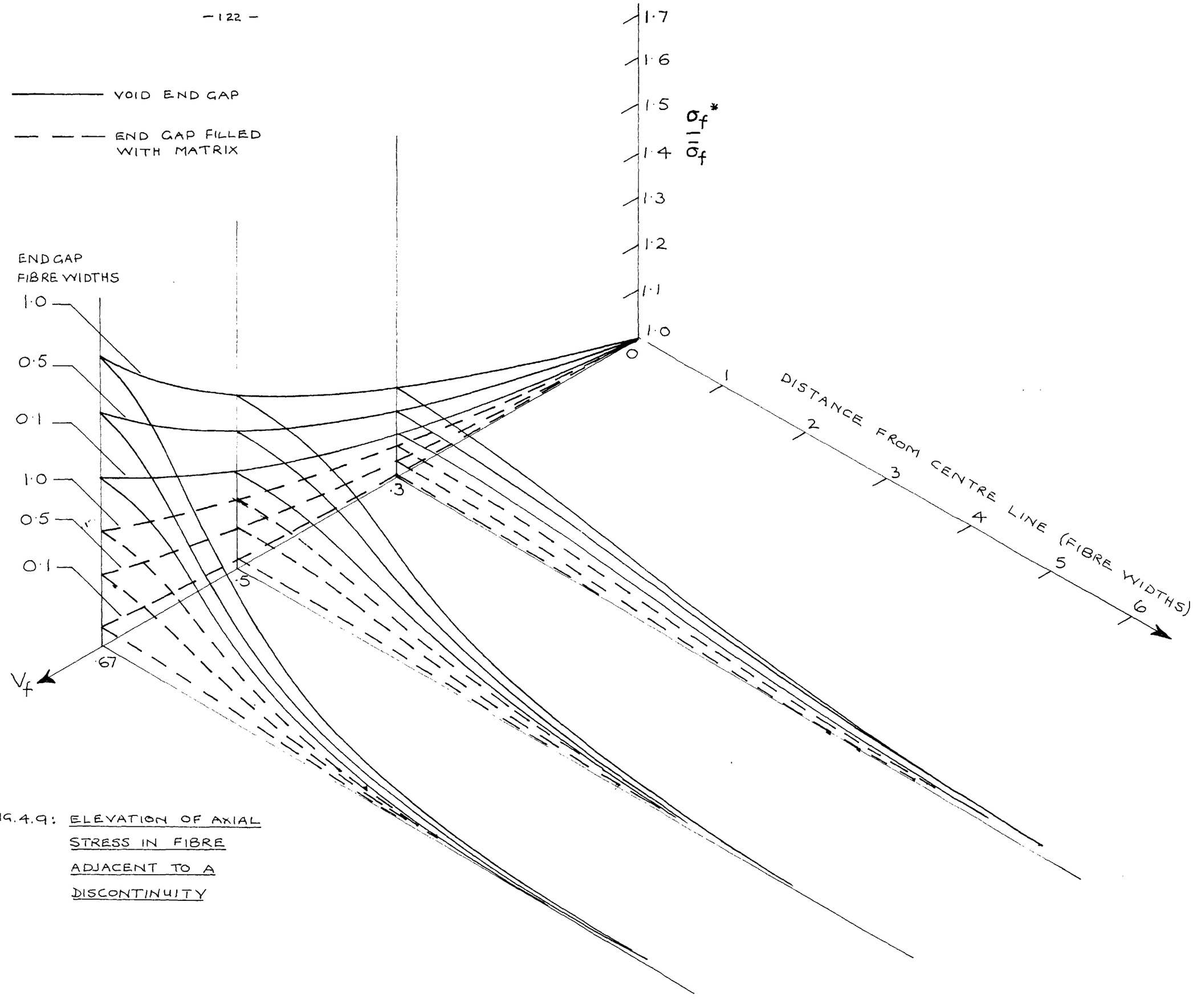

FIG. 4.9: ELEVATION OF AXIAL STRESS IN FIBRE ADJACENT TO A DISCONTINUITY

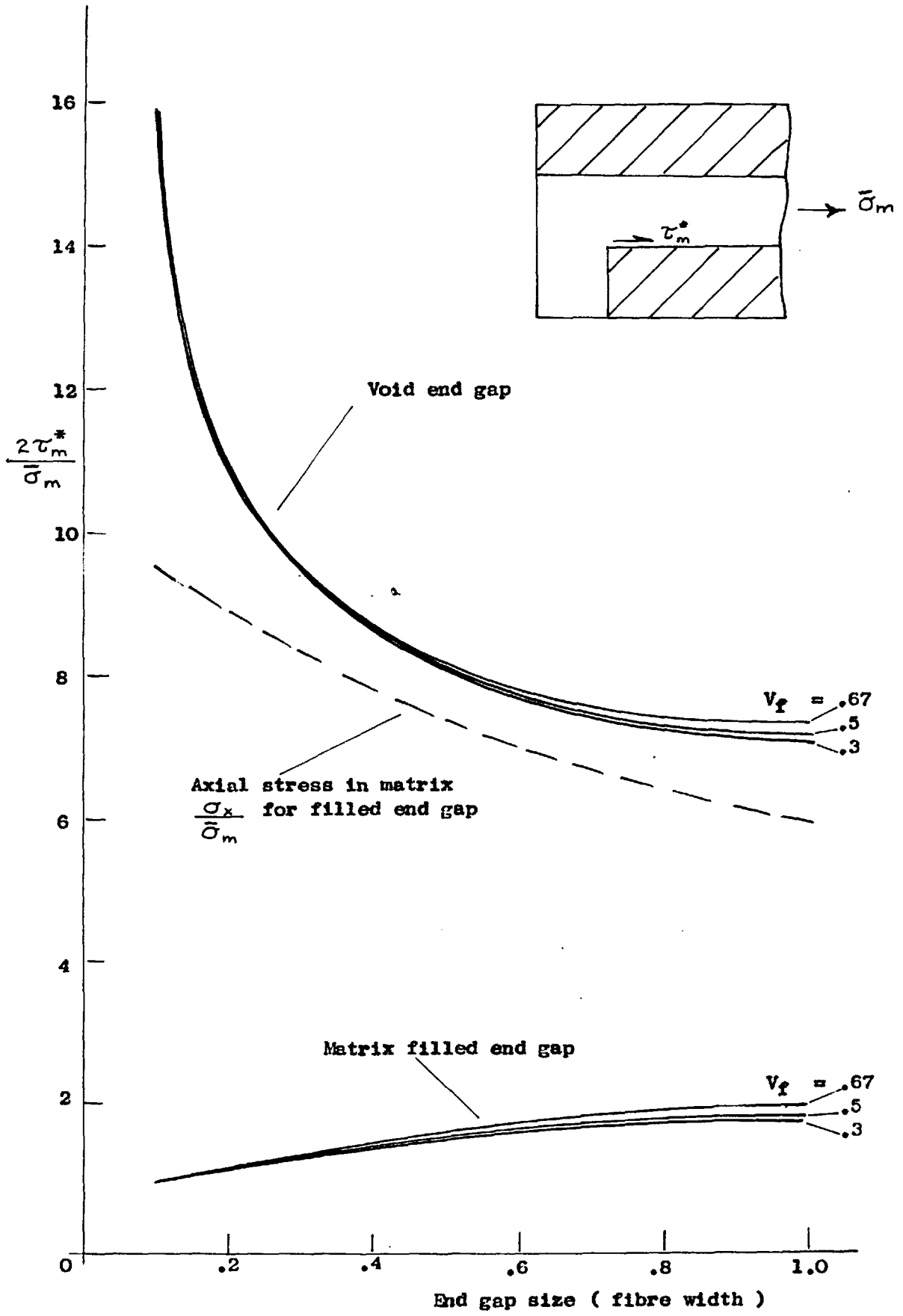

Fig. 4.10 : Maximum Interfacial Shear Stress v End Gap Size

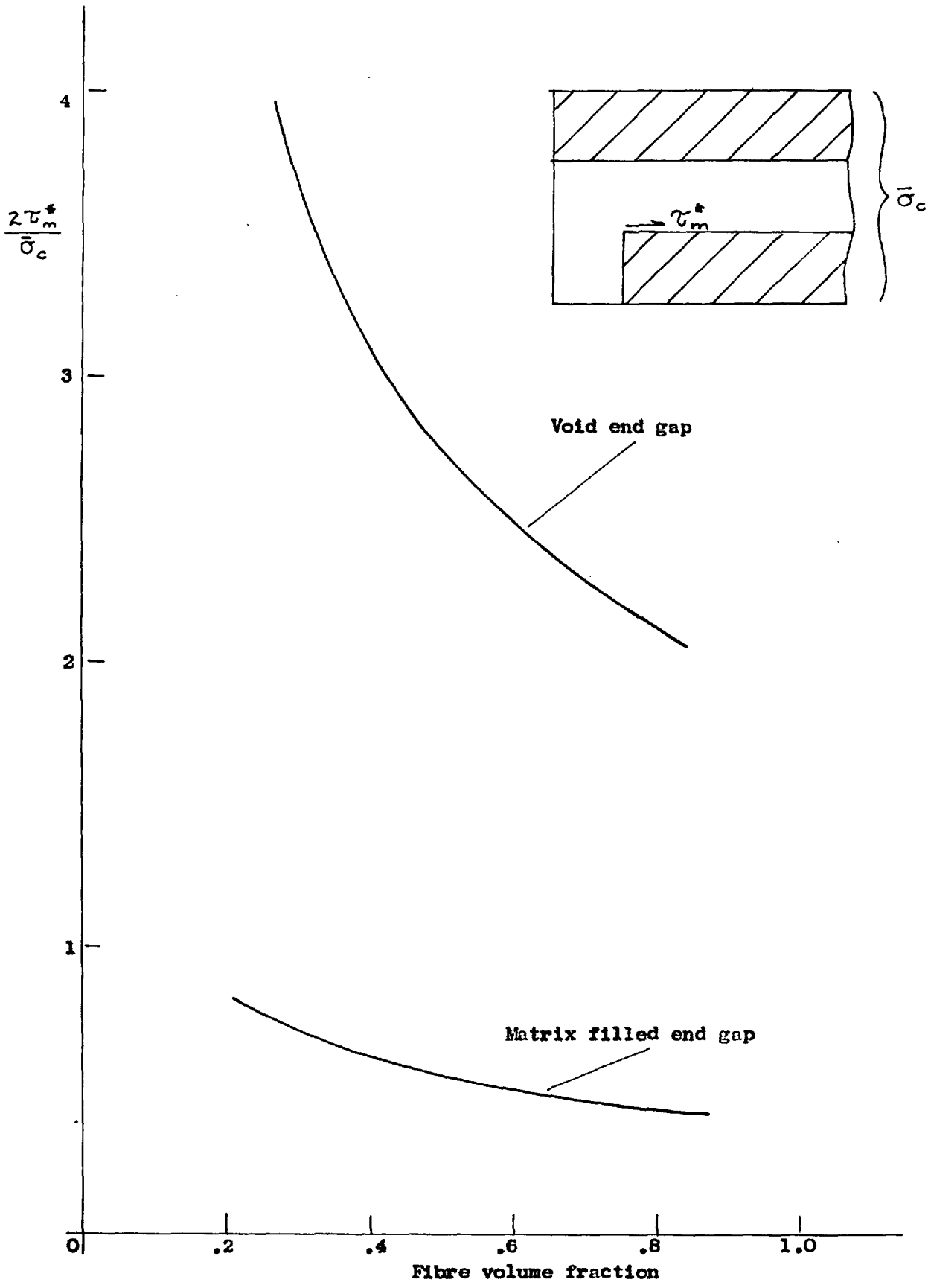

Fig. 4.11 : Maximum Interfacial Shear Stress v Fibre Volume Fraction

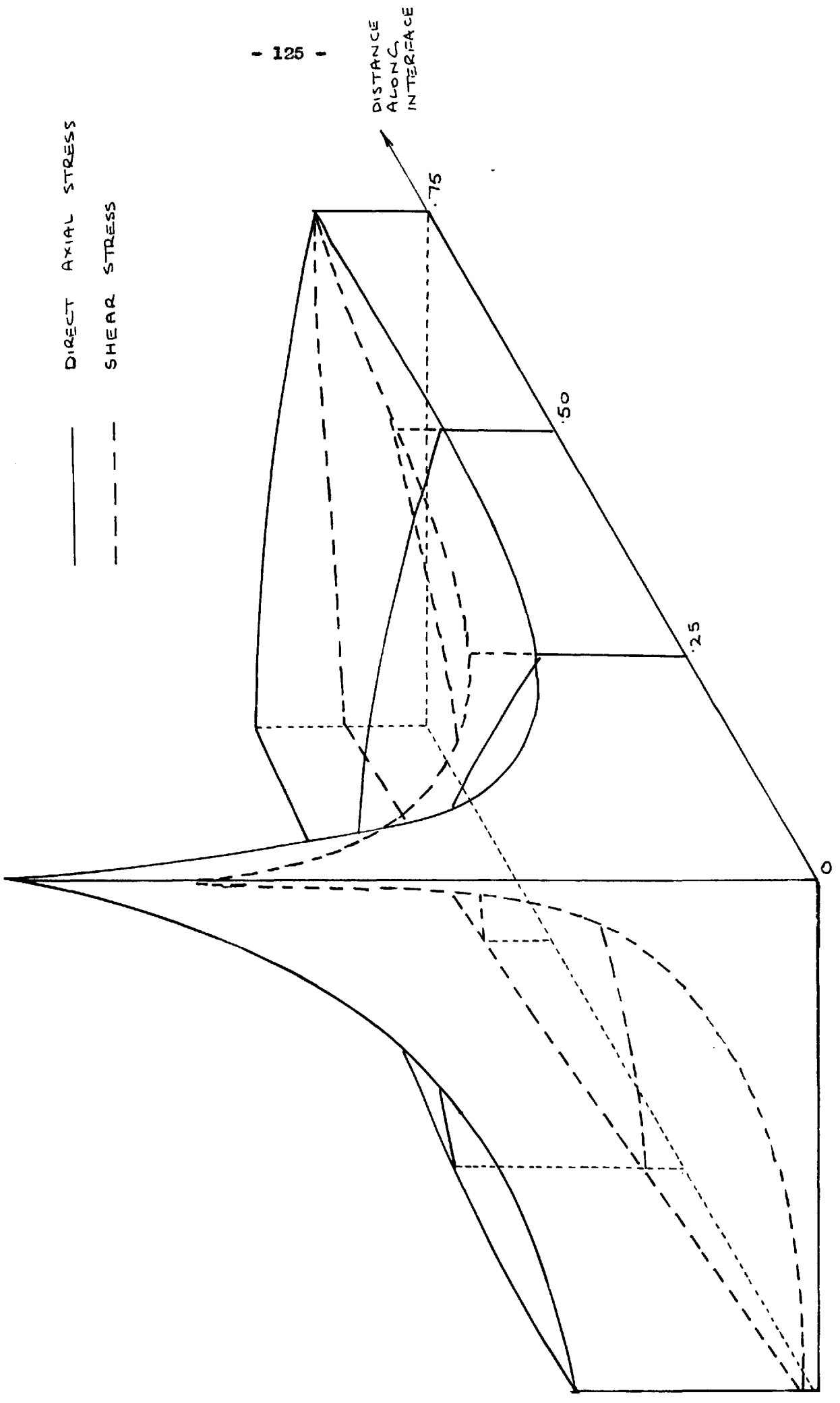

Fig. 4.12 : Stress Distribution Between Adjacent Fibres

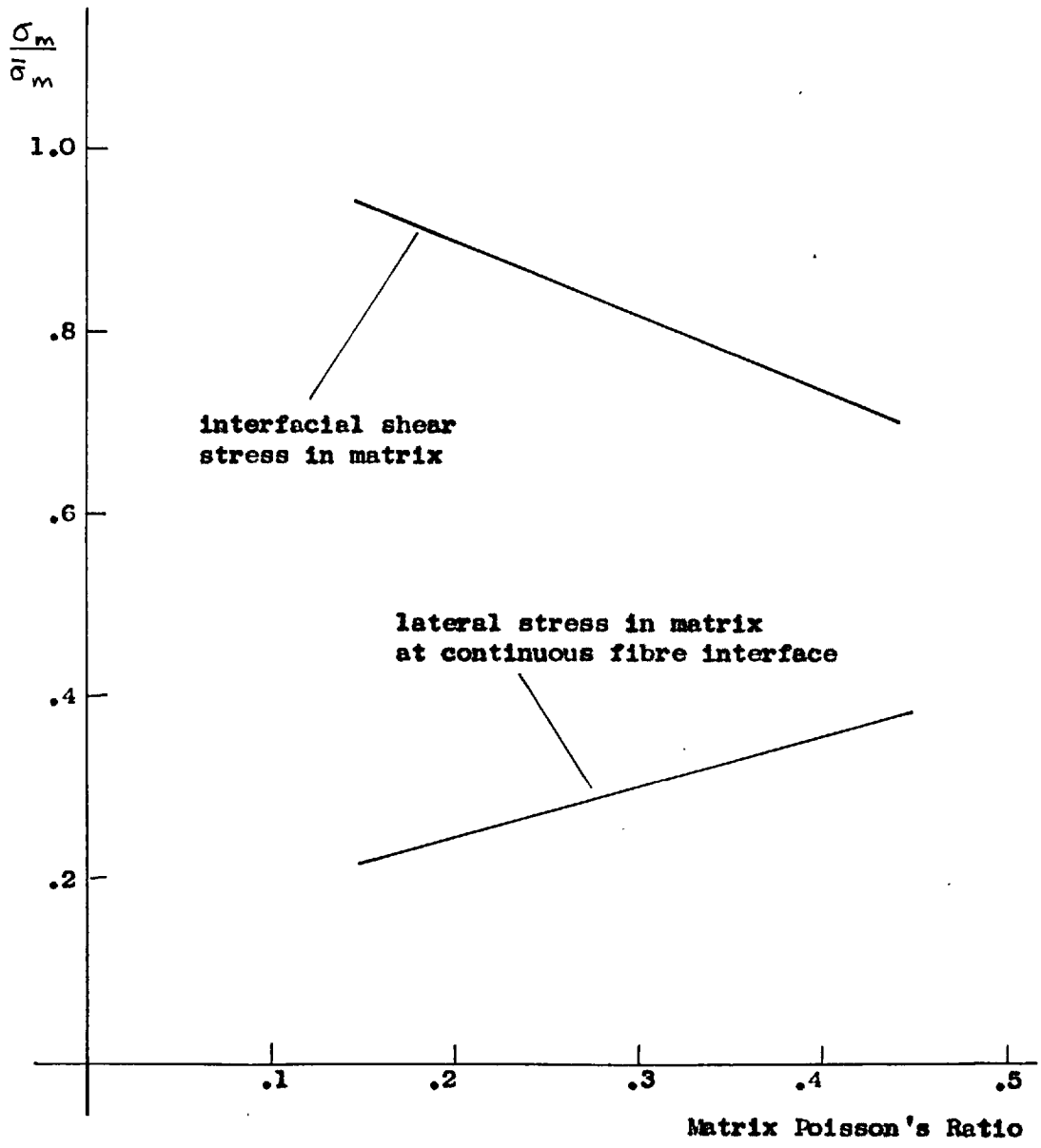

Fig. 4.13 : Effect of Poisson's Ratio

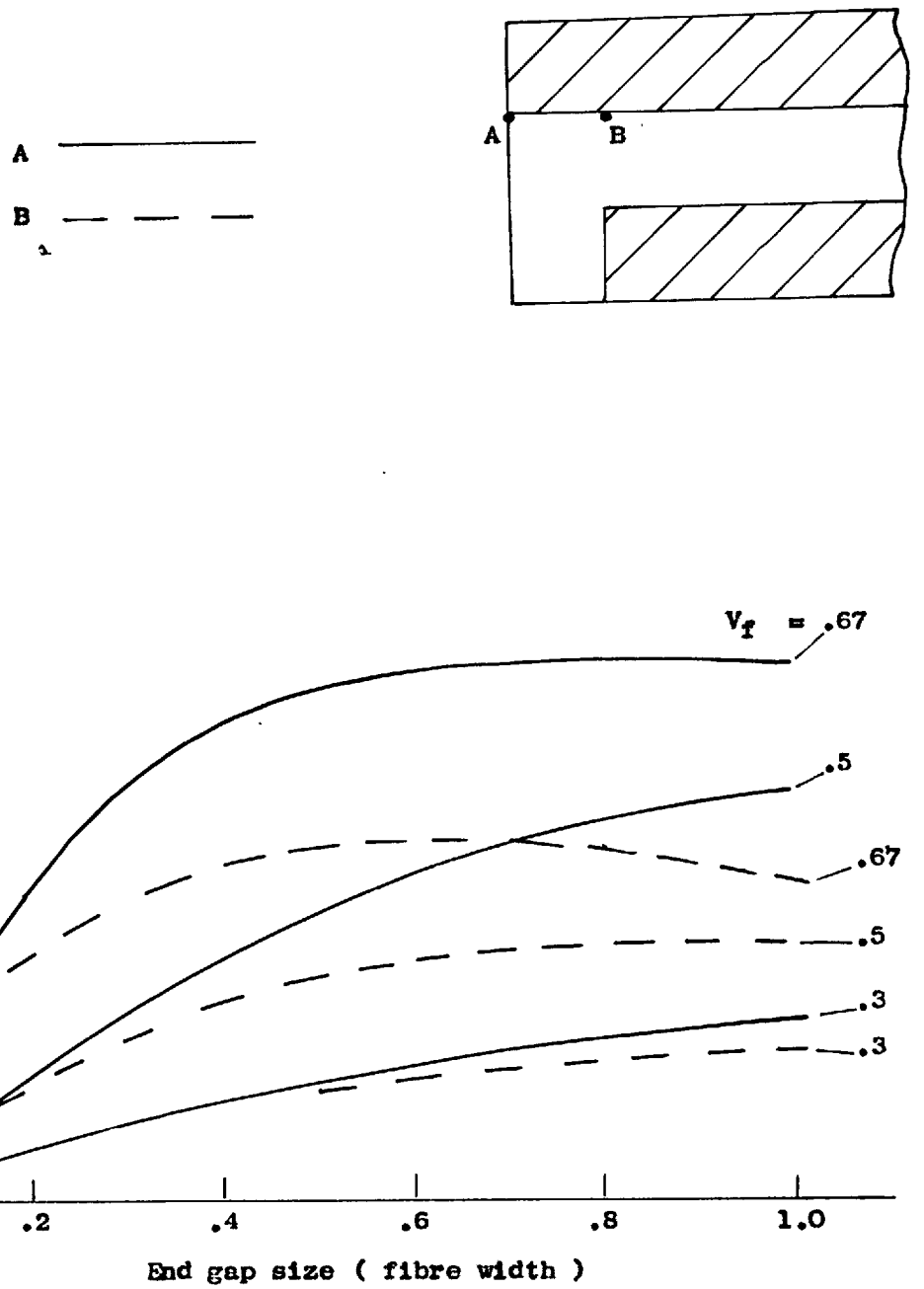

Fig. 4.14 : Lateral Direct Stress v End Gap Size

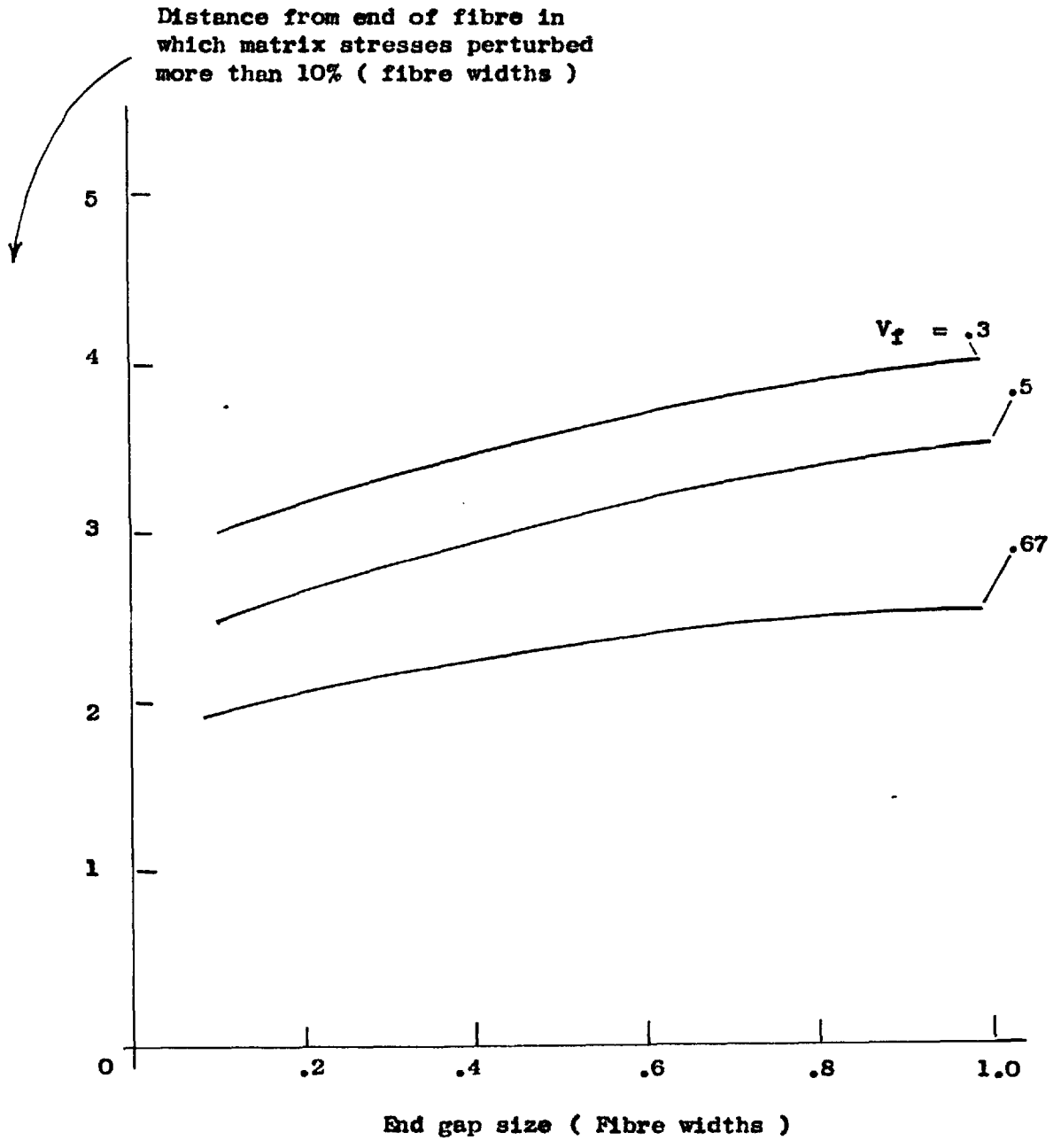

Fig. 4.15 : Extent of Matrix Perturbation

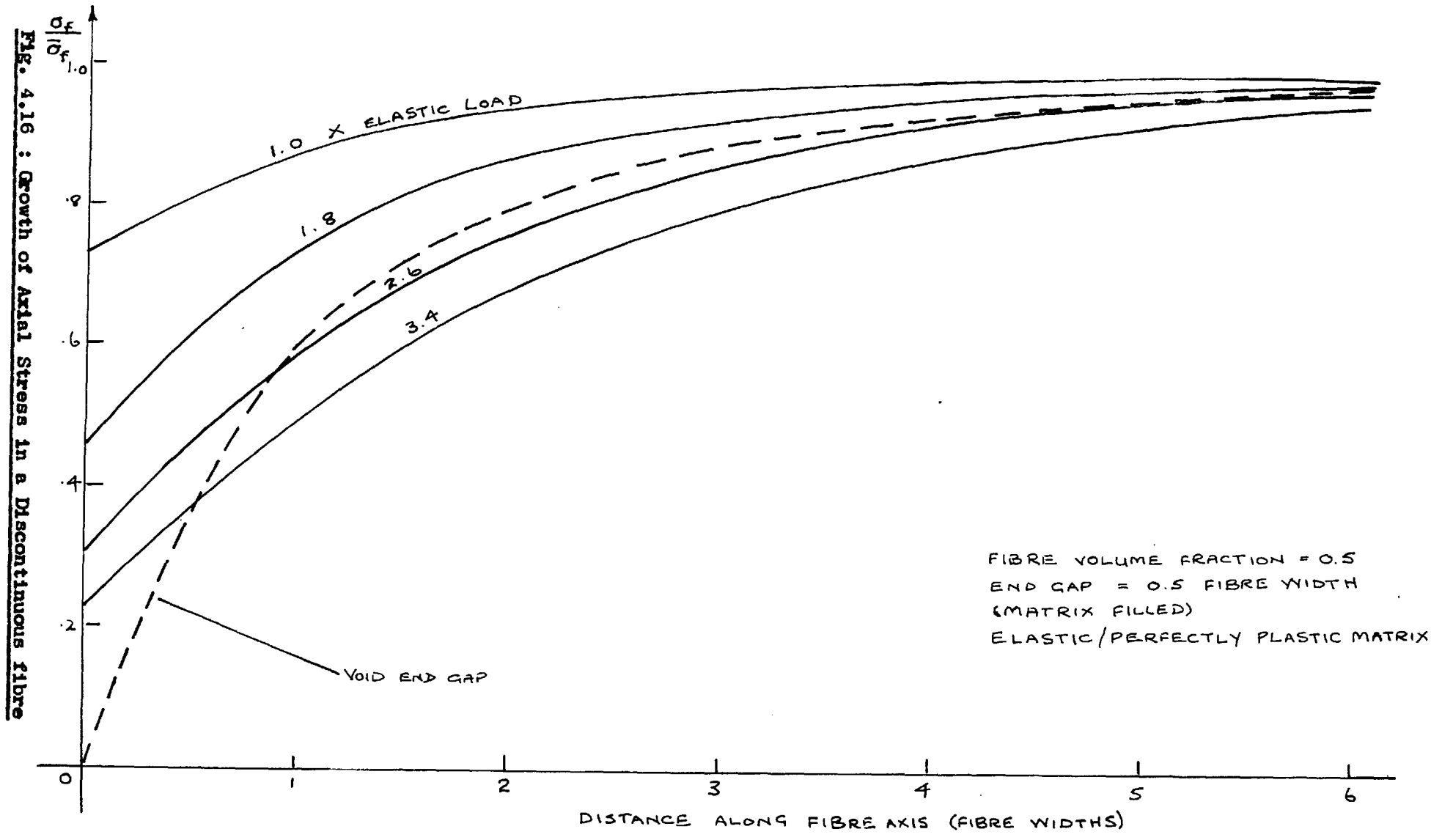

Fig. 4.16 : Growth of Axial Stress in a Discontinuous Fibre

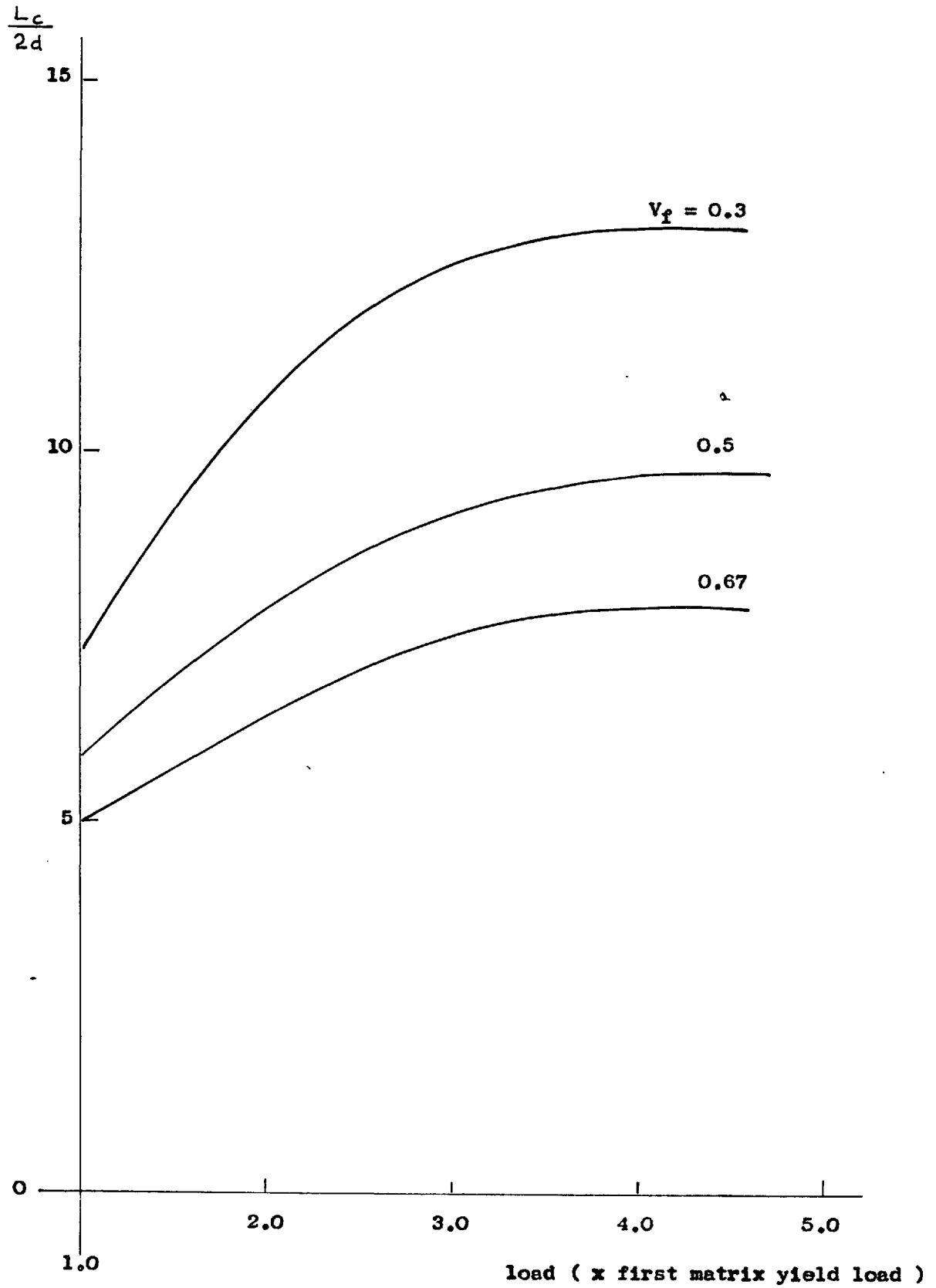

Fig. 4.17 : Variation of Critical Fibre Length as the Matrix Yield

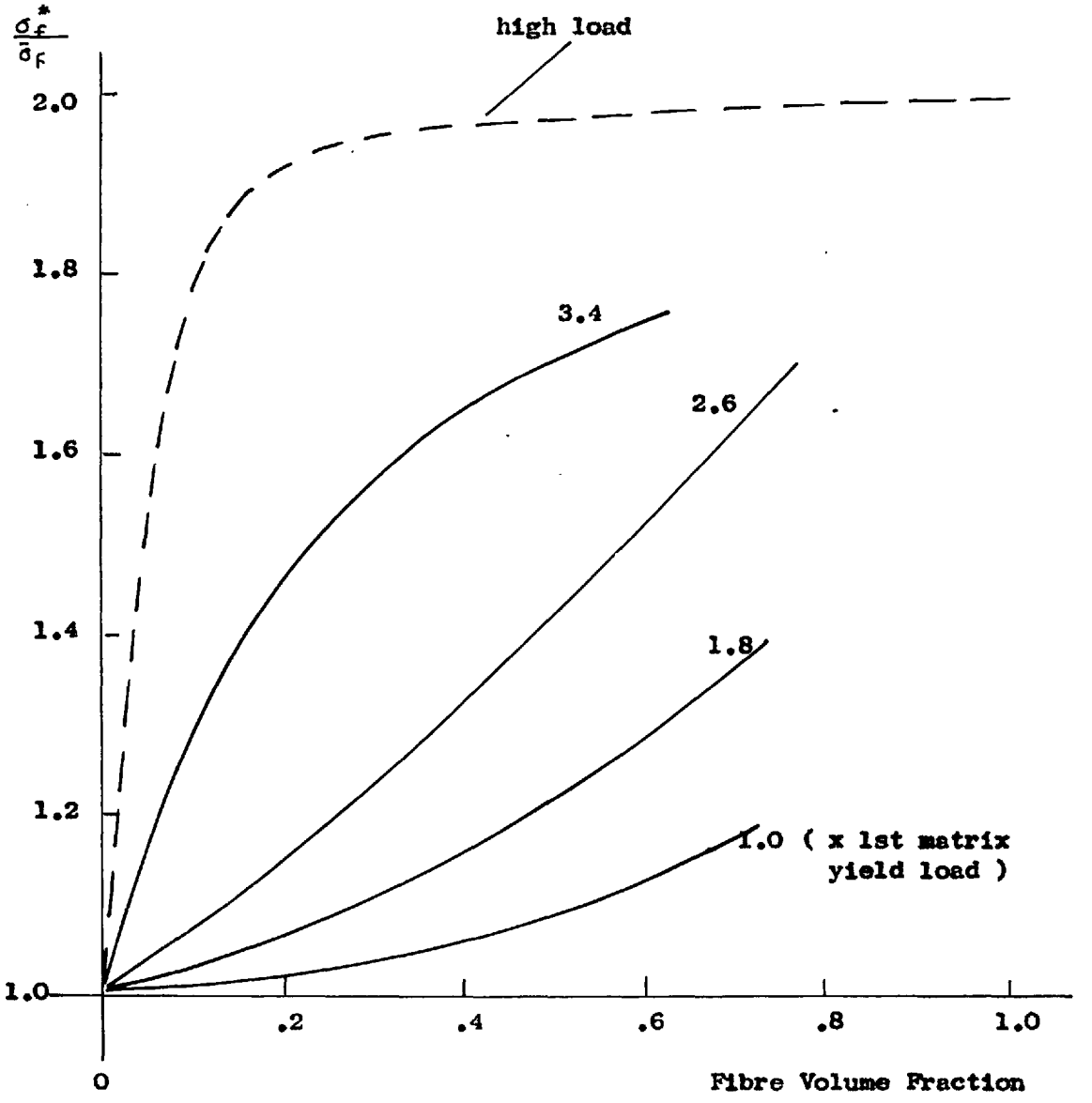

Fig. 4.18 : Elevation of Axial Stress in Fibre Adjacent to the Discontinuity when the Matrix has Yielded

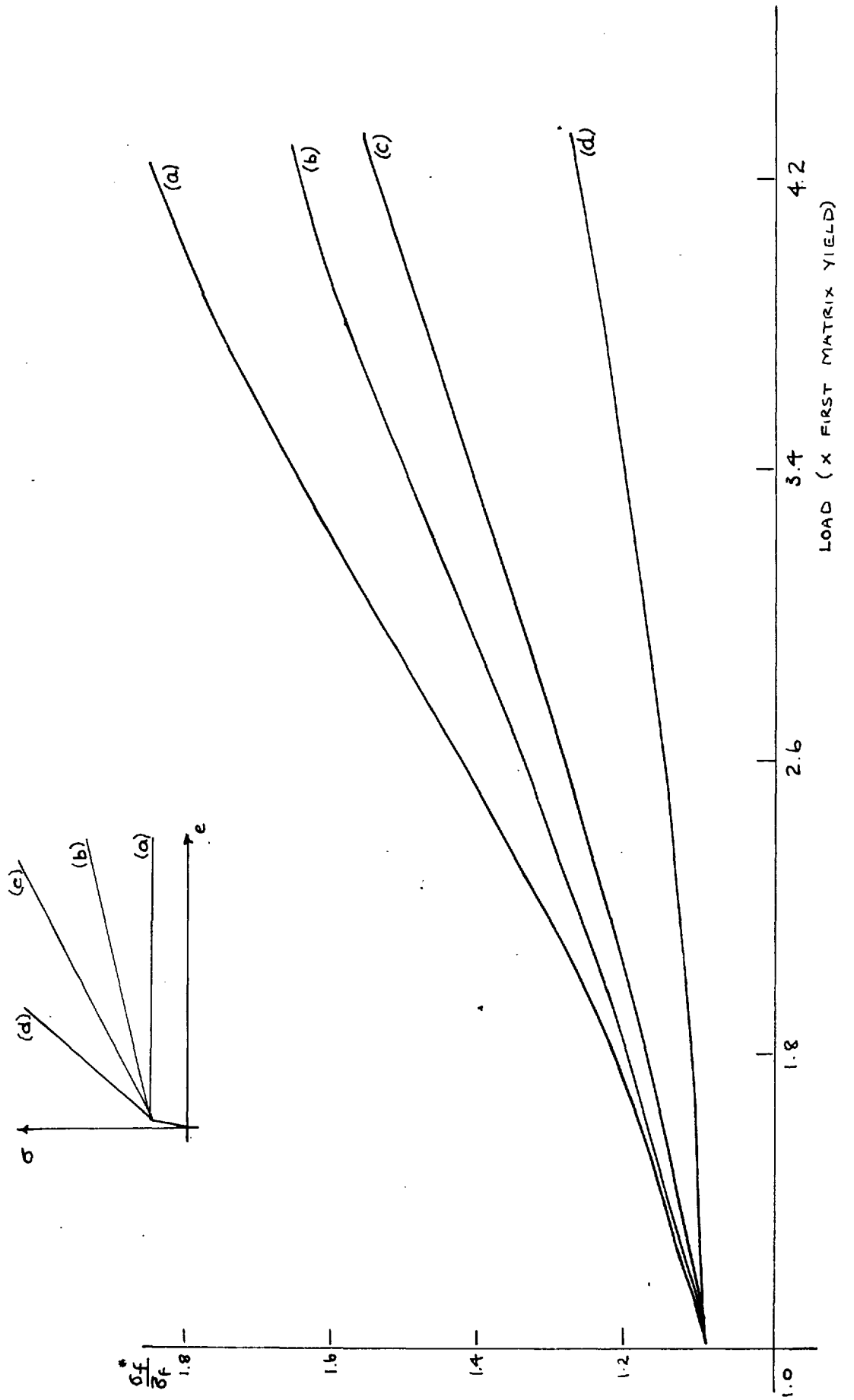

Fig. 4.19 : Effect of Matrix Work-hardening Characteristics on Continuous Fibre Axial Stress Concentration

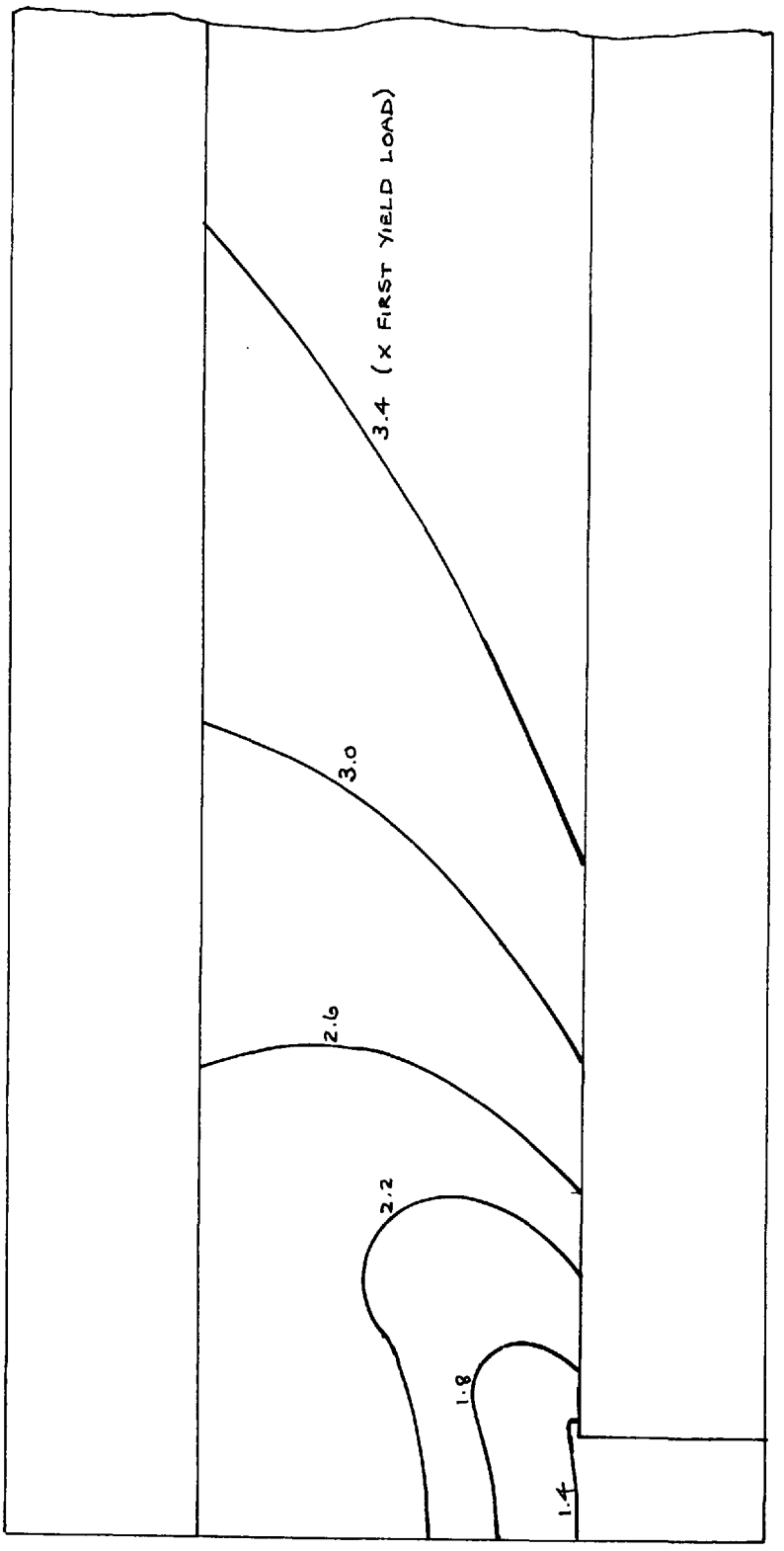

Fig. 4.20 : Growth of Plastic Enclaves

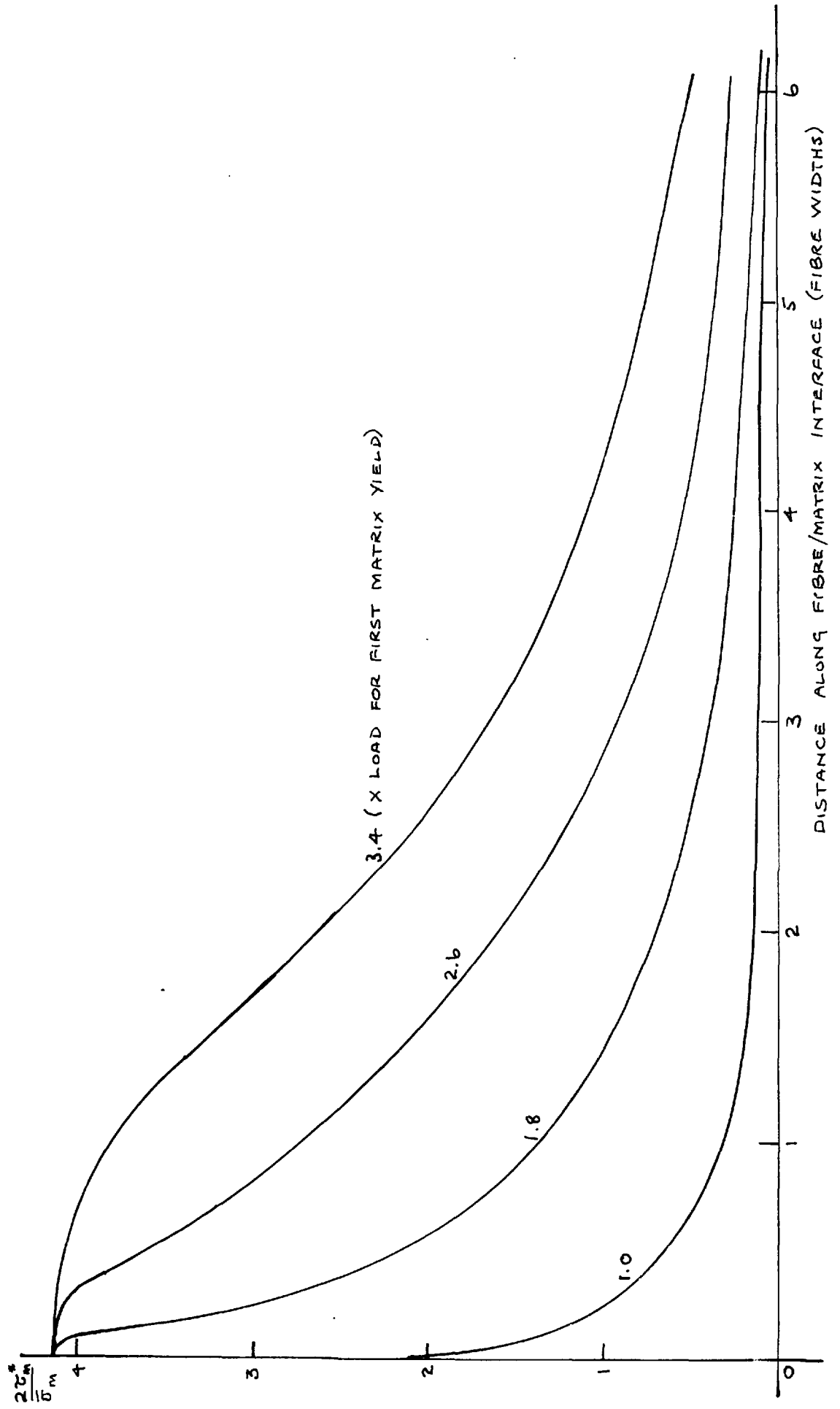

Fig. 4.21 : Variation of matrix shear stress along fibre/matrix interface

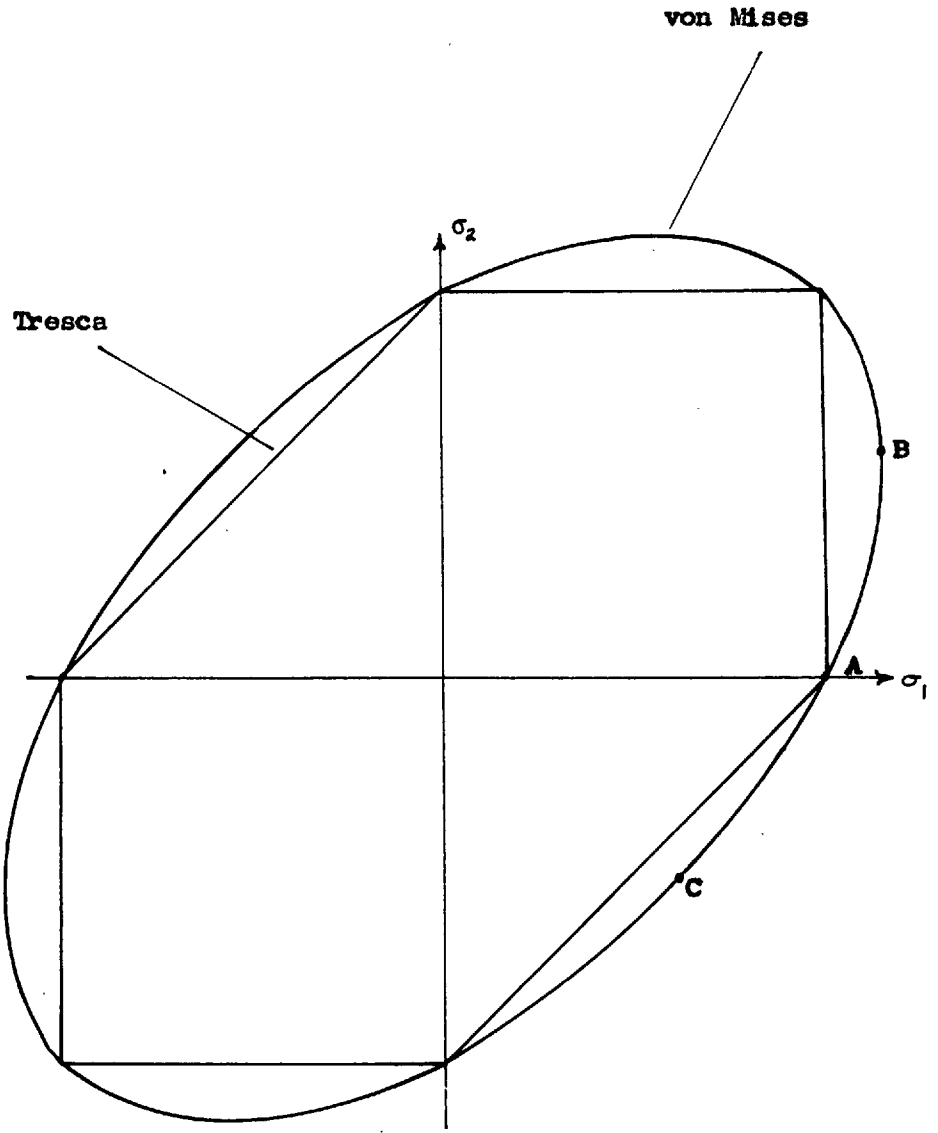

Fig. 4.22 : Criteria of Yielding

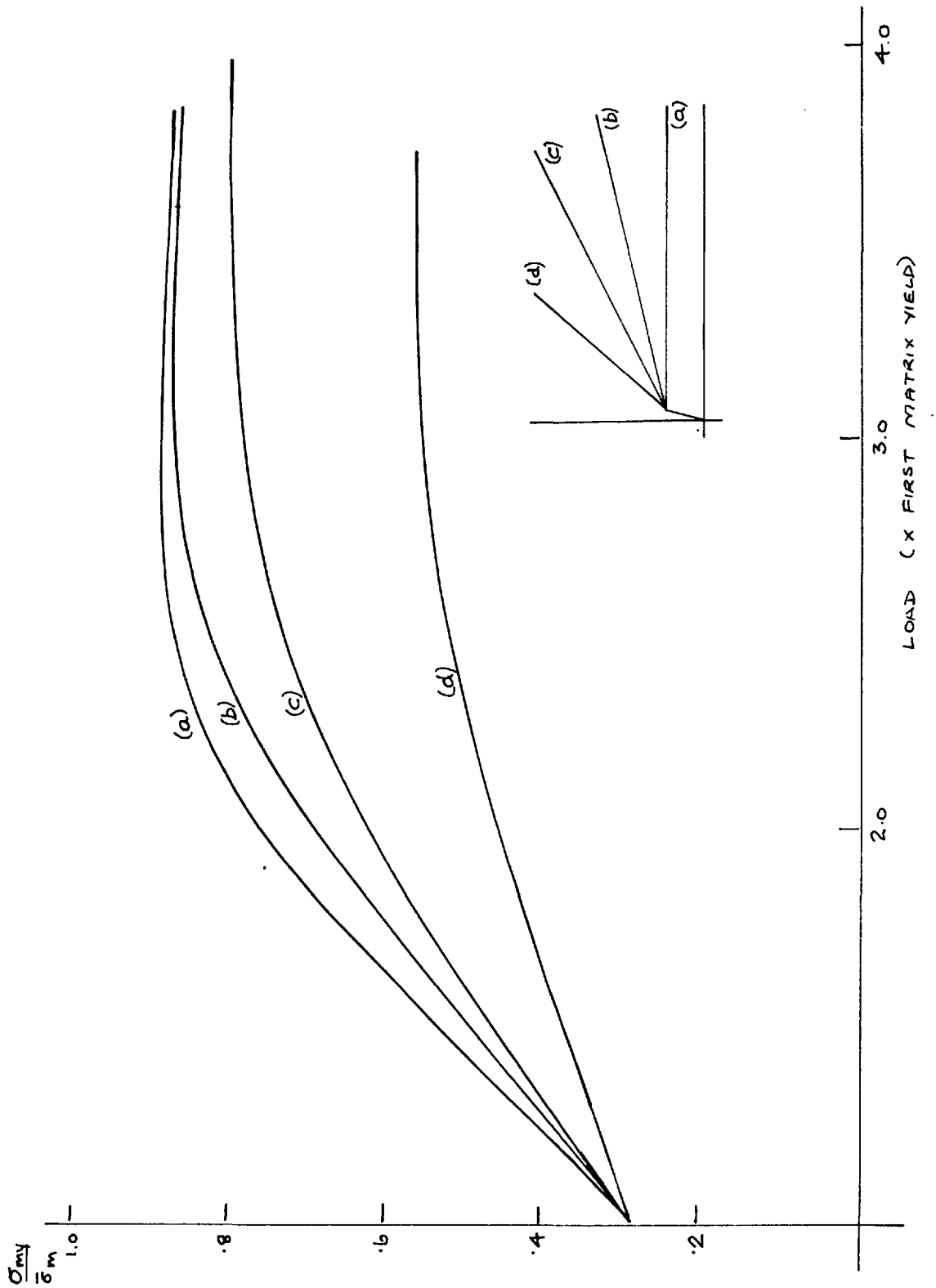

Fig. 4.23 : Variations in Lateral Matrix Stress on the Interface of a Fibre Adjacent to the Discontinuity

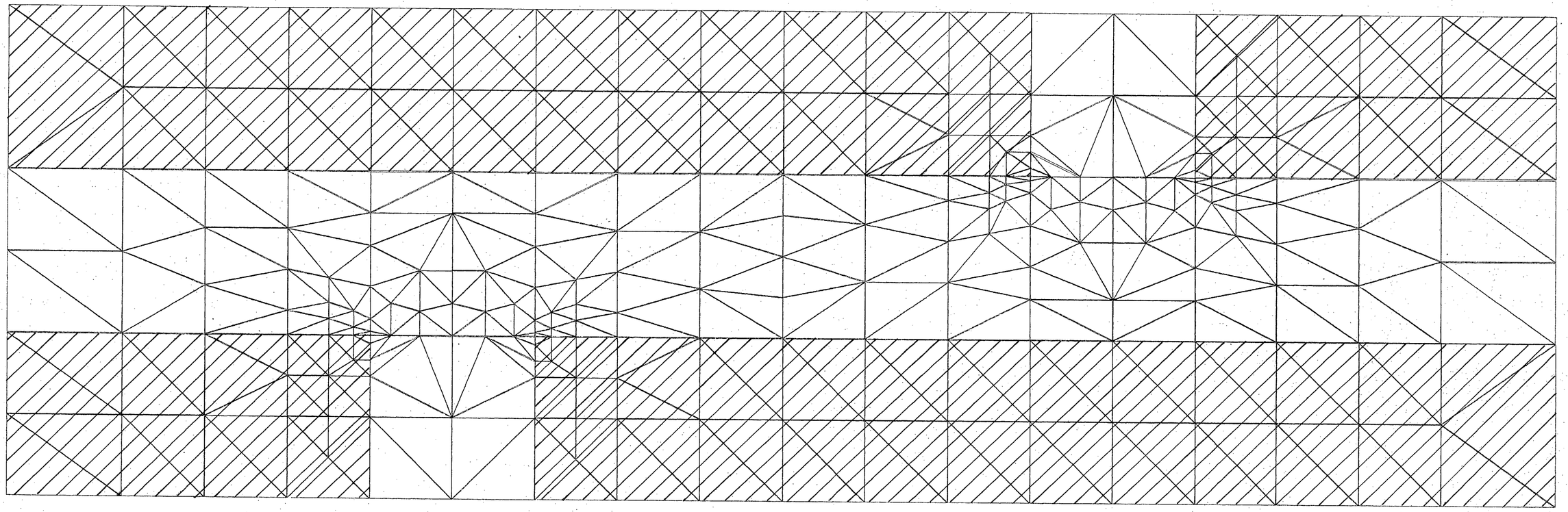

FIG. 5.1 : MIDDLE SECTION OF INTERACTING DISCONTINUITY MESH

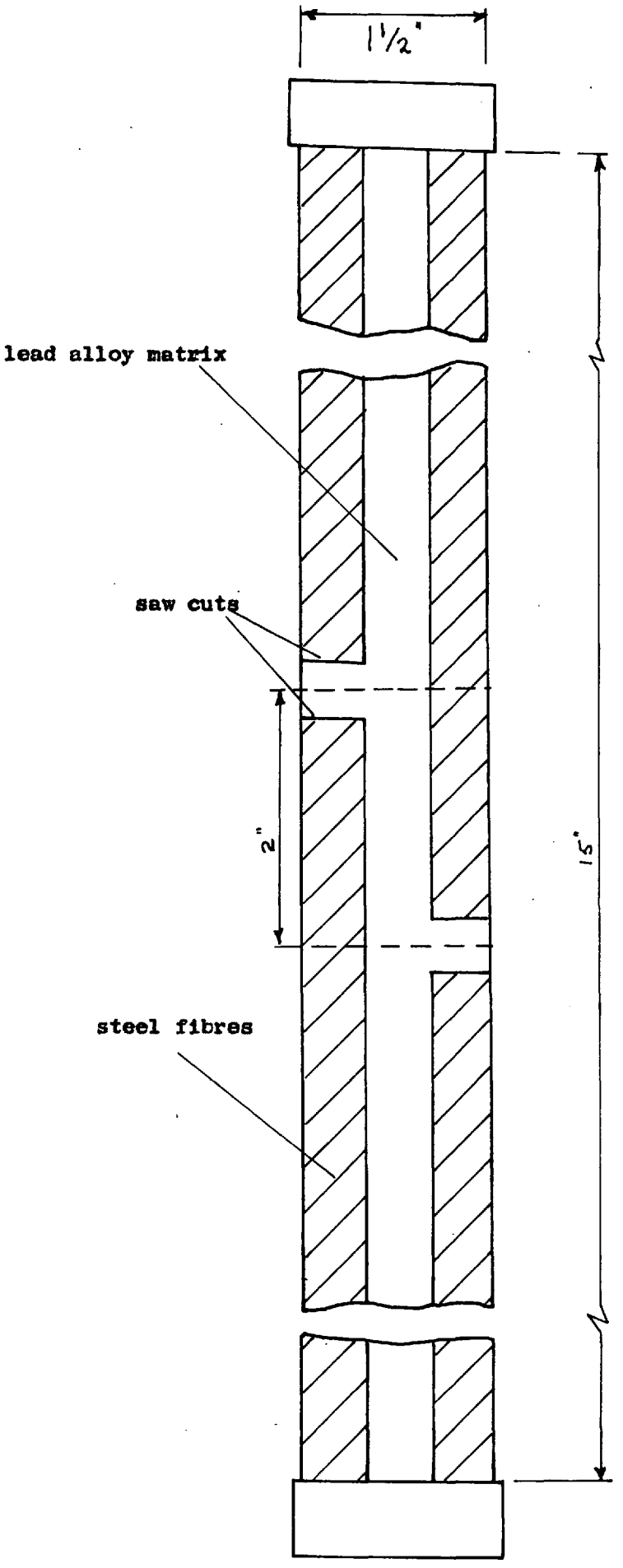

Fig. 5.2 : Experimental Interacting Discontinuity Model

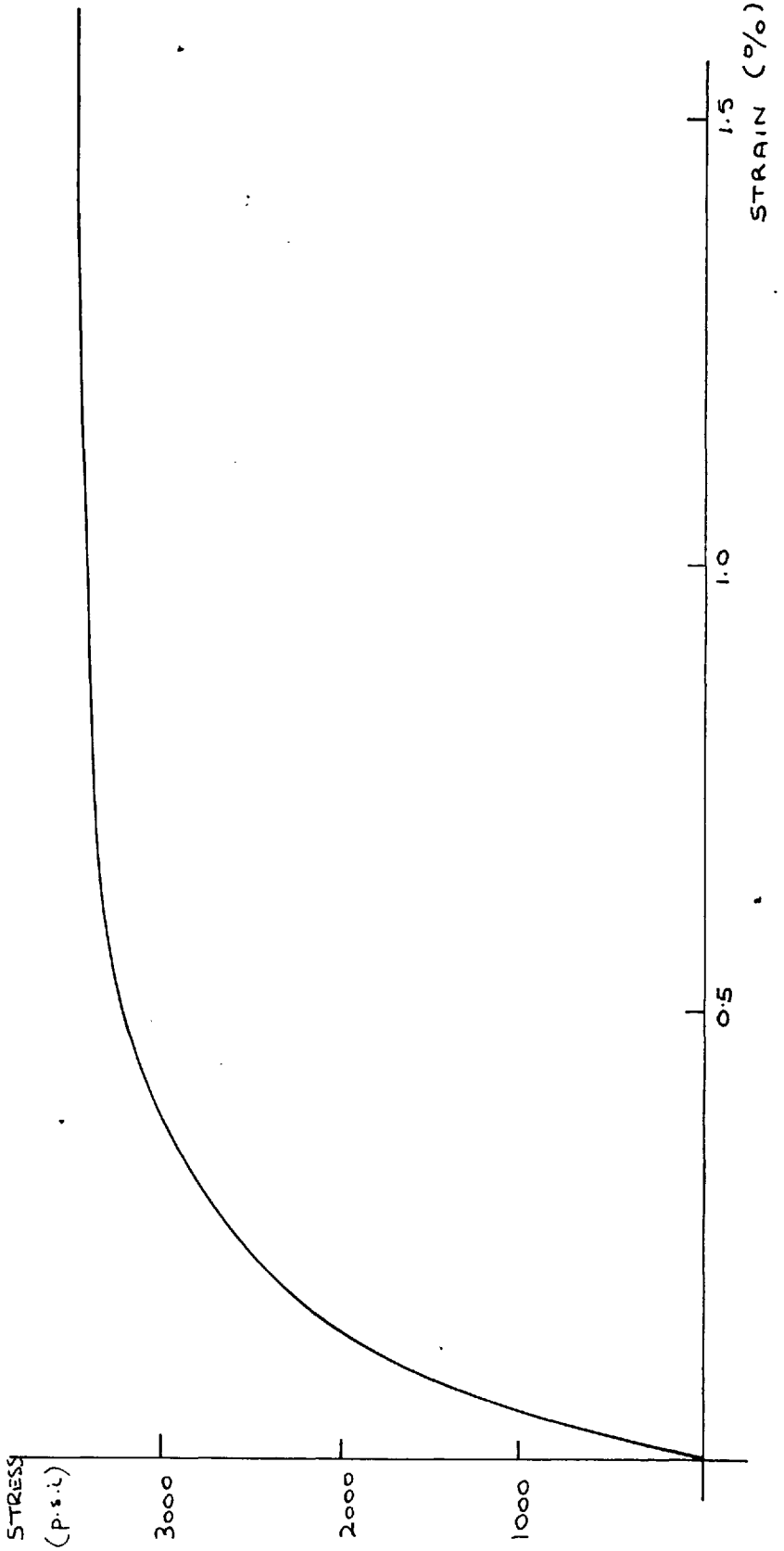

Fig. 5.3 : Stress-Strain Curve for Lead Alloy

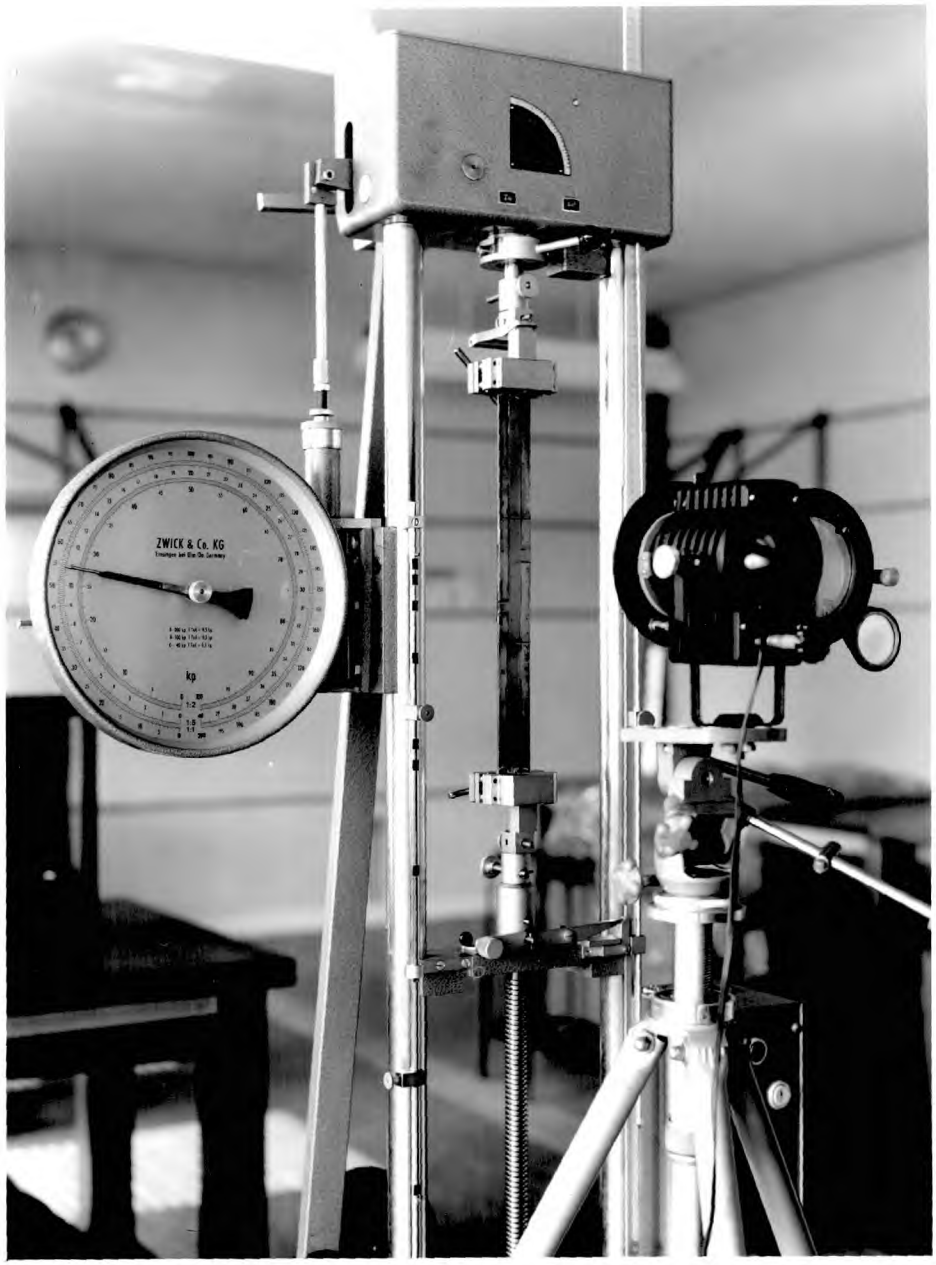

Fig. 5.4 : Photoelastic Coating Test Set Up



Fig. 5.5 : Photoelastic Coating Fringe Pattern

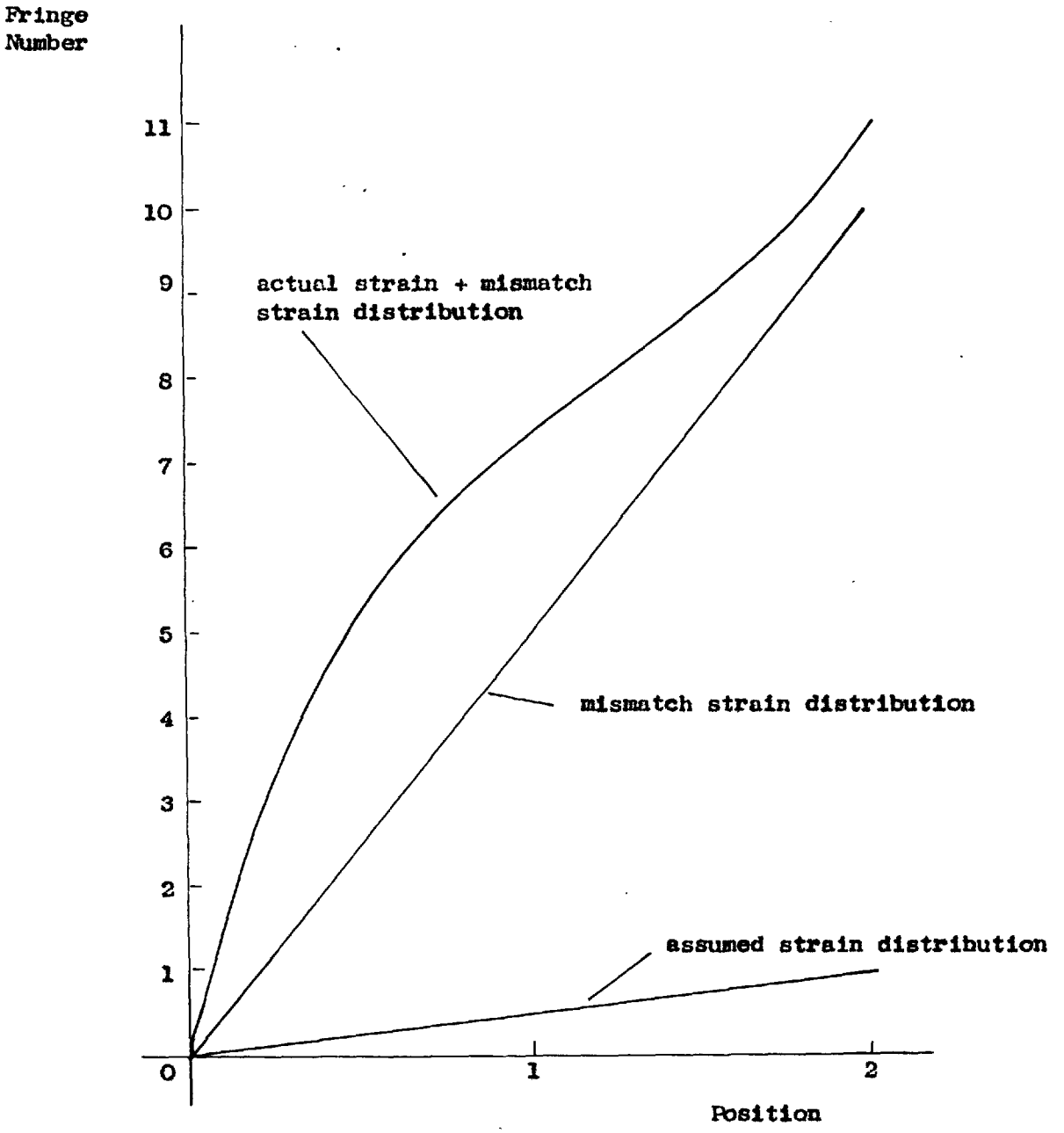

Fig. 5.6 : Mismatch Procedure



Fig. 5.7 : Moiré Fringe Pattern

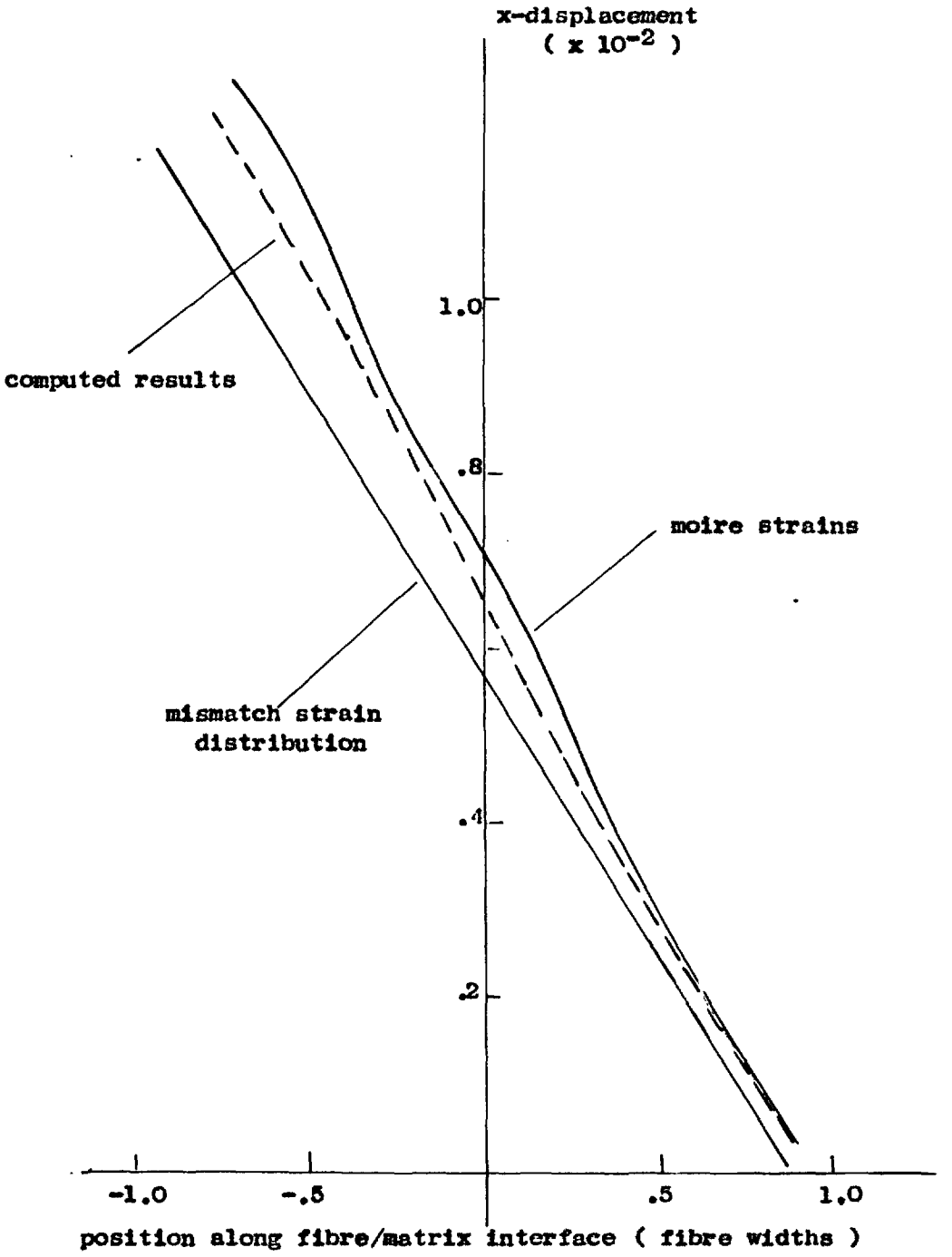

Fig. 5.8 : Comparison of Moiré and Computed Results

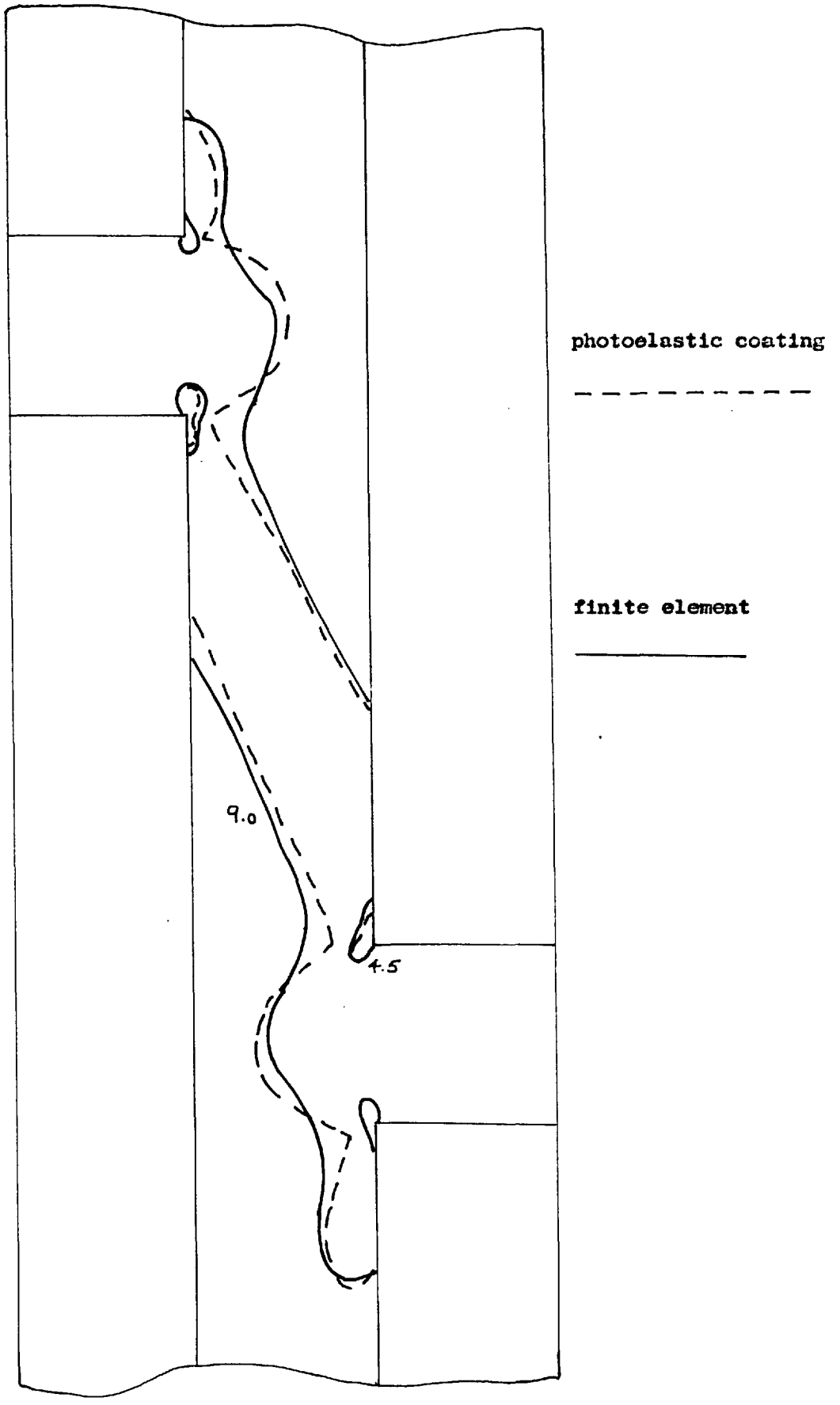

Fig. 5.9 : Comparison of Plastic Enclave Shapes as Predicted by the Finite Element and Photoelastic Coating Methods

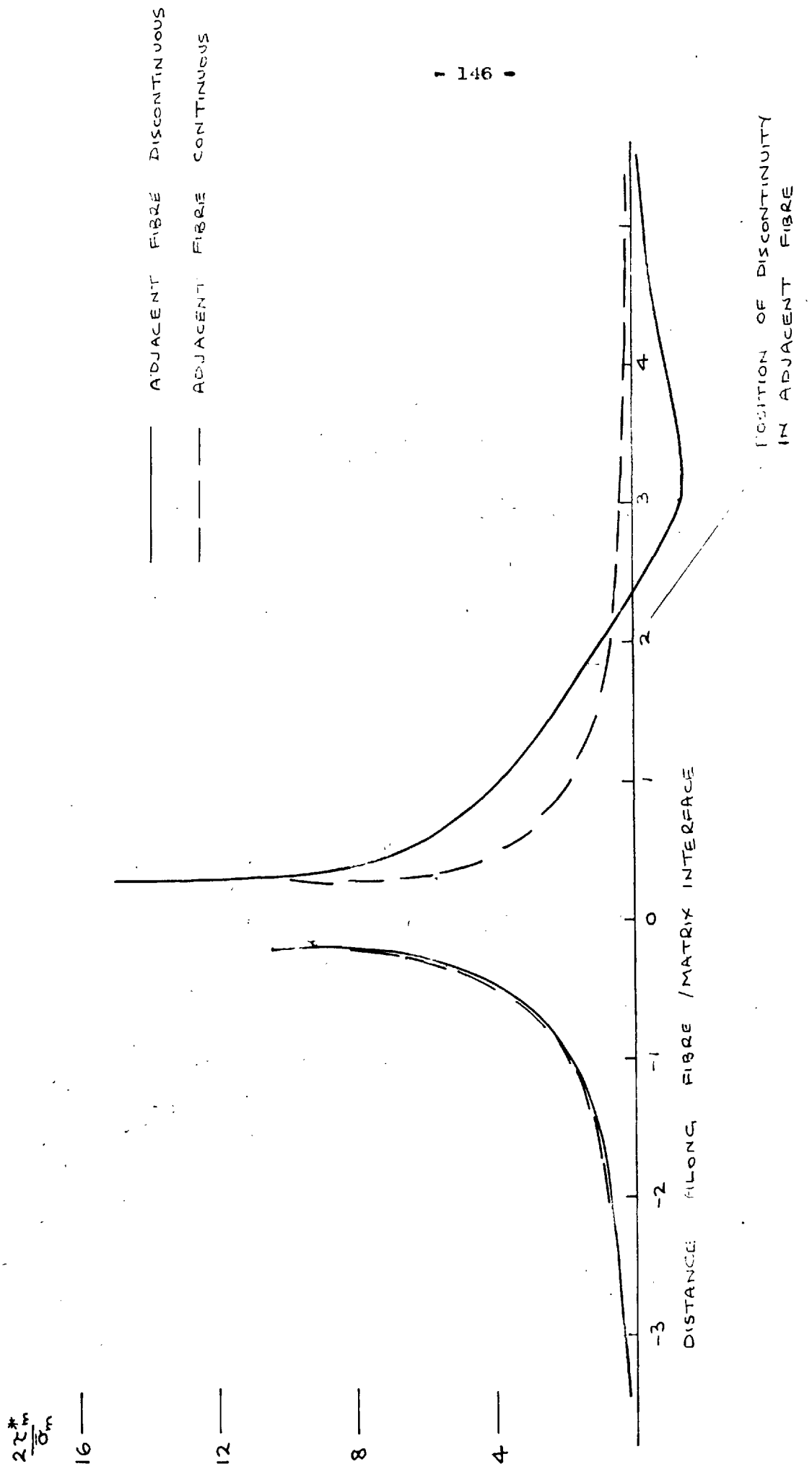

Fig. 5.10 : Interfacial Shear Stress Distribution

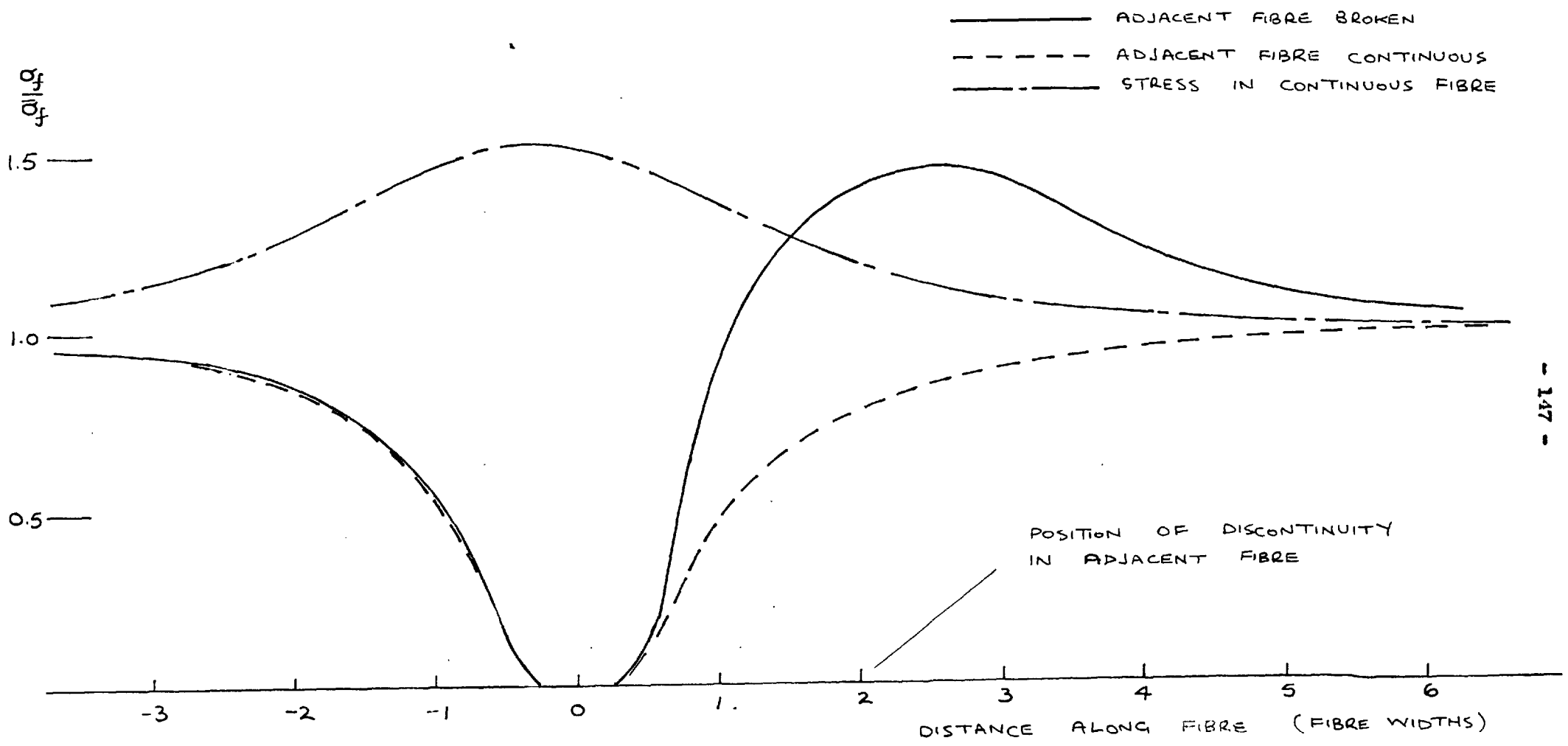

FIG. 5.11 : FIBRE AXIAL STRESS DISTRIBUTION

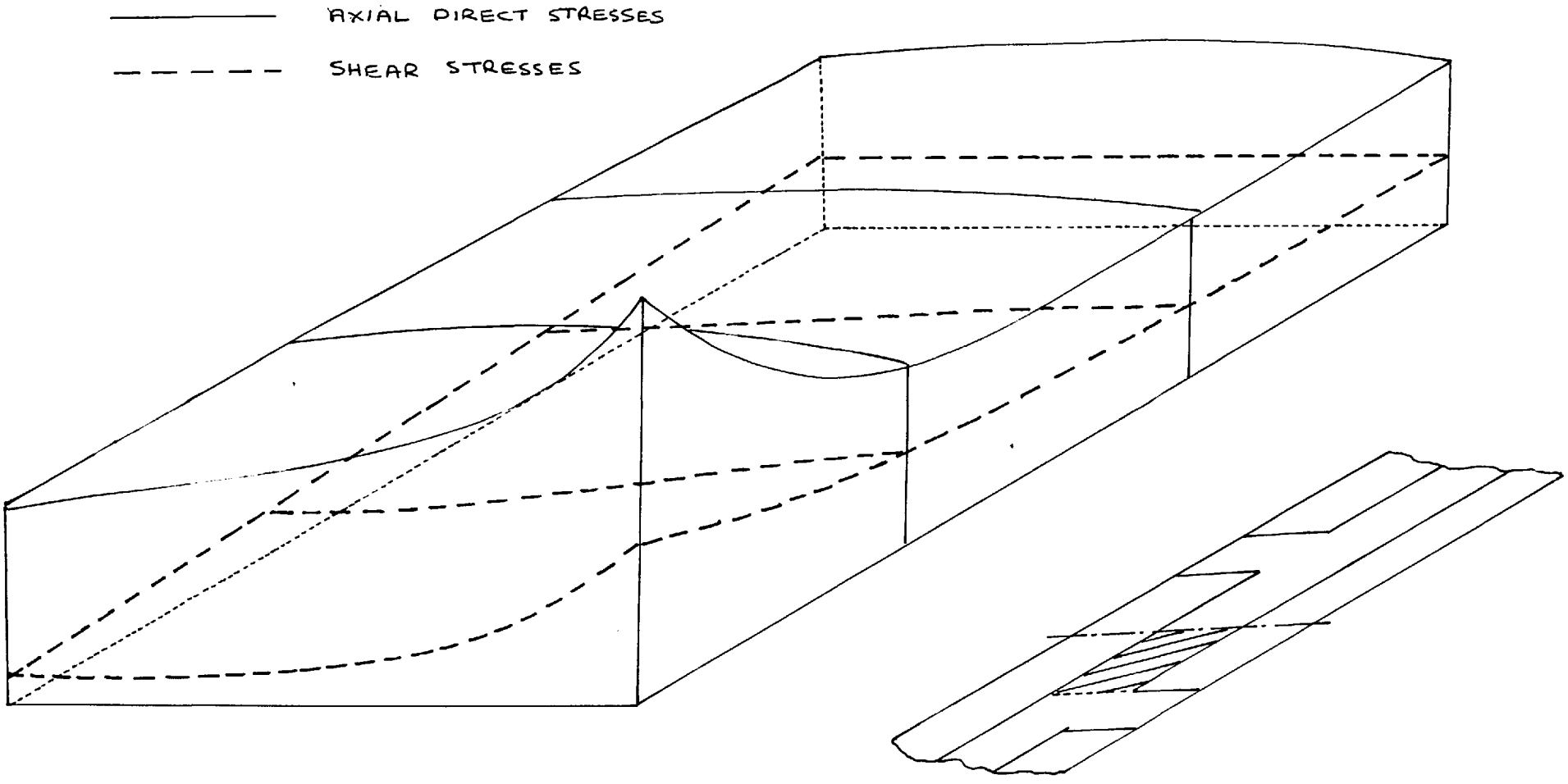

FIG. 5.12 : ELASTIC STRESS DISTRIBUTION IN REGION BETWEEN DISCONTINUITIES

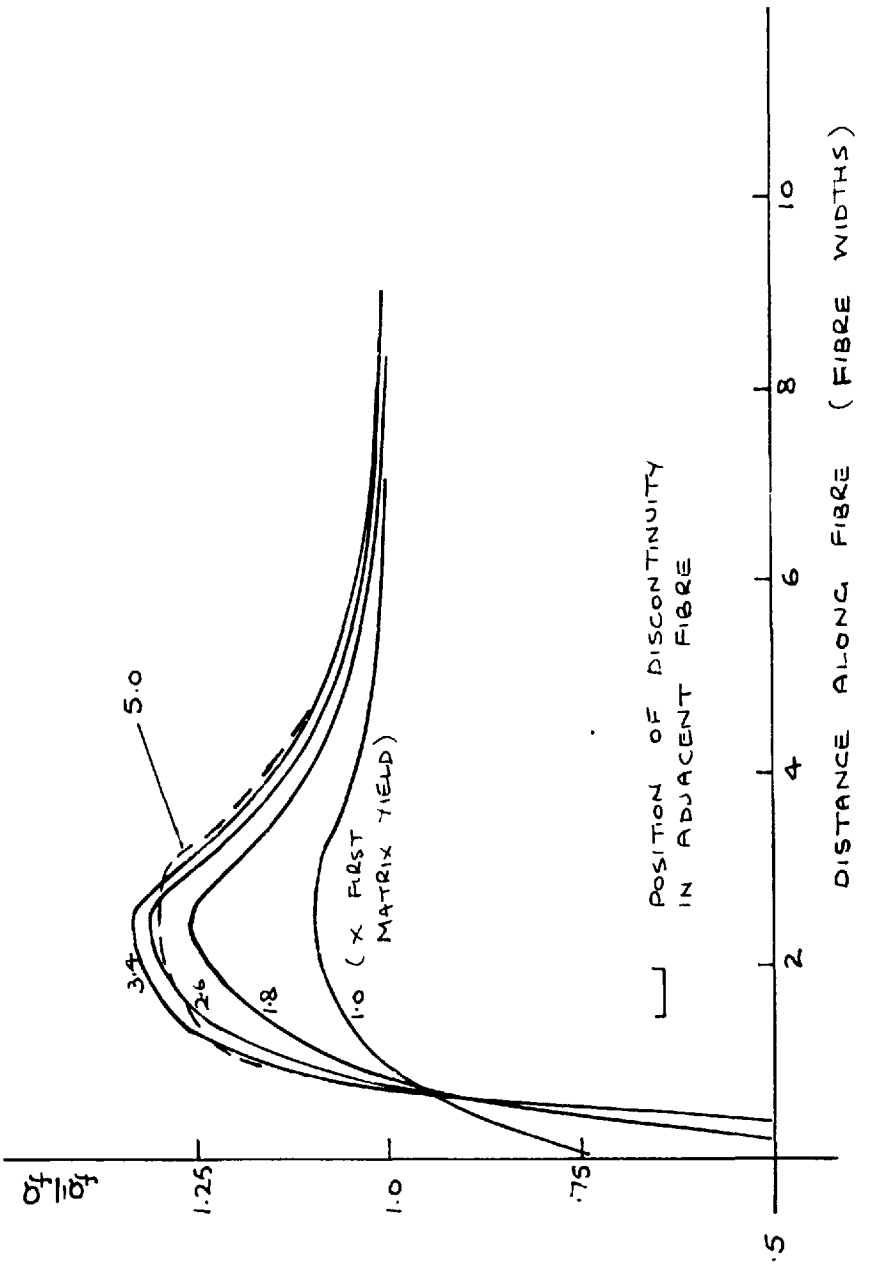

Fig. 5.13 : Axial Stress Distribution in Fibre when Adjacent Fibres Discontinuous

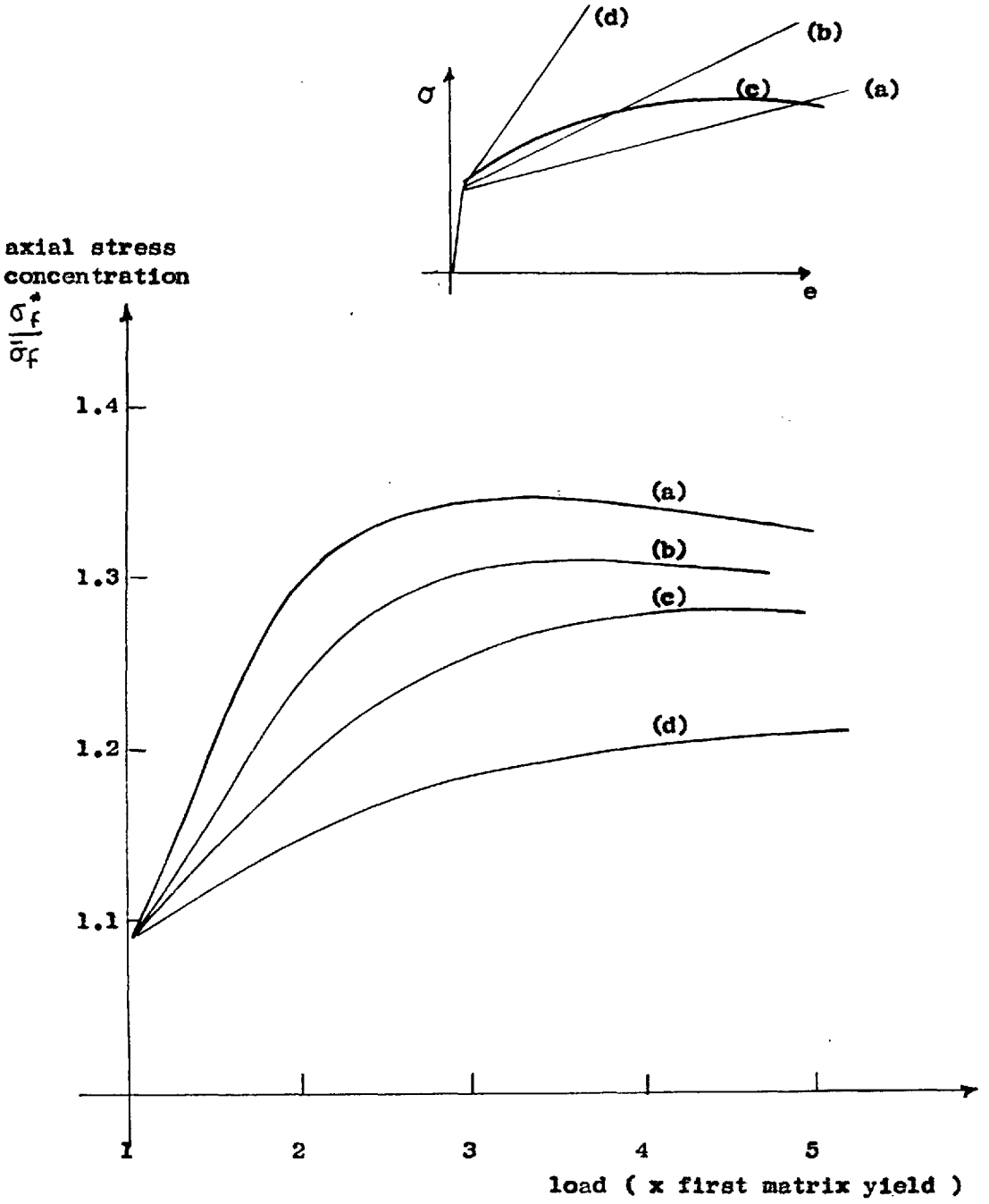

Fig. 5.14 : Effect of matrix work-hardening characteristics on the axial stress in a fibre opposite a discontinuity

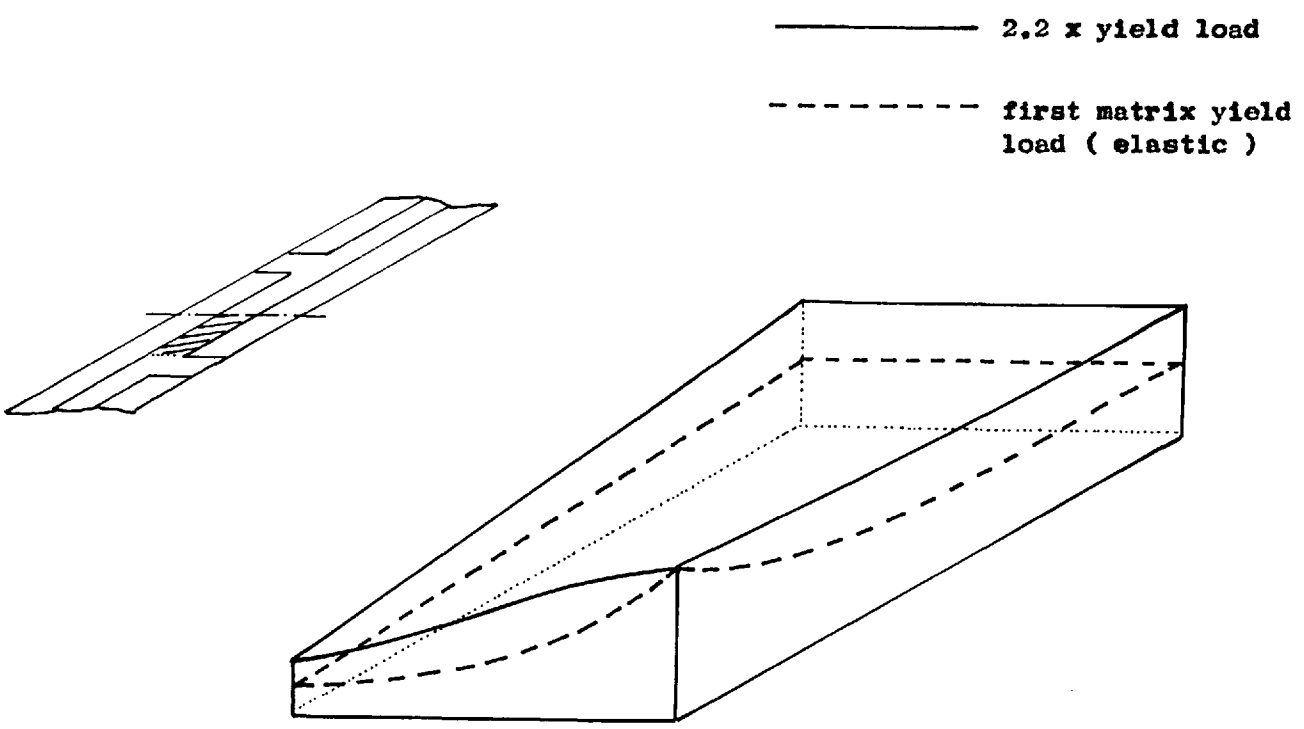

Shear stress contours

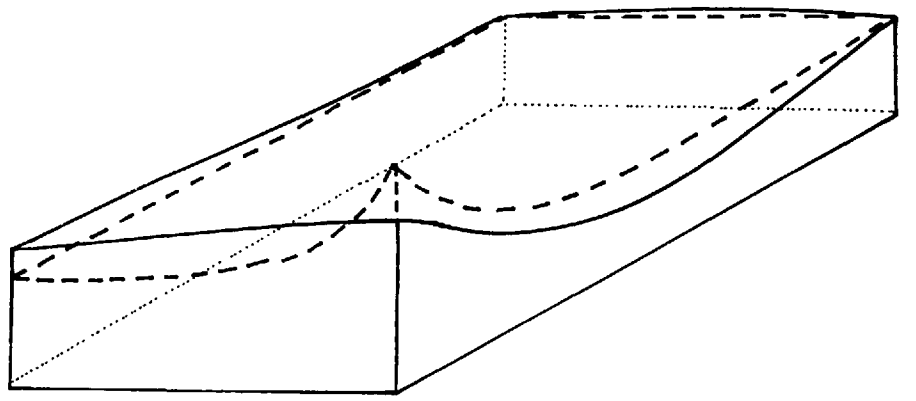

Direct (axial) stress contours

Fig. 5.15 : Stress distributions in matrix region between discontinuities in adjacent fibres

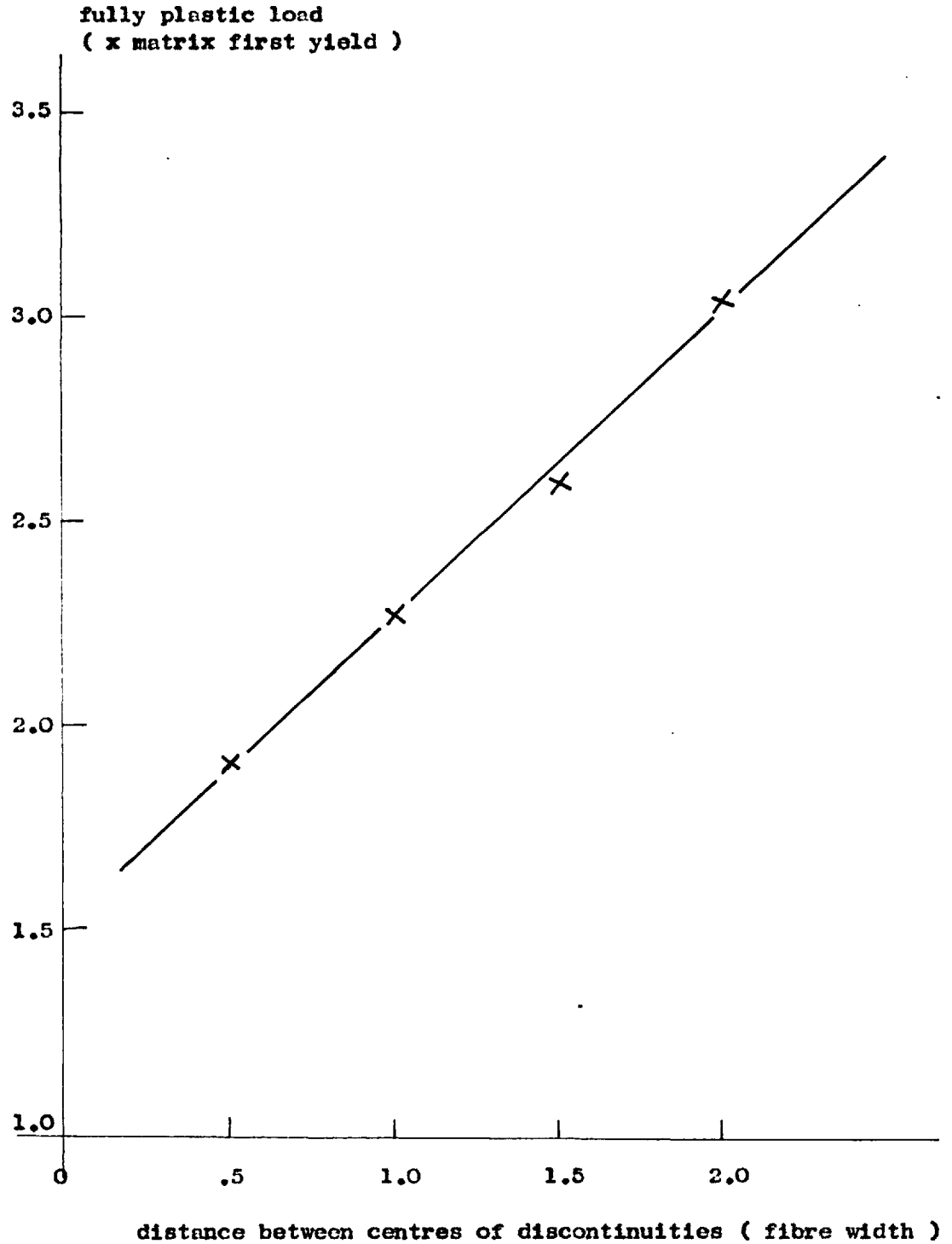

Fig. 5.16 : Relation Between Load Necessary to Create Fully Plastic Cross-section and Distance Between Centres of Discontinuities

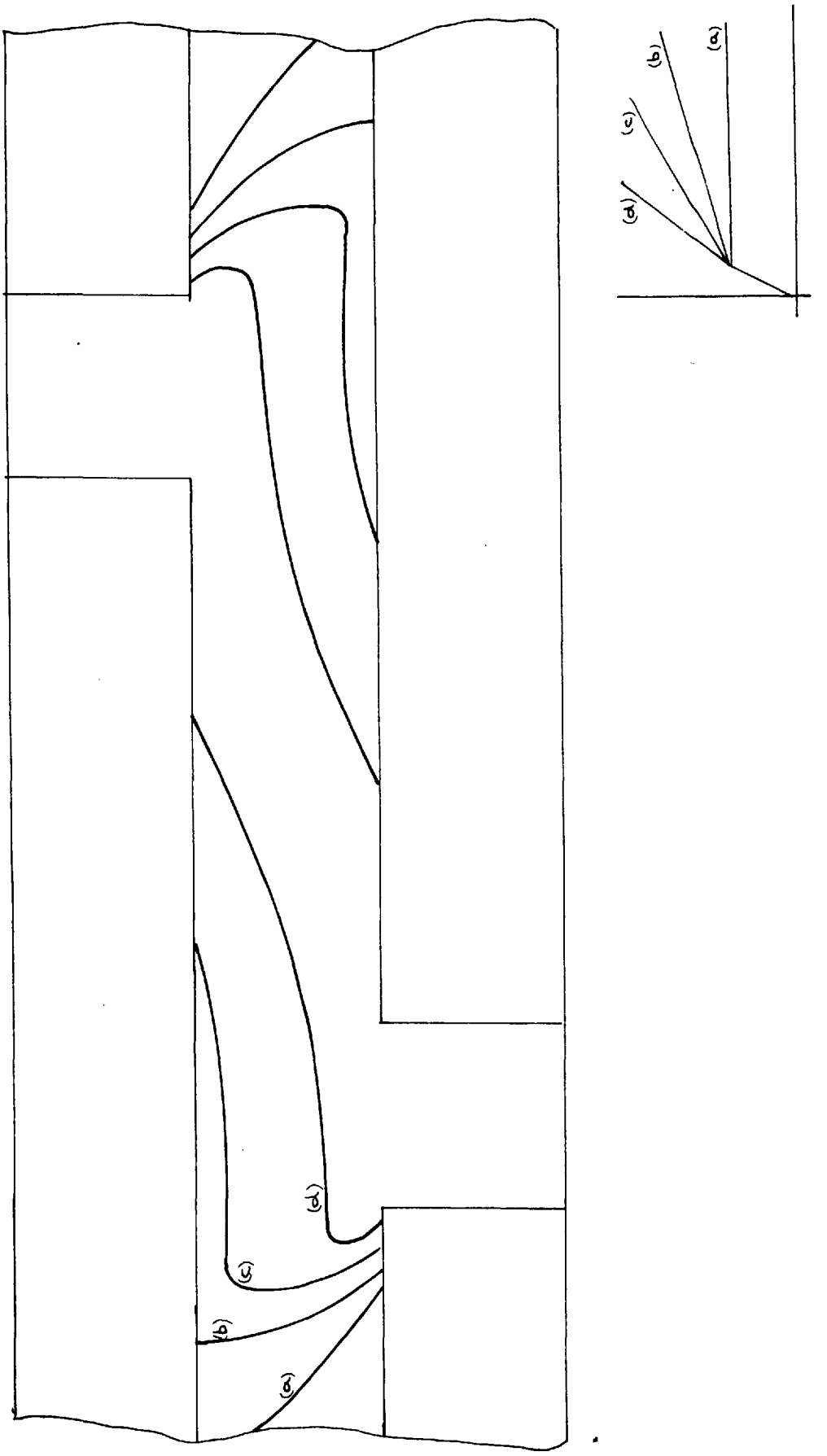

Fig. 5.17 : Effect of Matrix Work-hardening Characteristics on Plastic Enclave shape (For Same Load)

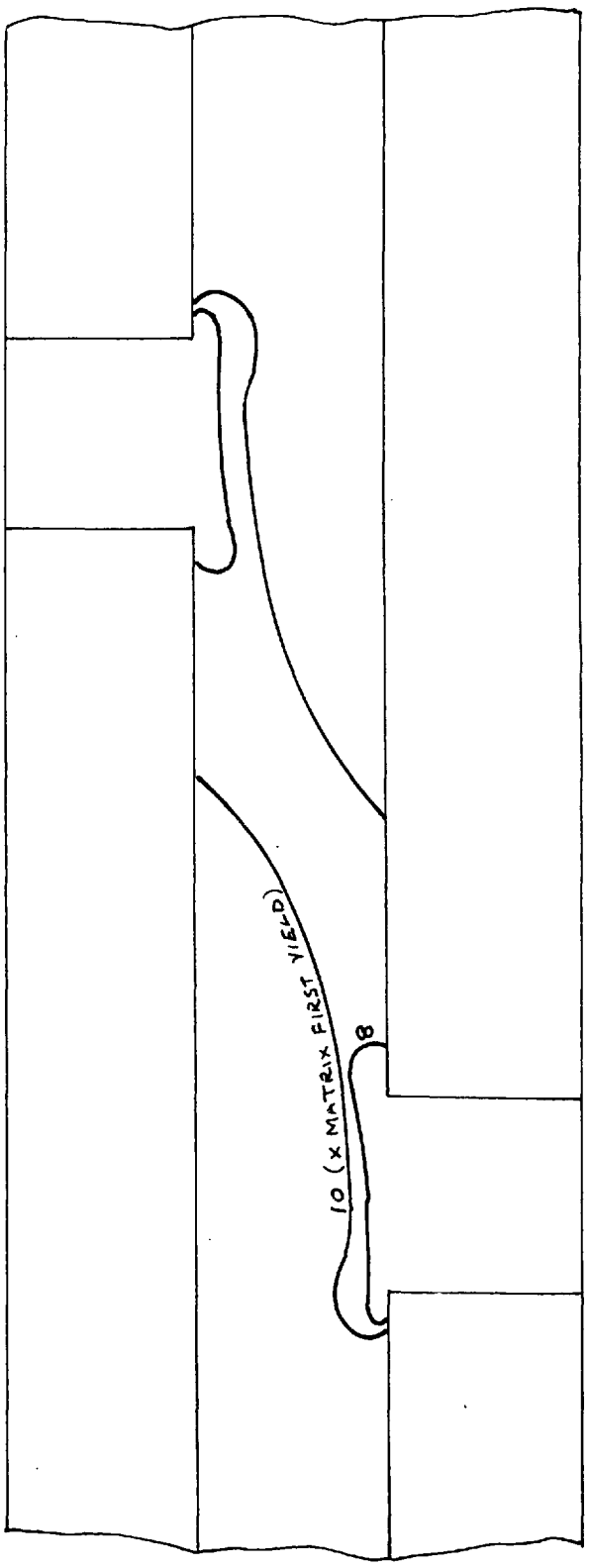

Fig. 5.18 : Extent of Matrix Fracture Assuming a Strain Limited Fracture Criterion

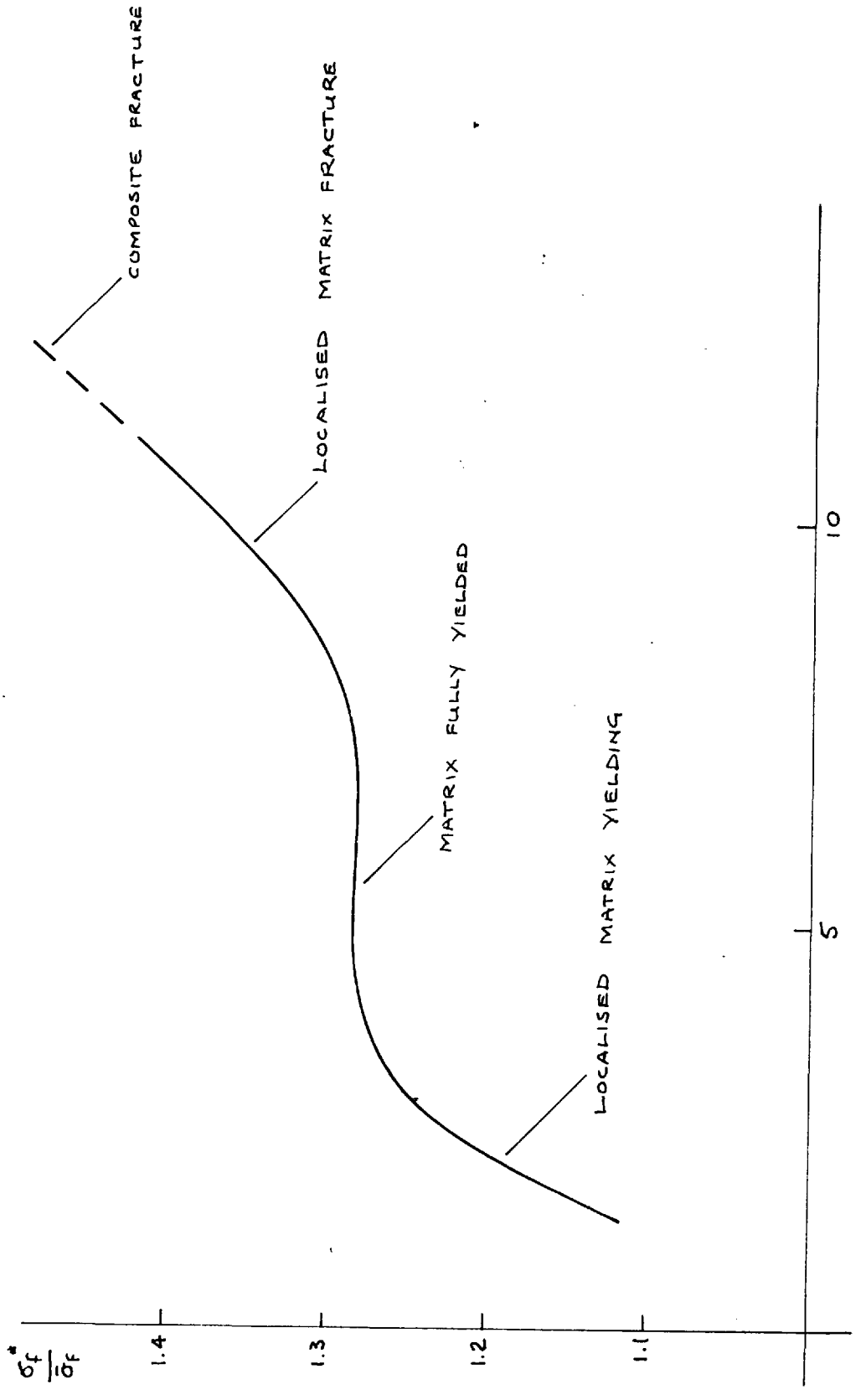

Fig. 5.19 : Axial Stress Concentration in Fibres Adjacent to the Discontinuous one

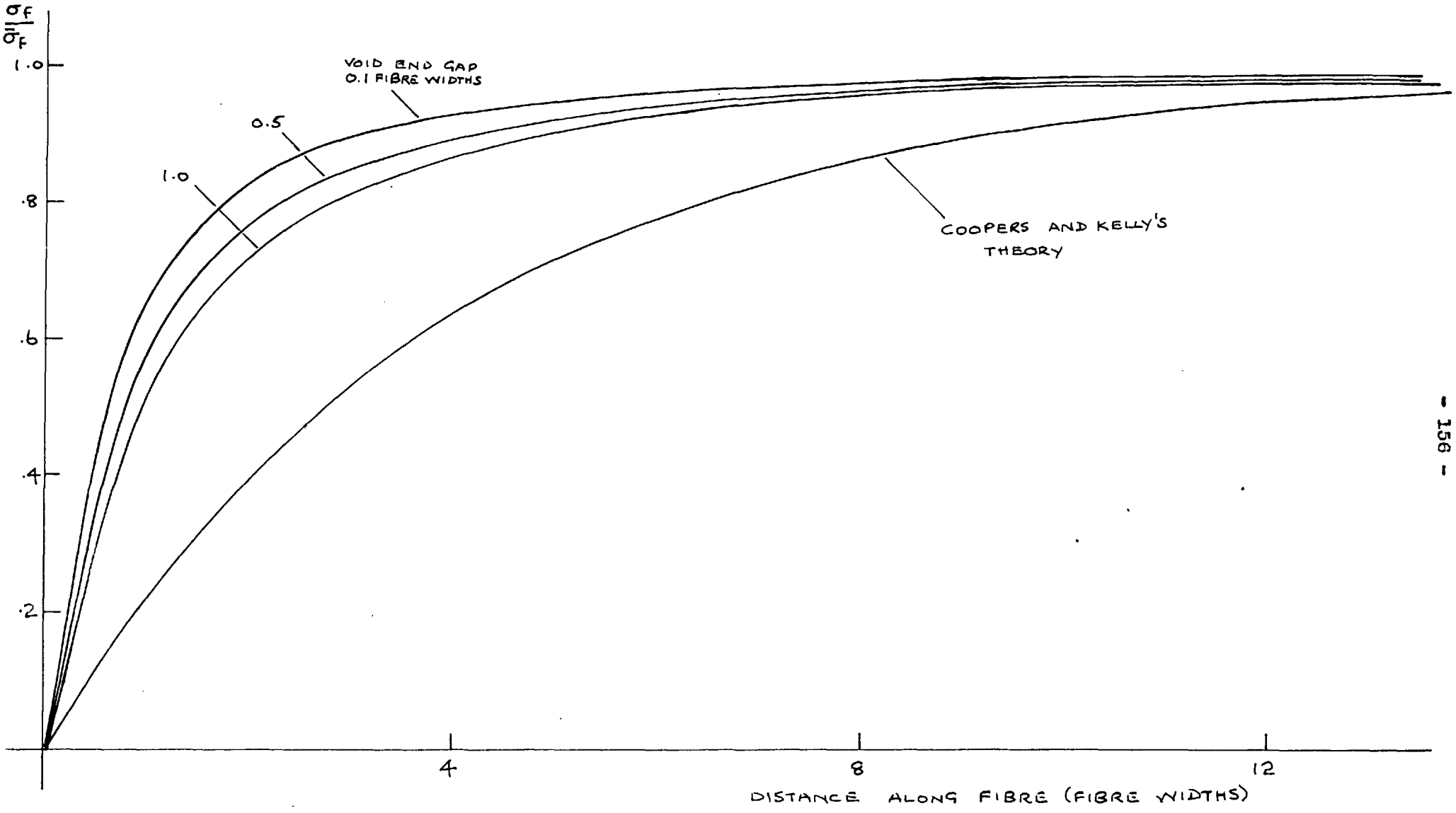

FIG. 6.1 : AXIAL STRESS BUILD-UP IN FIBRE COMPARISON OF THEORIES

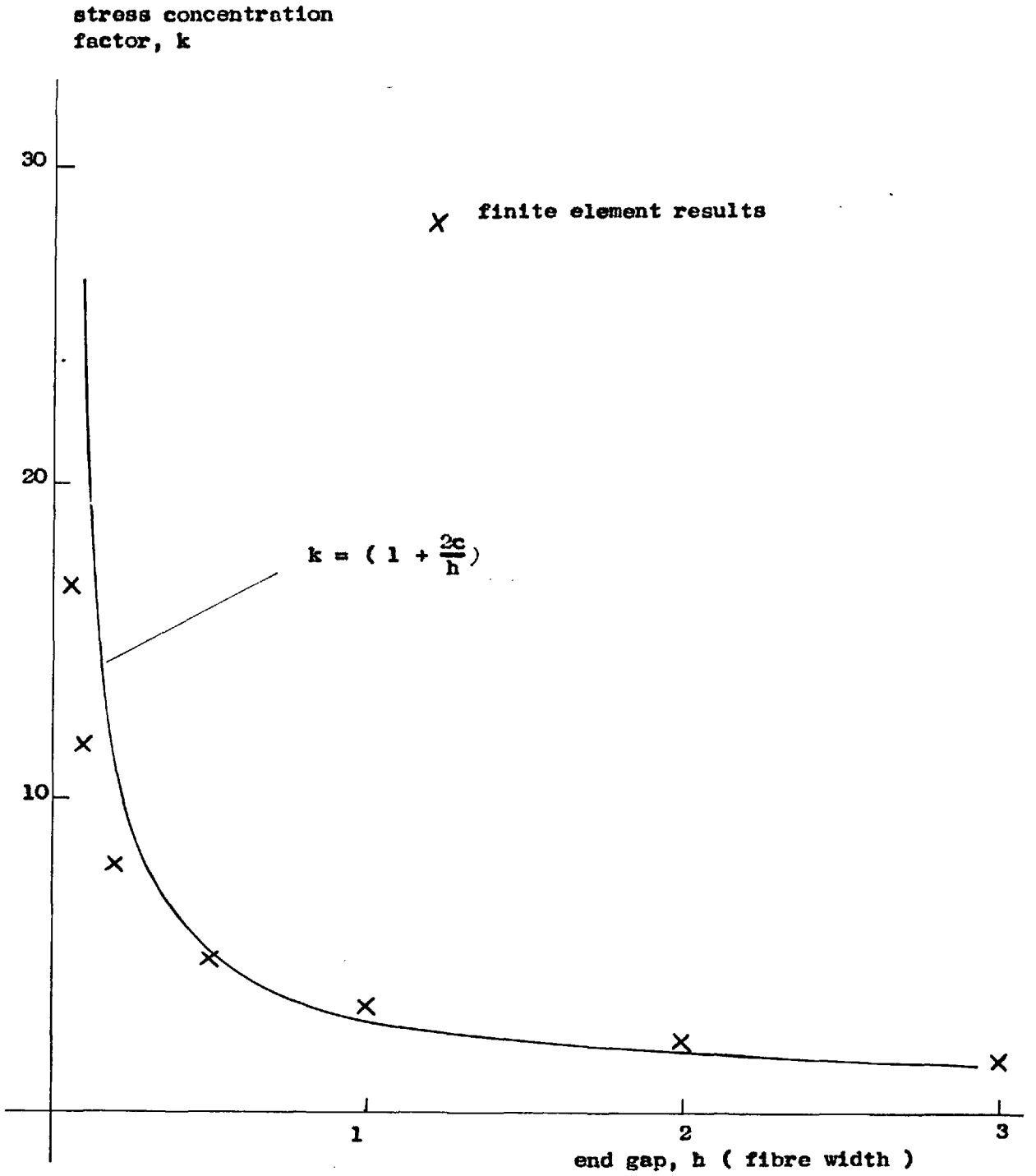

Fig. 6.2 : Comparison of finite element results and Inglis' formula for the stress concentration factor at a crack

APPENDIX 1

THE PARTIAL STIFFNESS METHOD

A numerical method for the solution of elastic/plastic problems using a partial stiffness concept has been derived by Marcal (1965). It has been modified by Marcal and King (1967) for use in finite element analysis. The basis of the method is described below.

The von Mises yield criterion for plane stress is,

$$\sigma_x^2 - \sigma_x\sigma_y + \sigma_y^2 + 3\tau_{xy}^2 = \bar{\sigma}^2 \qquad (A1.1)$$

This can be put in the form of an implicit differential,

$$3\sigma_x^1\, d\sigma_x + 3\sigma_y^1\, d\sigma_y + 6\tau_{xy}\, d\tau_{xy} = 2\bar{\sigma}\, d\bar{\sigma} \qquad (A1.2)$$

where σ^1 denotes a deviatoric stress

$$\text{e.g.} \quad \sigma_x^1 = \tfrac{1}{3}(2\sigma_x - \sigma_y)$$

The relation between equivalent stress, $\bar{\sigma}$, and equivalent plastic strain $\bar{e}_p$ can be obtained experimentlly. The slope of this curve, H^1, at a particular value of $\bar{e}_p$ is given by,

$$d\bar{\sigma} = H^1\, d\bar{e}_p \qquad (A1.3)$$

Equation (A1.2) can therefore be written,

$$\frac{3}{2}\frac{\sigma_x^1}{\bar{\sigma}}\, d\sigma_x + \frac{3}{2}\frac{\sigma_y^1}{\bar{\sigma}}\, d\sigma_y + 3\frac{\tau_{xy}}{\bar{\sigma}}\, d\tau_{xy} - H^1\, d\bar{e}_p = 0 \qquad (A1.4)$$

The Prandtl-Reuss stress-strain relations together with equation (A1.4) form a linear symmetric matrix.

$$\begin{bmatrix} \frac{1}{E} & -\frac{\nu}{E} & & \frac{3}{2}\frac{\sigma_x^1}{\bar{\sigma}} \\ -\frac{\nu}{E} & \frac{1}{E} & & \frac{3}{2}\frac{\sigma_y^1}{\bar{\sigma}} \\ & & \frac{1}{G} & 3\frac{\tau_{xy}}{\bar{\sigma}} \\ \frac{3}{2}\frac{\sigma_x^1}{\bar{\sigma}} & \frac{3}{2}\frac{\sigma_y^1}{\bar{\sigma}} & \frac{3\tau_{xy}}{\bar{\sigma}} & -H^1 \end{bmatrix} \begin{bmatrix} d\sigma_x \\ d\sigma_y \\ d\tau_{xy} \\ d\bar{e}_p \end{bmatrix} = \begin{bmatrix} de_x \\ de_y \\ d\gamma_{xy} \\ 0 \end{bmatrix}$$

$$\text{or} \quad \underline{P}\, d\sigma = de \qquad (A1.5)$$

By multiplying both sides by the inverse matrix $\underline{P}^{-1}$

$$d\sigma = \underline{P}^{-1}\, de \qquad (A1.6)$$

where the coefficients of $\underline{P}^{-1}$ may be written as,

$$\frac{\partial \sigma_i}{\partial e_j} \qquad \text{for } i = x, y, xy \text{ and } P \text{ and } j = x, y, xy \text{ and } 0$$

(σ_p is used to represent $\bar{e}_p$)

These $\partial\sigma/\partial e$ (partial stiffness) coefficients have to be modified for an elastic region which yields during the next increment of load. This area adjacent to the elastic/plastic interface is known as the transition region.

An estimate of the strains at a point is made based on the behaviour during the last increment of load. The proportion of these strains necessary to bring the present stresses up to a yield value is then calculated. Subsequent behaviour is assumed to be elastic/plastic and the partial stiffness coefficients are determined from the ratio of stresses at yield. Thus,

$$\left.\frac{\partial \sigma_i}{\partial e_j}\right|_{\text{mean}} = m \left.\frac{\partial \sigma_i}{\partial e_j}\right|_{\text{elastic}} (1-m) \left.\frac{\partial \sigma_i}{\partial e_j}\right|_{\text{elastic/plastic}}$$

where m is the ratio of the strain required to cause yielding and the estimated strain.

As the first increment of strains is not correct this procedure is repeated after the equilibrium equations have been solved. Convergence of the mean stiffness coefficients is obtained after only two iterations.

APPENDIX 2

FINITE ELEMENT COMPUTER ANALYSIS

The finite element method described in chapter 2 has been programmed in Fortran by Wilson (1963). His program has been extended by Marcal and King (1967) to include plastic behaviour and modified by the present author for the study of composite materials. This modified program is listed in Appendix 3.

The elastic analysis described below is that of Wilson (1963). It has been included here for the sake of completeness.

Elastic Analysis

The element stiffness matrices (equation (2.6)) are computed from the dimensions and material constants of each element. The element dimensions a_j, b_j, a_k and b_k shown in the diagram below are calculated from the nodal point co-ordinates

$$a_j = X_j - X_i \quad \text{etc.}$$

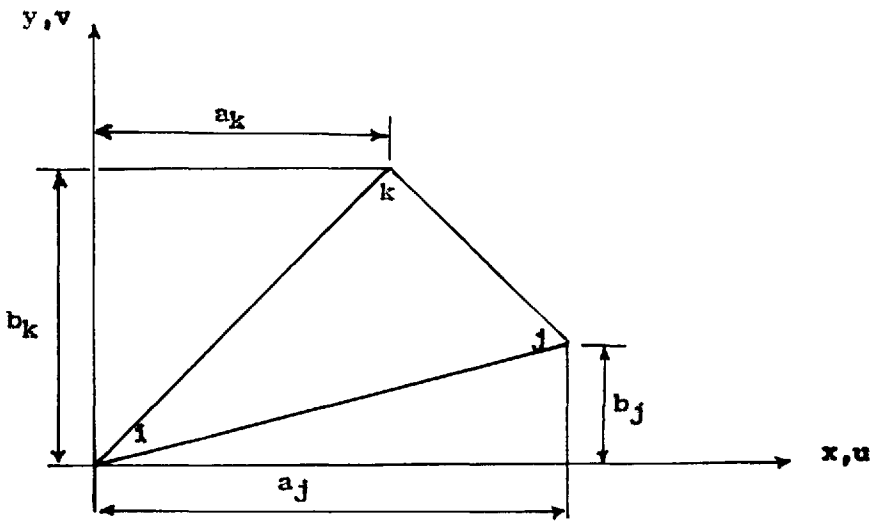

The displacements are assumed to follow a linear pattern given by,

$$u_{(x,y)} = u_i + C_1 x + C_2 y \qquad \text{(A2.1a)}$$

$$v_{(x,y)} = v_i + C_3 x + C_4 y \qquad \text{(A2.1b)}$$

where u and v are the x and y displacements respectively and the constants C_1 etc., are related to the corner displacements.

$$\begin{bmatrix} c_1 \\ c_2 \\ c_3 \\ c_4 \end{bmatrix} = \frac{1}{a_j b_k - a_k b_j} \begin{bmatrix} b_j - b_k & 0 & b_k & 0 & -b_j & 0 \\ a_k - a_j & 0 & -a_k & 0 & -a_j & 0 \\ 0 & b_j - b_k & 0 & b_k & 0 & -b_j \\ 0 & a_k - a_j & 0 & -a_k & 0 & a_j \end{bmatrix} \begin{bmatrix} u_i \\ v_i \\ u_j \\ v_j \\ u_k \\ v_k \end{bmatrix} \quad (A2.2)$$

The matrix $\underline{D}$ in equation (2.1) is given by,

$$\begin{bmatrix} e_x \\ e_y \\ \gamma_{xy} \end{bmatrix} = \frac{1}{a_j b_k - a_k b_j} \begin{bmatrix} b_j - b_k & 0 & b_k & 0 & -b_j & 0 \\ 0 & a_k - a_j & 0 & -a_k & 0 & a_j \\ a_k - a_j & b_j - b_k & -a_k & b_k & a_j & -b_j \end{bmatrix} \begin{bmatrix} u_i \\ v_i \\ u_j \\ v_j \\ u_k \\ v_k \end{bmatrix} \quad (A2.3)$$

which is obtained by differentiating the displacement function of the element

i.e. $$e_x = \frac{\partial u}{\partial x} = C_1 \quad ; \quad e_y = \frac{\partial v}{\partial y} = C_4$$

$$\gamma_{xy} = \frac{\partial u}{\partial y} + \frac{\partial v}{\partial x} = C_2 + C_3$$

The element stress-strain relation (equation (2.2)) is of the form, for plane stress,

$$\begin{bmatrix} \sigma_x \\ \sigma_y \\ \tau_{xy} \end{bmatrix} = \frac{E}{(1-\nu^2)} \begin{bmatrix} 1 & \nu & 0 \\ \nu & 1 & 0 \\ 0 & 0 & \frac{1-\nu}{2} \end{bmatrix} \begin{bmatrix} e_x \\ e_y \\ \gamma_{xy} \end{bmatrix} \quad (A2.4)$$

The uniform stresses acting on the edges of an element are replaced by stress resultants acting at the corners. Thus, equation (2.3) is,

$$\begin{bmatrix} F_x^i \\ F_y^i \\ F_x^j \\ F_y^j \\ F_x^k \\ F_y^k \end{bmatrix} = \frac{1}{2} \begin{bmatrix} b_j - b_k & 0 & a_k - a_j \\ 0 & a_k - a_j & b_j - b_k \\ b_k & 0 & -a_k \\ 0 & -a_k & b_k \\ -b_j & 0 & a_j \\ 0 & a_k & -b_j \end{bmatrix} \begin{bmatrix} \sigma_x \\ \sigma_y \\ \tau_{xy} \end{bmatrix} \quad (A2.5)$$

The element stiffness (equation (2.6)) is then obtained by combining these equations as explained on page 23 .

The assemblage stiffness (equation (2.7)) is found by a systematic addition of all the element stiffnesses. Since the complete stiffness matrix contains many zero terms only those which are non-zero are retained.

Equation (2.5) for a typical element q is,

$$\begin{bmatrix} F_i^{(q)} \\ F_j^{(q)} \\ F_k^{(q)} \end{bmatrix} = \begin{bmatrix} k_{ii}^{(q)} & k_{ij}^{(q)} & k_{ik}^{(q)} \\ k_{ji}^{(q)} & k_{jj}^{(q)} & k_{jk}^{(q)} \\ k_{ki}^{(q)} & k_{kj}^{(q)} & k_{kk}^{(q)} \end{bmatrix} \begin{bmatrix} r_i \\ r_j \\ r_k \end{bmatrix} \qquad \text{(A2.6)}$$

where in terms of an arbitary nodal point ,

$$F_l^{(q)} = \begin{bmatrix} F_x \\ F_y \end{bmatrix}_l^{(q)} \qquad \text{(A2.8)}$$

and for another nodal point in,

$$r_m^{(q)} = \begin{bmatrix} r_x \\ r_y \end{bmatrix}_m^{(q)} \qquad \text{(A2.9)}$$

and the stiffness coefficient k is of the form,

$$k_{lm}^{(q)} = \begin{bmatrix} k_{xx} & k_{xy} \\ k_{xy} & k_{yy} \end{bmatrix}_{lm}^{(q)} \qquad \text{(A2.10)}$$

which represents the forces developed on element q at nodal point due to unit displacements at nodal point m .

The general stiffness term K_{lm}, which is the sum of the forces acting on all the elements a nodal point l due to unit displacements at nodal point m, is given by

$$K_{lm} = \sum_q k_{lm}^{(q)} \qquad \text{(A2.11)}$$

The Gauss-Seidel iteration for the solution of equation (2.7)

involves the repeated calculation of new displacements from the equation,

$$r_n^{(s+1)} = K_{nn}^{-1} \left[R_n - \sum_{i=1,n-1} K_{ni} r_i^{(s+1)} - \sum_{i=n+1,N} K_{ni} r^{(s)} \right] \quad (A2.12)$$

where n is the number of the nodal point and s is the cycle of iteration.

The change in displacement, $\Delta r_n^{(s)}$, between two successive cycles of iteration is given by,

$$\Delta r_n^{(s)} = r_n^{(s+1)} - r_n^{(s)} \quad (A2.13)$$

and from equation (A2.12),

$$\Delta r_n^{(s)} = K_{nn}^{-1} \left[R_n - \sum_{i=1,n-1} K_{ni} r_i^{(s+1)} - \sum_{i=n,N} K_{ni} r_i^{(s)} \right] \quad (A2.14)$$

By using an over-relation factor, , the displacement is modified,

$$r_n^{(s+1)} = r_n^{(s)} + \beta \Delta r_n^{(s)} \quad (A2.15)$$

This greatly speeds up the convergence (see page 30). The computor program uses as a convergence criterion the expression,

$$\frac{\sum |\Delta r_n|}{\sum |r_n|} < \text{tolerance specified in data}$$

Strains and stresses are calculated from equations (A2.3) and (A2.4) respectively.

Elastic/Plastic Analysis

The steps taken in the computer program to solve an elastic/plastic problem using Marcal's partial stiffness method described in Appendix A1 are as follows:

1. The elastic problem is solved as described in the previous paragraphs.

2. The maximum equivalent stress is determined from von Mises'

yield criterion (equation (2.8)). This stress is taken as the yield stress of the material.

3. A increment of load is applied causing certain elements to exceed the yield stress.

4. The elastic strain increments that would be caused by the increase in load are calculated and used to determine whether or not each element has yielded.

5. The partial stiffness coefficients are calculated for the yielded elements from equation (A1.6).

6. The assemblage stiffness coefficients are formed and the equilibrium equations solved as in the elastic analysis.

7. Steps 5 and 6 are repeated three times, each time testing for yielding.

8. The increments of stresses are calculated and added to the existing stresses.

9. Displacements etc., are written out as required.

10. The program returns to step 3 for another increment of load.

APPENDIX 3

The Computer Program

The computer program follows closely the procedures of the finite element and partial stiffness methods described in Appendix 2.

The necessary input data is described in the listing, the format statements appearing at the end of the main program.

The values of the stresses used in chapters 4 and 5 are calculated using an averaging procedure due to Wilson. Points along a fibre/matrix interface are considered from each side of the interface separately (subroutine NPSIG).

The additions to the programs of Wilson and Marcal and King are described on page 25.

(a) Boundary Conditions:

(i) The flexibilities of boundary nodal points which are restricted to sliding along one or other co-ordinate axes are modified as described by Wilson (subroutine BOUMOD).

(ii) Boundary nodal points which displace in both directions but are restricted by an 'equal displacement' condition in one are treated differently. Each nodal point along the boundary in question is given a displacement equal to that of the end nodal point (either the x-displacement of nodal point B (DXNOPB) or the y-displacement of nodal point C (DYNOPC) whichever is appropriate).

(b) Preliminary Approximation:

The overall axial strain of the model (STRAIN) is calculated from the applied loads. Approximate x-displacements are calculated by multiplying STRAIN by the x-ordinate of each nodal point assuming the model homogeneous with an average elastic modulus (EC). Y-displacements

are determined by considering each phase in turn (fibre, matrix and fibre again).

This subroutine (NPDIAP) is ommitted by reading in BOTFIB = UPPFIB = 0.

(c) Matrix Yielding:

In order that the elements representing fibre and matrix can be treated separately in an elastic/plastic analysis the parameter JEL is set to 1 for a fibre element and 0 for a matrix element. The fibre elements always behave elastically while the matrix elements are allowed to yield.

For partial matrix yielding the elements that are to be allowed to yield are specified by reading in MORF = 2.

(d) Matrix Fracture:

The elastic modulus of a matrix element is set nearly zero when its plastic strain equals EPFAIL (subroutine ELACS). The value of EPFAIL which is read in as required should be 100. if no fracture is to occur.

```
C PLANE STRESS ELASTIC/PLASTIC FINITE ELEMENT ANALYSIS
C
C      DIMENSION AND COMMON STATEMENTS
C
       COMMON NPI(750),NPJ(750),NPK(750),ET(750),XU(750),
      1MORF(750),AJ(750),AK(750),BJ(750),BK(750),SIGXX(750),
      2SIGYY(750),SIGXY(750),TEX(750),TEY(750),TEXY(750),
      3XORD(450),YORD(450),XLOAD(450),YLOAD(450),DSX(450),
      4DSY(450),NP(450,10),NAP(450),SLOPE(450),LM(3),
      5SXX(450,9),SXY(450,9),SYX(450,9),SYY(450,9),
      6NSLOPE(450),NFIX(450),NPB(450),A(6,6),B(6,6),S(6,6),
      7NUMNP,NUMEL,NUMBC
       COMMON/PLAST/EX(750),EY(750),EXY(750),EPLAS(750)
       COMMON/HARDEN/COF(5)
       DIMENSION ARRAY(18)
       NAMELIST/PLLOAD/FACTO,NCPIN,NOPIN,NCYCM,INC,IPRINT,
      1ISKIP,TLOAD
       INTEGER T1
C
C      READ AND PRINT OF DATA
C
       READ(5,126) NREST
C  NREST CONTROLS QUANTITY OF OUTPUT FOR ELASTIC ANALYSIS ONLY.
C  WHEN NREST=1 OUTPUT CONTROLLED BY IKE, OTHERWISE
C  NREST=5   UNBALANCE CONDITIONS ONLY -------                (A)
C        4   (A) AND NODAL POINT DISPLACEMENTS ------------(B)
C        3   (B) AND NODAL POINT STRESSES
C        2   (A) AND NODAL POINT STRESSES
       READ(5,126) IKE
C  IKE = 1 GIVES FULL ELASTIC OUTPUT, IKE = 0 SUPPRESSES
C  ELASTIC OUTPUT
       READ(5,126) MONT
C  MONT CONTROLS OUTPUT OF NODAL POINT STRESSES FOR PLASTIC
C  LOAD INCREMENTS.
C  MONT = 1 GIVES OUTPUT, MONT = 0 SUPPRESSES OUTPUT
       WRITE(6,99)
       READ(5,126) NARRAY
C  NARRAY IS THE NUMBER OF TITLE LINES
       DO 150 I=1,NARRAY
       READ(5,100) ARRAY
  150  WRITE(6,100) ARRAY
       READ(5,1)NUMEL,NUMNP,NUMBC,NCPIN,NOPIN,NCYCM,TOLER,XFAC,T1
C  NUMBER OF ELEMENTS, NUMBER OF NODAL POINTS, NUMBER OF
C  BOUNDARY CONDITIONS, UNBALANCE CONDITION PRINT-OUT INTERVAL,
C  FULL OUTPUT PRINT-OUT INTERVAL, MAXIMUM NUMBER OF CYCLES,
C  TOLERANCE AND OVER-RELAXATION FACTOR RESPECTIVELY.
C  IF T1 NON-ZERO DATA PRINT-OUT SUPPRESSED
       WRITE(6,101)NUMEL
       WRITE(6,102)NUMNP
       WRITE(6,103)NUMBC
       WRITE(6,104)NCPIN
       WRITE(6,105)NOPIN
       WRITE(6,106)NCYCM
       WRITE(6,107)TOLER
       WRITE(6,108)XFAC
       READ(5,125)EF,EM,AF,AM,GNUF,GNUM
C  EF AND EM ARE ELASTIC MODULI OF FIBRE AND MATRIX RESPECTIVELY
C  AF AND AM ARE CROSS-SECTIONAL AREAS OF FIBRE AND MATRIX
C  GNUF AND GNUM ARE POISSON'S RATIOS OF FIBRE AND MATRIX
```

```
      READ(5,2) (N,NPI(N),NPJ(N),NPK(N),ET(N),XU(N),MORF(N),
     1N=1,NUMEL)
      CALL GNUMOD(EF,EM,GNUF,GNUM)
C   IF MORF = 0 ELEMENT IS MATRIX, IF MORF = 1 ELEMENT IS FIBRE
      READ(5,3) (M,XORD(M),YORD(M),XLOAD(M),YLOAD(M),DSX(M),
     1DSY(M), M=1,NUMNP)
      IF (T1) 57,155,57
  155 WRITE(6,110)
      WRITE(6,2)(N,NPI(N),NPJ(N),NPK(N),ET(N),XU(N),MORF(N),
     1N=1,NUMEL)
C   ELEMENT NUMBER, CORNER NODAL POINT NUMBERS, ELASTIC MODULUS,
C   POISSON'S RATIO AND MORF RESPECTIVELY
      WRITE(6,111)
      WRITE(6,109) (M,XORD(M),YORD(M),XLOAD(M),YLOAD(M),DSX(M),
     1DSY(M), M=1,NUMNP)
C   NODAL POINT NUMBER, X AND Y CO-ORDINATES, X AND Y LOADS AND
C   INITIAL X AND Y DISPLACEMENTS RESPECTIVELY
      WRITE(6,112)
   57 CONTINUE
      DO 58 L=1,NUMBC
      READ(5,4)NPB(L),NFIX(L),SLOPE(L)
C   NFIX=0  NODAL POINT IS FIXED
C   NFIX=1  NODAL POINT CAN MOVE IN Y-DIRN. ONLY
C   NFIX=2  NODAL POINT CAN MOVE IN X-DIRN. ONLY
C   NFIX=2 AND SLOPE NON-ZERO NODAL POINT MOVES ALONG SLOPE
C   NFIX=3  NODAL POINT RESTRAINED IN X-DIRECTION SO AS TO
C           DISPLACE A DISTANCE EQUAL TO THAT OF NOPB
C   NFIX=4  NODAL POINT RESTRAINED IN Y-DIRECTION SO AS TO
C           DISPLACE A DISTANCE EQUAL TO THAT OF NOPC
      IF(T1) 58,909,58
  909 WRITE(6,4)NPB(L),NFIX(L),SLOPE(L)
   58 CONTINUE
      READ(5,6) MINC,COF(1),COF(2),COF(3)
C   MINC IS NUMBER OF PLASTIC LOAD INCREMENTS, COF(1) ETC.
C   ARE WORK-HARDENING COEFFICIENTS
      READ(5,129)BOTFIB,UPPFIB
C   BOTFIB IS YORD OF UPPER EDGE OF LOWER FIBRE
C   UPPFIB IS YORD OF LOWER EDGE OF UPPER FIBRE
      READ(5,113) XBOUND,YBOUND,NOPB,NOPC,NOPD
C   XBOUND AND YBOUND ARE THE LENGTHS OF THE X AND Y AXES
C   RESPECTIVELY, NOPB AND NOPD ARE THE NUMBERS OF THE NODAL
C   POINTS AT THE EXTREMITIES OF THESE AXES, NOPC IS THE NUMBER
C   OF THE POINT (X = XBOUND,Y = YBOUND)
      FVF=AF/(AF+AM)
      READ(5,130) EPFAIL
C   PUT EPFAIL = 100.0 IF NO FRACTURE IS ALLOWED, OTHERWISE
C   EPFAIL IS 0. FOR BRITTLE SYSTEMS AND (EP)MAX FOR DUCTILE
C   SYSTEMS
C   FVF IS FIBRE VOLUME FRACTION
      EC=AF*EF+AM*EM
      GNUC=AF*GNUF+AM*GNUM
C   EC AND GNUC ARE ELASTIC MODULUS AND POISSON'S RATIO OF
C   THE COMPOSITE RESPECTIVELY
      IF (T1) 61,59,61
   59 CONTINUE
      WRITE(6,131)
      WRITE(6,127)EF,EM,GNUF,GNUM
      WRITE(6,128)EC,GNUC
      WRITE(6,132)FVF
```

```
      WRITE(6,133)
      WRITE(6,114)XBOUND,YBOUND,NOPB,NOPC,NOPD
      WRITE(6,134)BOTFIB,UPPFIB
      WRITE(6,8)
      WRITE(6,7)
      WRITE(6,6)MINC,COF(1),COF(2),COF(3)
   61 CONTINUE
C
      IPRINT = 0
C  WHEN IPRINT = 1 OUTPUT CONTROLLED BY ISKIP
C  IPRINT = 0 GIVES FULL ELASTIC/PLASTIC OUTPUT.
      ISKIP = 0
C  ISKIP = 0 GIVES FULL OUTPUT OF NODAL POINT DISPLACEMENTS
C  AND ELEMENT STRESSES AND STRAINS. ISKIP = 1 GIVES OUTPUT
C  OF STRAINS IN PLASTIC ELEMENTS ONLY
      INC=1
      MINC=MINC+1
      JEL=1
C  IF JEL = 1 ELEMENT IS ELASTIC. IF JEL = 0 ELEMENT IS PLASTIC
      FACTOR=0.
      WRITE(6,99)
C
C     MODIFICATION OF LOADS AND ELEMENT DIMENSIONS
C
  160 CONTINUE
      CALL MODIM
  777 CONTINUE
C
C     INITIALIZATION
C
      NCYCLE=0
      NUMPT=NCPIN
      NUMOPT=NOPIN
      WLOAD=0.
      IF (IKE.EQ.0.AND.INC.EQ.1) GO TO 75
  243 WRITE(6,119)
   75 CONTINUE
      DO 175 L=1,NUMNP
      WLOAD=WLOAD+XLOAD(L)
      NSLOPE(L)=-1
      DO 170 M=1,9
      SXX(L,M)=0.0
      SYX(L,M)=0.0
      SXY(L,M)=0.0
      SYY(L,M)=0.0
  170 NP(L,M)=0
      NP(L,10)=0
  175 NP(L,1)=L
      IF(WLOAD.EQ.XLOAD(NOPB)) WLOAD=0.
C
C     FORMATION OF STIFFNESS ARRAY
      CALL STIFF(JEL,ISTORE,INC,FACTOR)
C
C     COUNT OF ADJACENT NODAL POINTS
      CALL NPSUM
C
C     INVERSION OF NODAL POINT STIFFNESSES
      CALL NPSTIN
C
```

```
C       MODIFICATION OF BOUNDARY FLEXIBILITIES
        CALL BOUMOD(NSLMAX)
C
C       PRELIMINARY APPROXIMATION TO NODAL POINT DISPLACEMENTS
        IF(INC.GT.1) GO TO 244
        CALL NPDIAP(XBOUND,YBOUND,BOTFIB,UPPFIB,EC,NOPB,GNUF,
       1GNUM,WLOAD)
C
C       ITERATION ON NODAL POINT DISPLACEMENTS
  244   SUM=0.
        SUMD=0.
        CALL NPITER(SUM,SUMD,NSLMAX,NOPB,NOPC,NOPD,XFAC)
C
C       CYCLE COUNT AND PRINT CHECK
C
        NCYCLE=NCYCLE +1
        IF(NCYCLE-NUMPT) 305,300,300
  300   NUMPT=NUMPT+NCPIN
        IF(IKE.EQ.0.AND.INC.EQ.1) GO TO 76
        WRITE(6,120)NCYCLE,SUM,SUMD
   76   CONTINUE
  305   IF(SUM.GT.TOLER) GO TO 310
        NCYCLE=NUMOPT
        NUMOPT=NUMOPT+NOPIN
        GO TO 400
  310   IF(NCYCM-NCYCLE) 400,400,315
  315   IF(NCYCLE-NUMOPT) 244,320,320
  320   NUMOPT=NUMOPT+NOPIN
  400   CONTINUE
        IF(NREST.EQ.5.AND.MINC.EQ.1) GO TO 1000
C       PRINT OF DISPLACEMENTS AND STRESSES
C
        IF (NREST.EQ.2.AND.MINC.EQ.1) GO TO 62
        IF (IKE.EQ.0.AND.INC.EQ.1) GO TO 62
        IF (NCYCLE.LT.NCYCM.AND.INC.GT.1) GO TO 62
        IF (IPRINT.NE.0.OR.ISKIP.NE.0) GO TO 999
        WRITE(6,121)
        WRITE(6,122)(M,DSX(M),DSY(M),M=1,NUMNP)
        IF (NREST.EQ.4.AND.MINC.EQ.1) GO TO 1000
  999   CONTINUE
        IF (NREST.GT.1.AND.MINC.EQ.1) GO TO 62
        IF (IPRINT.NE.0.AND.ISKIP.EQ.0) GO TO 62
        IF (ISKIP.EQ.0) GO TO 63
        WRITE(6,135)
        GO TO 62
   63   CONTINUE
        WRITE(6,123)
   62   CONTINUE
        CALL SIGOUT(INC,JFL,NCYCLE,NCYCM,PSCALE,TLOAD,FACTOR,
       1MINC,ISKIP,IPRINT,NREST,IKE,EPFAIL)
C
C       CALCULATION OF NODAL POINT STRESSES
C
        IF (NREST.GT.3.AND.MINC.EQ.1) GO TO 1000
        IF (NREST.GT.3.AND.INC.EQ.1) GO TO 801
        IF (IKE.EQ.0.AND.INC.EQ.1) GO TO 801
        IF (NCYCLE.LT.NCYCM.AND.INC.GT.1) GO TO 801
        IF (MONT.EQ.0.AND.INC.GT.1) GO TO 801
        WRITE (6,823)
```

```
      WRITE (6,824)
      CALL NPSIG(INC)
C
  801 CONTINUE
      IF(SUM-TOLER) 1000,1000,430
  430 IF(NCYCM-NCYCLE) 1000,1000,243
 1000 CONTINUE
      IF(INC.EQ.1) WRITE(6,136) FACTOR
      IF(MINC.EQ.1)STOP
C
C     CALCULATION OF PLASTIC LOAD INCREMENTS
C
  440 ISTORE=0
      IF(MINC.LE.INC)STOP
      IF(INC.GT.1) JEL = 0
      ISKIP = 0
      IPRINT = 0
      READ(5,PLLOAD)
      IF(INC.GT.1) GO TO 71
      PSCALE = FACTO
      TLOAD = PSCALE + 1.
      GO TO 51
   71 TLOAD = TLOAD + PSCALE*FACTO
      PSCALE = PSCALE*FACTO
   51 CONTINUE
      CALL PLACS(FACTO,FACTOR,EPFAIL)
      WRITE(6,PLLOAD)
      INC=INC+1
      JEL=0
      GO TO 777
C
C     FORMAT STATEMENTS
C
    1 FORMAT(6I4,2E12.5,1I1)
    2 FORMAT(4I4,1X,E12.4,12X,E12.4,18X,I1)
    3 FORMAT(1I4,4F8.5,2F12.8)
    4 FORMAT(2I4,F12.8)
    5 FORMAT(3E15.8)
    6 FORMAT(I12,18X,3E12.5)
    7 FORMAT(23HONO. PLASTIC INCREMENTS,9X,
     128H WORK HARDENING COEFFICIENTS,//)
    8 FORMAT(////////,13H PLASTIC DATA,//)
   99 FORMAT (1H1)
  100 FORMAT(18A4)
  101 FORMAT(29HONUMBER OF ELEMENTS           =,I4/)
  102 FORMAT(29H NUMBER OF NODAL POINTS       =,I4/)
  103 FORMAT(29H NUMBER OF BOUNDARY POINTS    =,I4/)
  104 FORMAT(29H CYCLE PRINT INTERVAL         =,I4/)
  105 FORMAT(29H OUTPUT INTERVAL OF RESULTS   =,I4/)
  106 FORMAT(29H CYCLE LIMIT                  =,I4/)
  107 FORMAT(29H TOLERANCE LIMIT              =,E12.4/)
  108 FORMAT(29H OVER RELAXATION FACTOR       =1F6.3)
  109 FORMAT(1I8,6F12.5)
  110 FORMAT (24H1EL.    I    J    K        E,19X,8H POISSON)
  111 FORMAT (44H1      NP        X-ORD        Y-ORD       X-LOAD,
     15X,31H Y-LOAD       X-DISP       Y-DISP)
  112 FORMAT (20H1BOUNDARY CONDITIONS,//)
  113 FORMAT(2F12.8,3I4)
  114 FORMAT(8HOXBOUND=,F7.2,4X,7HYBOUND=,F7.2,7X,
```

```
     115HNOPB IS N.P. NO.I3.4X.15HNOPC IS N.P. NO.I3.4X.
     215HNOPD IS N.P. NO.I3.//)
  119 FORMAT(34H0       CYCLE        DISPL UNBALANCE.4X.
     112H TOTAL DISPL)
  120 FORMAT(111.2E20.6)
  121 FORMAT (42H1NODAL POINT X-DISPLACEMENT Y-DISPLACEMENT)
  122 FORMAT(111.2E15.8)
  123 FORMAT (30H1  ELEMENT              X-STRESS.11X.
     19H Y-STRESS.10X.10H XY-STRESS.9X.11H MAX-STRESS.
     23X.11H MIN-STRESS.6X.10H DIRECTION)
  124 FORMAT(1110.3F20.8.5X.3F15.8)
  125 FORMAT(2E12.4.4F6.2)
  126 FORMAT (111)
  127 FORMAT(4H0EF=.E12.4.4X.4H EM=.E12.4.4X.6H GNUF=.F6.3.
     14X.6H GNUM=.F6.3./)
  128 FORMAT(4H0EC=.E12.4.24X.6H GNUC=.F6.3.//)
  129 FORMAT(2F7.2)
  130 FORMAT(F20.8)
  131 FORMAT (1H1.19HMATERIAL PROPERTIES.//)
  132 FORMAT(23H FIBRE VOLUME FRACTION=.F5.2)
  133 FORMAT(///////.16H MESH DIMENSIONS.///)
  134 FORMAT(8H BOTFIB=.F7.2.3X.8H UPPFIB=.F7.2)
  135 FORMAT (30H1  ELEMENT              X-STRAIN.11X.
     151H Y-STRAIN            XY-STRAIN         PLASTIC-STRAIN)
  136 FORMAT(//.26H0EQUIVALENT YIELD STRESS =.F12.3)
  698 FORMAT(114.4F8.5)
  823 FORMAT (30H1  ELEMENT              X-STRESS.11X.
     19H Y-STRESS.10X.10H XY-STRESS.9X.11H MAX-STRESS.
     23X.11H MIN-STRESS.6X.10H MAX SHEAR)
  824 FORMAT(//.30H MATRIX STRESSES WRITTEN FIRST.//)
      END
```

```
      SUBROUTINE GNUMOD(EF,EM,GNUF,GNUM)
C
C     ELASTIC CONSTANTS OF FIBRE AND MATRIX
C
      COMMON NPI(750),NPJ(750),NPK(750),ET(750),XU(750),
     1MORF(750),AJ(750),AK(750),BJ(750),BK(750),SIGXX(750),
     2SIGYY(750),SIGXY(750),TEX(750),TEY(750),TEXY(750),
     3XORD(450),YORD(450),XLOAD(450),YLOAD(450),DSX(450),
     4DSY(450),NP(450,10),NAP(450),SLOPE(450),LM(3),
     5SXX(450,9),SXY(450,9),SYX(450,9),SYY(450,9),
     6NSLOPE(450),NFIX(450),NPB(450),A(6,6),B(6,6),S(6,6),
     7NUMNP,NUMEL,NUMBC
      DO 1 N=1,NUMEL
      IF(ET(N).LT.1.E1) GO TO 1
      IF(MORF(N).EQ.0.OR.MORF(N).EQ.2) GO TO 2
      ET(N)=EF
      XU(N)=GNUF
      GO TO 1
    2 ET(N)=EM
      XU(N)=GNUM
    1 CONTINUE
      RETURN
      END
```

```
      SUBROUTINE MODIM
C
C     MODIFICATION OF LOADS AND ELEMENT DIMENSIONS
C
      COMMON NPI(750),NPJ(750),NPK(750),ET(750),XU(750),
     1MORF(750),AJ(750),AK(750),BJ(750),BK(750),SIGXX(750),
     2SIGYY(750),SIGXY(750),TEX(750),TEY(750),TEXY(750),
     3XORD(450),YORD(450),XLOAD(450),YLOAD(450),DSX(450),
     4DSY(450),NP(450,10),NAP(450),SLOPE(450),LM(3),
     5SXX(450,9),SXY(450,9),SYX(450,9),SYY(450,9),
     6NSLOPE(450),NFIX(450),NPB(450),A(6,6),B(6,6),S(6,6),
     7NUMNP,NUMEL,NUMBC
      COMMON/PLAST/EX(750),EY(750),EXY(750),EPLAS(750)
      LAMORF=0
      DO 16 N=1,NUMEL
      ET(N)=ABS(ET(N))
      EPLAS(N)=0.
      TEX(N)=0.
      TEY(N)=0.
      TEXY(N)=0.
      I=NPI(N)
      J=NPJ(N)
      K=NPK(N)
      AJ(N)=XORD(J)-XORD(I)
      AK(N)=XORD(K)-XORD(I)
      BJ(N)=YORD(J)-YORD(I)
      BK(N)=YORD(K)-YORD(I)
  176 AREA=(AJ(N)*BK(N)-BJ(N)*AK(N))/2.
      IF(MORF(N).GT.LAMORF) LAMORF=MORF(N)
      IF (AREA.GT.0.) GO TO 16
      WRITE(6,711)N
      STOP
   16 CONTINUE
      IF(LAMORF.EQ.1) RETURN
C  WHEN LAMORF = 2 ONLY PARTIAL YIELDING OF THE MATRIX IS
C  ALLOWED I.E. BY THOSE ELEMENTS WITH MORF = 2
      DO 3 N=1,NUMEL
      IF(MORF(N).EQ.0) MORF(N)=1
      IF(MORF(N).EQ.2) MORF(N)=0
    3 CONTINUE
  711 FORMAT (32H0ZERO OR NEGATIVE AREA, EL. NO.=1I4)
      RETURN
      END
```

```
      SUBROUTINE STIFF(JEL,ISTORE,INC,FACTOR)
C
C     FORMATION OF ELEMENT STIFFNESSES
C
      COMMON NPI(750),NPJ(750),NPK(750),ET(750),XU(750),
     1MORF(750),AJ(750),AK(750),BJ(750),BK(750),SIGXX(750),
     2SIGYY(750),SIGXY(750),TEX(750),TEY(750),TEXY(750),
     3XORD(450),YORD(450),XLOAD(450),YLOAD(450),DSX(450),
     4DSY(450),NP(450,10),NAP(450),SLOPE(450),LM(3),
     5SXX(450,9),SXY(450,9),SYX(450,9),SYY(450,9),
     6NSLOPE(450),NFIX(450),NPB(450),A(6,6),B(6,6),S(6,6),
     7NUMNP,NUMEL,NUMBC
      COMMON/PLAST/EX(750),EY(750),EXY(750),EPLAS(750)
      DO 200 N=1,NUMEL
      AREA=.5/(AJ(N)*BK(N)-AK(N)*BJ(N))
      A(1,1)=BJ(N)-BK(N)
      A(1,2)=0.0
      A(1,3)=BK(N)
      A(1,4)=0.0
      A(1,5)=-BJ(N)
      A(1,6)=0.0
      A(2,1)=0.0
      A(2,2)=AK(N)-AJ(N)
      A(2,3)=0.0
      A(2,4)=-AK(N)
      A(2,5)=0.0
      A(2,6)=AJ(N)
      A(3,1)=AK(N)-AJ(N)
      A(3,2)=BJ(N)-BK(N)
      A(3,3)=-AK(N)
      A(3,4)=BK(N)
      A(3,5)=AJ(N)
      A(3,6)=-BJ(N)
      IF(MORF(N).EQ.1) JEL=1
      CALL SIGEPS(B,6,EX(N),EY(N),EXY(N),SIGXX(N),SIGYY(N),
     1SIGXY(N),XU(N),ET(N),EPLAS(N),ISTORE,JEL,FACTOR)
      IF(INC.GT.1) JEL = 0
      DO 17I=1,3
      DO 17J=1,3
   17 B(I,J)=B(I,J)*AREA
C
      DO 182 J=1,6
      DO 182 I=1,3
      S(I,J)=0.0
      DO 182 K=1,3
  182 S(I,J)=S(I,J)+B(I,K)*A(K,J)
      DO 183 J=1,6
      DO 183 I=1,3
  183 B(J,I)=S(I,J)
      DO 184 J=1,6
      DO 184 I=1,6
      S(I,J)=0.0
      DO 184 K=1,3
  184 S(I,J)=S(I,J)+B(I,K)*A(K,J)
C
C     FORMATION OF ASSEMBLAGE STIFFNESS MATRIX
C
      LM(1)=NPI(N)
      LM(2)=NPJ(N)
```

```
      LM(3)=NPK(N)
      DO 200 L=1,3
      DO 200 M=1,3
      LX=LM(L)
      MX=0
  185 MX=MX+1
      IF(NP(LX,MX)-LM(M)) 190,195,190
  190 IF(NP(LX,MX)) 185,195,185
  195 NP(LX,MX)=LM(M)
      IF (MX-10) 196,702,702
  702 WRITE(6,712)LX
      STOP
  196 SXX(LX,MX)=SXX(LX,MX)+S(2*L-1,2*M-1)
      SXY(LX,MX)=SXY(LX,MX)+S(2*L-1,2*M)
      SYX(LX,MX)=SYX(LX,MX)+S(2*L,2*M-1)
  200 SYY(LX,MX)=SYY(LX,MX)+S(2*L,2*M)
  712 FORMAT (33HOOVER 8 N.P. ADJACENT TO N.P. NO.1I4)
      RETURN
      END
```

```
      SUBROUTINE NPSUM
C
C     COUNT OF ADJACENT NODAL POINTS
C
      COMMON NPI(750),NPJ(750),NPK(750),ET(750),XU(750),
     1MORF(750),AJ(750),AK(750),BJ(750),BK(750),SIGXX(750),
     2SIGYY(750),SIGXY(750),TEX(750),TEY(750),TEXY(750),
     3XORD(450),YORD(450),XLOAD(450),YLOAD(450),DSX(450),
     4DSY(450),NP(450,10),NAP(450),SLOPE(450),LM(3),
     5SXX(450,9),SXY(450,9),SYX(450,9),SYY(450,9),
     6NSLOPE(450),NFIX(450),NPB(450),A(6,6),B(6,6),S(6,6),
     7NUMNP,NUMEL,NUMBC
      DO 206 M=1,NUMNP
      MX =1
  205 MX=MX+1
      IF (NP(M,MX)) 206,206,205
  206 NAP(M)=MX-1
      RETURN
      END
```

```
      SUBROUTINE NPSTIN
C
C     INVERSION OF NODAL POINT STIFFNESSES
C
      COMMON NPI(750),NPJ(750),NPK(750),ET(750),XU(750),
     1MORF(750),AJ(750),AK(750),BJ(750),BK(750),SIGXX(750),
     2SIGYY(750),SIGXY(750),TEX(750),TEY(750),TEXY(750),
     3XORD(450),YORD(450),XLOAD(450),YLOAD(450),DSX(450),
     4DSY(450),NP(450,10),NAP(450),SLOPE(450),LM(3),
     5SXX(450,9),SXY(450,9),SYX(450,9),SYY(450,9),
     6NSLOPE(450),NFIX(450),NPB(450),A(6,6),B(6,6),S(6,6),
     7NUMNP,NUMEL,NUMBC
      DO 210 M=1,NUMNP
      COMM=SXX(M,1)*SYY(M,1)-SXY(M,1)*SYX(M,1)
      TEMP=SYY(M,1)/COMM
      SYY(M,1)=SXX(M,1)/COMM
      SXX(M,1)=TEMP
      SXY(M,1)=-SXY(M,1)/COMM
  210 SYX(M,1)=-SYX(M,1)/COMM
      RETURN
      END
```

```
      SUBROUTINE BOUMOD(NSLMAX)
C
C     MODIFICATION OF BOUNDARY FLEXIBILITIES
C
      COMMON NPI(750),NPJ(750),NPK(750),ET(750),XU(750),
     1MORF(750),AJ(750),AK(750),BJ(750),BK(750),SIGXX(750),
     2SIGYY(750),SIGXY(750),TEX(750),TEY(750),TEXY(750),
     3XORD(450),YORD(450),XLOAD(450),YLOAD(450),DSX(450),
     4DSY(450),NP(450,10),NAP(450),SLOPE(450),LM(3),
     5SXX(450,9),SXY(450,9),SYX(450,9),SYY(450,9),
     6NSLOPE(450),NFIX(450),NPB(450),A(6,6),B(6,6),S(6,6),
     7NUMNP,NUMEL,NUMBC
      NSLMAX=0.
      DO 240 L=1,NUMBC
      M=NPB(L)
      NSLOPE(M)=NFIX(L)
      IF(NSLOPE(M).GT.NSLMAX) NSLMAX=NSLOPE(M)
      IF(NSLOPE(M).GT.2) GO TO 240
      NP(M,1)=0
      IF(NFIX(L)-1) 225,220,215
  215 CONTINUE
      C=(SXX(M,1)*SLOPE(L)-SXY(M,1))/(SYX(M,1)*SLOPE(L)-SYY(M,1))
      R=1.-C*SLOPE(L)
      SXX(M,1)=(SXX(M,1)-C*SYX(M,1))/R
      SXY(M,1)=(SXY(M,1)-C*SYY(M,1))/R
      SYX(M,1)=SXX(M,1)*SLOPE(L)
      SYY(M,1)=SXY(M,1)*SLOPE(L)
      GO TO 240
  220 SYY(M,1)=SYY(M,1)-SYX(M,1)*SXY(M,1)/SXX(M,1)
      GO TO 230
  225 SYY(M,1)=0.0
  230 SXX(M,1)=0.0
  235 SXY(M,1)=0.0
      SYX(M,1)=0.0
  240 CONTINUE
      RETURN
      END
```

```
      SUBROUTINE NPDIAP(XBOUND,YBOUND,BOTFIB,UPPFIB,EC,NOPB,GNUF,
     1GNUM,WLOAD)
C
C     PRELIMINARY APPROXIMATION TO NODAL POINT DISPLACEMENTS
C
      COMMON NPI(750),NPJ(750),NPK(750),ET(750),XU(750),
     1MORF(750),AJ(750),AK(750),BJ(750),BK(750),SIGXX(750),
     2SIGYY(750),SIGXY(750),TEX(750),TEY(750),TEXY(750),
     3XORD(450),YORD(450),XLOAD(450),YLOAD(450),DSX(450),
     4DSY(450),NP(450,10),NAP(450),SLOPE(450),LM(3),
     5SXX(450,9),SXY(450,9),SYX(450,9),SYY(450,9),
     6NSLOPE(450),NFIX(450),NPB(450),A(6,6),B(6,6),S(6,6),
     7NUMNP,NUMEL,NUMBC
      IF (BOTFIB.EQ.0..AND.UPPFIB.EQ.0.) RETURN
      STRAIN=WLOAD/(YBOUND*EC)
      IF(WLOAD.EQ.0.) STRAIN=DSX(NOPB)/XBOUND
      DO 253 M=1,NUMNP
      DSX(M)=XORD(M)*STRAIN
      IF(YORD(M).GT.BOTFIB) GO TO 251
      DSY(M)=-GNUF*STRAIN*YORD(M)
      IF(YORD(M).EQ.BOTFIB) DSYBF=DSY(M)
      GO TO 253
  251 CONTINUE
      IF(YORD(M).GT.UPPFIB) GO TO 252
      DSY(M)=-GNUM*STRAIN*(YORD(M)-BOTFIB) + DSYBF
      IF(YORD(M).EQ.UPPFIB) DSYUF=DSY(M)
      GO TO 253
  252 CONTINUE
      DSY(M)=-GNUF*STRAIN*(YORD(M)-UPPFIB) + DSYUF
  253 CONTINUE
      RETURN
      END
```

```
      SUBROUTINE NPITER(SUM,SUMD,NSLMAX,NOPB,NOPC,NOPD,XFAC)
C
C     ITERATION ON NODAL POINT DISPLACEMENTS
C
      COMMON NPI(750),NPJ(750),NPK(750),ET(750),XU(750),
     1MORF(750),AJ(750),AK(750),BJ(750),BK(750),SIGXX(750),
     2SIGYY(750),SIGXY(750),TEX(750),TEY(750),TEXY(750),
     3XORD(450),YORD(450),XLOAD(450),YLOAD(450),DSX(450),
     4DSY(450),NP(450,10),NAP(450),SLOPE(450),LM(3),
     5SXX(450,9),SXY(450,9),SYX(450,9),SYY(450,9),
     6NSLOPE(450),NFIX(450),NPB(450),A(6,6),B(6,6),S(6,6),
     7NUMNP,NUMEL,NUMBC
      DXNOPB=0.
      DYNOPC=0.
      DO 290 M=1,NUMNP
      NUM=NAP(M)
      IF (SXX(M,1)+SYY(M,1)) 275,290,275
  275 FRX=XLOAD(M)
      FRY=YLOAD(M)
      DO 280 L=2,NUM
      N=NP(M,L)
      FRX=FRX-SXX(M,L)*DSX(N)-SXY(M,L)*DSY(N)
  280 FRY=FRY-SYX(M,L)*DSX(N)-SYY(M,L)*DSY(N)
      DX=SXX(M,1)*FRX+SXY(M,1)*FRY-DSX(M)
      DY=SYX(M,1)*FRX+SYY(M,1)*FRY-DSY(M)
      IF(M.EQ.NOPB) DXNOPB = DX
      IF(NSLOPE(M).EQ.3) DX = DXNOPB
      IF(NSLMAX.LT.4) GO TO 281
      IF(M.EQ.NOPC) DYNOPC = DY
      IF(NSLOPE(M).EQ.4) DY = DYNOPC
      IF(M.EQ.NOPD) DY = DYNOPC
  281 CONTINUE
      DSX(M)=DSX(M)+XFAC*DX
      DSY(M)=DSY(M)+XFAC*DY
      SUMD=SUMD+ABS(DSX(M))+ABS(DSY(M))
  285 SUM=SUM+ABS(DX)+ABS(DY)
  290 CONTINUE
      SUM=SUM/SUMD
      RETURN
      END
```

```
      SUBROUTINE SIGOUT(INC,JEL,NCYCLE,NCYCM,PSCALE,TLOAD,
     1FACTOR,MINC,ISKIP,IPRINT,NREST,IKE,EPFAIL)
C
C     CALCULATION OF ELEMENT STRESSES
C
      COMMON NPI(750),NPJ(750),NPK(750),ET(750),XU(750),
     1MORF(750),AJ(750),AK(750),BJ(750),BK(750),SIGXX(750),
     2SIGYY(750),SIGXY(750),TEX(750),TEY(750),TEXY(750),
     3XORD(450),YORD(450),XLOAD(450),YLOAD(450),DSX(450),
     4DSY(450),NP(450,10),NAP(450),SLOPE(450),LM(3),
     5SXX(450,9),SXY(450,9),SYX(450,9),SYY(450,9),
     6NSLOPE(450),NFIX(450),NPB(450),A(6,6),B(6,6),S(6,6),
     7NUMNP,NUMEL,NUMBC
      COMMON/PLAST/EX(750),EY(750),EXY(750),EPLAS(750)
      DO 998 N=1,NUMEL
      IF(INC.GT.1) JEL=0
      I=NPI(N)
      J=NPJ(N)
      K=NPK(N)
      EPX=(BJ(N)-BK(N))*DSX(I)+BK(N)*DSX(J)-BJ(N)*DSX(K)
      EPY=(AK(N)-AJ(N))*DSY(I)-AK(N)*DSY(J)+AJ(N)*DSY(K)
      GAM= (AK(N)-AJ(N))*DSX(I)-AK(N)*DSX(J)+AJ(N)*DSX(K)
     1    +(BJ(N)-BK(N))*DSY(I)+BK(N)*DSY(J)-BJ(N)*DSY(K)
      COMM=1./(AJ(N)*BK(N)-AK(N)*BJ(N))
      EX(N)=EPX*COMM
      EY(N)=EPY*COMM
      EXY(N)=GAM*COMM
      IF(NCYCLE.LT.NCYCM) GO TO 82
      TEX(N)=TEX(N)+EX(N)
      TEY(N)=TEY(N)+EY(N)
      TEXY(N)=TEXY(N)+EXY(N)
   82 CONTINUE
      IF(INC.GT.1.AND.MORF(N).NE.1) GO TO 11
      COMM=COMM*ET(N)/(1.-XU(N)**2)
      X=COMM*(EPX+XU(N)*EPY)
      Y=COMM*(EPY+XU(N)*EPX)
      XY=COMM*GAM*(1.-XU(N))*.5
      IF(INC.EQ.1.OR.NCYCLE.LT.NCYCM) GO TO 81
      TIM=ET(N)/(1.-XU(N)**2)
      X=TIM*(TEX(N)+XU(N)*TEY(N))
      Y=TIM*(TEY(N)+XU(N)*TEX(N))
      XY=TIM*TEXY(N)*(1.-XU(N))*.5
   81 CONTINUE
      IF(MORF(N).EQ.1) GO TO 19
      FACT=ZERO(X,Y,XY)
      IF(FACT.GT.FACTOR)FACTOR=FACT
   19 CONTINUE
      SIGXX(N)=X
      SIGYY(N)=Y
      SIGXY(N)=XY
      GO TO 12
   11 X=SIGXX(N)
      Y=SIGYY(N)
      XY=SIGXY(N)
      EP=EPLAS(N)
      CALL SIGEPS(B,6,EX(N),EY(N),EXY(N),X,Y,XY,XU(N),ET(N),
     1EP,1,JEL,FACTOR)
   12 CONTINUE
      IF(INC.EQ.1) GO TO 67
```

```
      IF(NCYCLE.LT.NCYCM) GO TO 67
      SIGXX(N)=X
      SIGYY(N)=Y
      SIGXY(N)=XY
      EPLAS(N)=EP
   67 CONTINUE
      C=(X+Y)/2.0
      R=SQRT(((Y-X)/2.0)**2+XY**2)
      XMAX=C+R
      XMIN=C-R
      XYMAX = 0.5*(XMAX-XMIN)
      IF (MORF(N).EQ.1) EP=0.
      IF (ISKIP.EQ.0) GO TO 997
      IF (NCYCLE.LT.NCYCM.AND.INC.GT.1) GO TO 997
      IF(MORF(N).NE.7) GO TO 68
      WRITE(6,125) N,TEX(N),TEY(N),TEXY(N),EP
      GO TO 997
   68 CONTINUE
      IF (EP.GT.0.) WRITE(6,124) N,TEX(N),TEY(N),TEXY(N),EP
  997 PA=0.5*57.29578*ATAN(2.*XY/(Y-X))
      IF (2.*X-XMAX-XMIN) 405,420,420
  405 IF (PA) 410,420,415
  410 PA=PA+90.0
      GO TO 420
  415 PA=PA-90.0
  420 CONTINUE
      IF (NREST.GT.1.AND.MINC.EQ.1) GO TO 998
      IF (IKE.EQ.0.AND.INC.EQ.1) GO TO 998
      IF (NCYCLE.LT.NCYCM.AND.INC.GT.1) GO TO 998
      IF (IPRINT.NE.0.OR.ISKIP.NE.0) GO TO 998
      IF(MORF(N).NE.7) GO TO 69
      WRITE(6,126) N,TEX(N),TEY(N),TEXY(N),EP,XYMAX
      WRITE(6,124) N,X,Y,XY,XMAX,XMIN,PA
      GO TO 998
   69 CONTINUE
      WRITE(6,124) N,TEX(N),TEY(N),TEXY(N),EP,XYMAX
      WRITE(6,124) N,X,Y,XY,XMAX,XMIN,PA
  998 CONTINUE
  124 FORMAT(1110,3F20.8,5X,3F15.8)
  125 FORMAT(1110,3F20.8,5X,F15.8,12H    FRACTURED)
  126 FORMAT(1110,3F20.8,5X,2F15.8,12H    FRACTURED)
      RETURN
      END
```

```
      SUBROUTINE NPSIG(INC)
C
C     CALCULATION OF NODAL POINT STRESSES
C
      COMMON NPI(750),NPJ(750),NPK(750),ET(750),XU(750),
     1MORF(750),AJ(750),AK(750),BJ(750),BK(750),SIGXX(750),
     2SIGYY(750),SIGXY(750),TEX(750),TEY(750),TEXY(750),
     3XORD(450),YORD(450),XLOAD(450),YLOAD(450),DSX(450),
     4DSY(450),NP(450,10),NAP(450),SLOPE(450),LM(3),
     5SXX(450,9),SXY(450,9),SYX(450,9),SYY(450,9),
     6NSLOPE(450),NFIX(450),NPB(450),A(6,6),B(6,6),S(6,6),
     7NUMNP,NUMEL,NUMBC
      DO 900 M=1,NUMNP
      ITCT=1
      GO TO 803
  802 ITCT=2
  803 X=0.
      Y=0.
      XY=0.
      SRX=0.
      SRY=0.
      R=0.
      DO 860 N=1,NUMEL
      IF(ITCT.EQ.2.AND.MORF(N).EQ.1) GO TO 804
      IF(ITCT.EQ.2.AND.MORF(N).EQ.0) GO TO 860
      IF (MORF(N).EQ.1) GO TO 860
  804 I=NPI(N)
      J=NPJ(N)
      K=NPK(N)
      IF (M-I) 830,850,830
  830 IF (M-J) 835,845,835
  835 IF (M-K) 860,840,860
  840 I=NPK(N)
      K=NPI(N)
      GO TO 850
  845 I=NPJ(N)
      J=NPI(N)
  850 AA=ABS(XORD(J)+XORD(K)-2.*XORD(I))
      BB=ABS(YORD(J)+YORD(K)-2.*YORD(I))
      RY=BB/(AA+BB)
      SRY=SRY+RY
      Y=Y+SIGYY(N)*RY
      RX=AA/(AA+BB)
      SRX=SRX+RX
      X=X+SIGXX(N)*RX
      R=R+1.
      XY=XY+SIGXY(N)
  860 CONTINUE
      IF(R.EQ.0..AND.ITCT.EQ.1) GO TO  802
      IF(R.EQ.0.) GO TO 900
      X=X/SRX
      Y=Y/SRY
      XY=XY/R
      C=(X+Y)/2.0
      R=SQRT(((Y-X)/2.0)**2+XY**2)
      XMAX=C+R
      XMIN=C-R
      XYMAX = 0.5*(XMAX-XMIN)
      PA=0.5*57.29578*ATAN(2.*XY/(Y-X))
```

```
      IF (2.*X-XMAX-XMIN) 805,820,820
  805 IF (PA) 810,820,815
  810 PA=PA+90.0
      GO TO 820
  815 PA=PA-90.0
  820 CONTINUE
      IF (X.EQ.0..AND.Y.EQ.0..AND.XY.EQ.0.) GO TO 899
      WRITE (6,124)  M,X,Y,XY,XMAX,XMIN,XYMAX
  899 CONTINUE
      IF (ITCT.EQ.1) GO TO 802
  900 CONTINUE
  124 FORMAT(1I10,3F20.8,5X,3F15.8)
      RETURN
      END
```

```
      SUBROUTINE ELACS(FACTO,FACTOR,EPFAIL)
C
C     ELASTIC INCREMENT OF STRAINS,LOADS AND DISPLACEMENTS
C
      COMMON NPI(750),NPJ(750),NPK(750),ET(750),XU(750),
     1MORF(750),AJ(750),AK(750),BJ(750),BK(750),SIGXX(750),
     2SIGYY(750),SIGXY(750),TEX(750),TEY(750),TEXY(750),
     3XORD(450),YORD(450),XLOAD(450),YLOAD(450),DSX(450),
     4DSY(450),NP(450,10),NAP(450),SLOPE(450),LM(3),
     5SXX(450,9),SXY(450,9),SYX(450,9),SYY(450,9),
     6NSLOPE(450),NFIX(450),NPB(450),A(6,6),B(6,6),S(6,6),
     7NUMNP,NUMEL,NUMBC
      COMMON/PLAST/EX(750),EY(750),EXY(750),EPLAS(750)
      DO 14 N=1,NUMEL
      EX(N)=EX(N)*FACTO
      EY(N)=EY(N)*FACTO
      EXY(N)=EXY(N)*FACTO
      TXINC=B(1,1)*EX(N)+B(1,2)*EY(N)+B(1,3)*EXY(N)
      TYINC=B(2,1)*EX(N)+B(2,2)*EY(N)+B(2,3)*EXY(N)
      TXYINC=B(3,1)*EX(N)+B(3,2)*EY(N)+B(3,3)*EXY(N)
      TX=SIGXX(N)+TXINC
      TY=SIGYY(N)+TYINC
      TXY=SIGXY(N)+TXYINC
      TZERO=ZERO(TX,TY,TXY)
      IF(TZERO,LT,FACTOR,OR,MORF(N),GT,0) GO TO 14
      IF(EPLAS(N),LT,EPFAIL) GO TO 14
      ET(N)=.1E0
      SIGXX(N)=0.
      SIGYY(N)=0.
      SIGXY(N)=0.
      MORF(N)=7
   14 CONTINUE
      DO 15 N=1,NUMNP
      XLOAD(N)=XLOAD(N)*FACTO
      YLOAD(N)=YLOAD(N)*FACTO
      DSX(N)=DSX(N)*FACTO
      DSY(N)=DSY(N)*FACTO
   15 CONTINUE
      RETURN
      END
```

```
      SUBROUTINE SIGEPS(B,N,EPX,EPY,EXY,X,Y,XY,GNU,E,EP,
     1ISTORE,JEL,FACTOR)
C
C     FORMATION OF STRESS/STRAIN RELATION
C
      DIMENSION B(N,N),DUMP(6),A(6,6)
      DIVE=1.0/E
      DIVGNU=-GNU*DIVE
      DIV=1.-GNU*GNU
      COMM=E/DIV
      G=0.5*E/(1.0+GNU)
      DIVG=1./G
      DO 5 I=1,6
    5 DUMP(I)=0.
      DO 1 I=1,4
      DO 1 J=1,4
      A(I,J)=0.
    1 B(I,J)=0.0
      B(1,1)=COMM
      B(1,2)=COMM*GNU
      B(2,1)=B(1,2)
      B(2,2)=B(1,1)
      B(3,3)=G
      IF(JEL.EQ.1) RETURN
      FPLAS=0.0
      T=ZERO(X,Y,XY)
      IF(T.GE.FACTOR.OR.EP.GT.0.) GO TO 2
      XINC=B(1,1)*EPX+B(1,2)*EPY+B(1,3)*EXY
      YINC=B(2,1)*EPX+B(2,2)*EPY+B(2,3)*EXY
      XYINC=B(3,1)*EPX+B(3,2)*EPY+B(3,3)*EXY
      TZERO=ZERO(X+XINC,Y+YINC,XY+XYINC)
      IF(TZERO.LE.FACTOR) GO TO 4
      FPLAS=(FACTOR-T)/(TZERO-T)
    2 XINC=XINC*FPLAS
      YINC=YINC*FPLAS
      XYINC=XYINC*FPLAS
      A(1,1)=DIVE
      A(1,2)=DIVGNU
      A(2,1)=DIVGNU
      A(2,2)=A(1,1)
      A(3,3)=DIVG
      A(1,4)=0.5*(2.0*(X+XINC)-(Y+YINC))
      A(2,4)=-0.5*(X+XINC)+(Y+YINC)
      A(3,4)=3.0*(XY+XYINC)
      IF(T.LT.FACTOR) T=FACTOR
      TR=1./T
      A(1,4)=A(1,4)*TR
      A(2,4)=A(2,4)*TR
      A(3,4)=A(3,4)*TR
      A(4,4)=-WORK(EP)
      A(4,1)=A(1,4)
      A(4,2)=A(2,4)
      A(4,3)=A(3,4)
      CALL INVERT(A,4,DUMP,1,DETERM,6)
      DO 3 I=1,4
      DO 3 J=1,4
    3 B(I,J)=B(I,J)*FPLAS+A(I,J)*(1.-FPLAS)
    4 IF(ISTORE.NE.1) RETURN
      XINC=B(1,1)*EPX+B(1,2)*EPY+B(1,3)*EXY
```

```
      YINC=B(2,1)*EPX+B(2,2)*EPY+B(2,3)*EXY
      XYINC=B(3,1)*EPX+B(3,2)*EPY+B(3,3)*EXY
      X=X+XINC
      Y=Y+YINC
      XY=XY+XYINC
      EP=EP+B(4,1)*EPX+B(4,2)*EPY+B(4,3)*EXY
      RETURN
      END
```

```
      FUNCTION ZERO(X,Y,XY)
C
C     FORMATION OF EQUIVALENT YIELD STRESS
C
      ZERO=SQRT(X*X-X*Y+Y*Y+3.*XY*XY)
      RETURN
      END
```

```
      FUNCTION WORK(EP)
C
C     INELASTIC STRESS/STRAIN RELATION - WORK HARDENING
C     CHARACTERISTICS
C
      COMMON/HARDEN/COF(5)
      WORK=COF(1)+EP*COF(2)*2.+3.*EP*EP*COF(3)
      RETURN
      END
```

```
      SUBROUTINE INVERT(A,N,B,M,DETERM,IDIM)
C     MATRIX INVERSION WITH ACCOMPANYING SOLUTION OF LINEAR
C     EQUATIONS
C
      DIMENSION IPIVOT( 150),A(IDIM,IDIM),B(IDIM,M),INDEX( 150,2)
     1,PIVOT( 150)
C
C     INITIALIZATION
C
    9 CALL DVCHK(IOV)
   10 DETERM=1.0
      DO 20  J=1,150
      IPIVOT(J)=0
      INDEX(J,1)=0
      INDEX(J,2)=0
      PIVOT(J)=0.0
   20 CONTINUE
      SWAP=0.0
      L=0
      L1=0
      T=0.0
   30 DO 550 I=1,N
C
C     SEARCH FOR PIVOT ELEMENT
C
   40 AMAX=0.0
   41 IROW=0
   42 ICOLUM=0
   45 DO 105 J=1,N
   50 IF (IPIVOT(J)-1) 60, 105, 60
   60 DO 100 K=1,N
   70 IF (IPIVOT(K)-1) 80, 100, 740
   80 IF (ABS(AMAX)-ABS(A(J,K))) 85, 100, 100
   85 IROW=J
   90 ICOLUM=K
   95 AMAX=A(J,K)
  100 CONTINUE
  105 CONTINUE
  106 IF(IROW) 110,750,110
  110 IPIVOT(ICOLUM)=IPIVOT(ICOLUM)+1
C
C     INTERCHANGE ROWS TO PUT PIVOT ELEMENT ON DIAGONAL
C
  130 IF (IROW-ICOLUM) 140, 260, 140
  140 DETERM=-DETERM
  150 DO 200 L=1,N
  160 SWAP=A(IROW,L)
  170 A(IROW,L)=A(ICOLUM,L)
      A(ICOLUM,L)=SWAP
  200 CONTINUE
  205 IF(M) 260, 260, 210
  210 DO 250 L=1,M
  220 SWAP=B(IROW,L)
  230 B(IROW,L)=B(ICOLUM,L)
      B(ICOLUM,L)=SWAP
  250 CONTINUE
  260 INDEX(I,1)=IROW
  270 INDEX(I,2)=ICOLUM
  310 PIVOT(I)=A(ICOLUM,ICOLUM)
```

```
      320 DETERM=DETERM*PIVOT(I)
C
C     DIVIDE PIVOT ROW BY PIVOT ELEMENT
C
      330 A(ICOLUM,ICOLUM)=1.0
      340 DO 350 L=1,N
          A(ICOLUM,L)=A(ICOLUM,L)/PIVOT(I)
      350 CONTINUE
      351 CALL DVCHK(IOV)
      352 IF(IOV-1) 355,750,355
      355 IF(M) 380, 380, 360
      360 DO 370 L=1,M
          B(ICOLUM,L)=B(ICOLUM,L)/PIVOT(I)
      370 CONTINUE
C
C     REDUCE NON-PIVOT ROWS
C
      380 DO 550L1=1,N
      390 IF(L1-ICOLUM) 400, 550, 400
      400 T=A(L1,ICOLUM)
      420 A(L1,ICOLUM)=0.0
      430 DO 450 L=1,N
          A(L1,L)=A(L1,L)-A(ICOLUM,L)*T
      450 CONTINUE
      455 IF(M) 550, 550, 460
      460 DO 500 L=1,M
          B(L1,L)=B(L1,L)-B(ICOLUM,L)*T
      500 CONTINUE
      550 CONTINUE
C
C     INTERCHANGE COLUMNS
C
      600 DO 710 I=1,N
      610 L=N+1-I
      620 IF (INDEX(L,1)-INDEX(L,2)) 630, 710, 630
      630 JROW=INDEX(L,1)
      640 JCOLUM=INDEX(L,2)
      650 DO 705 K=1,N
      660 SWAP=A(K,JROW)
      670 A(K,JROW)=A(K,JCOLUM)
      700 A(K,JCOLUM)=SWAP
      705 CONTINUE
      710 CONTINUE
      740 RETURN
      750 DETERM=0.0
      760 GO TO 740
          END
```